Littoral Wetlands and Lake Inflow Dynamics

by

Hrund Ólöf Andradóttir

B.S., Civil Engineering, University of Iceland, 1994
M.S., Environmental Engineering, Massachusetts Institute of Technology, 1997

Submitted to the Department of Civil and Environmental Engineering
in partial fulfillment of the requirements for the degree of

Doctor of Philosophy in Civil and Environmental Engineering

at the

MASSACHUSETTS INSTITUTE OF TECHNOLOGY

May 2000

Author .....
.....
Department of Civil and Environmental Engineering
May 12, 2000

Certified by .....
Heidi M. Nepf
Associate Professor
Thesis Supervisor

Accepted by .....
Daniele Veneziano
Chairman, Department Committee on Graduate Students

Littoral Wetlands and Lake Inflow Dynamics

by

Hrund Ólöf Andradóttir

Submitted to the Department of Civil and Environmental Engineering
on May 12, 2000, in partial fulfillment of the
requirements for the degree of
Doctor of Philosophy in Civil and Environmental Engineering

Abstract

Wetlands are increasingly recognized as important water treatment systems, which efficiently remove nutrients, suspended sediments, metals and anthropogenic chemicals through sediment settling and various chemical and biological processes. This thesis tackles three interconnected aspects of wetland physics. The first is wetland circulation, which is one of the most important design parameters when constructing wetlands for water quality improvement because it regulates the residence time distribution, and thus the removal efficiency of the system. Field work demonstrates that wetland circulation changes from laterally well mixed during low flows to short-circuiting during storms, which in combination with a reduced nominal residence time undermines the wetland treatment performance. The second important physical mechanism is thermal mediation, i.e. the temperature modification of the water that flows through the wetland. This change in water temperature is specifically important in littoral wetlands, where it can alter the intrusion depth in the downstream lake. Numerical analysis in conjunction with field observations shows that littoral wetlands located in small or forested watersheds can raise the water temperature of the lake inflow during summer enough to create surface inflows when a plunging inflow would otherwise exist. Consequently, more land borne nutrients and chemicals enter the epilimnion where they can enhance eutrophication and the risk of human exposure. The third and last physical mechanism considered in this thesis is the exchange flows generated between littoral wetlands and lakes. Field experiments show that during summer and fall, when river flows are low, buoyancy- and wind-driven exchange flows dominate the wetland circulation and flushing dynamics. More importantly, they can enhance the flushing by as high as a factor of ten, thus dramatically impairing the wetland potential for removal and thermal mediation.

Thesis Supervisor: Heidi M. Nepf
Title: Associate Professor

Acknowledgments

First of all, I would like to thank my advisor, Heidi Nepf, for her help and mentoring during the last six years. Besides initiating really interesting projects, she has given me the freedom to tackle the research problems I like, and been very supportive throughout my studies. Financial support from the National Institute of Environmental Health Sciences, Superfund Basic Research Program, Grant No. P42-ES04675 is also greatly appreciated.

In addition, I would like to thank my committee members: Eric Adams, for helping me better conceptualize and formalize my work on wetland thermal mediation; Rocky Geyer, for giving me great ideas on how to better collect field data, and teaching me about estuarine exchange flow mechanisms; Harry Hemond, for his insight and interest in physical limnology.

I would also like to thank the past and present members of my research group, especially Paul Fricker, for his continuous involvement with my work, and help with field data collection. In addition, I wish to thank my fellow students in the Parsons Lab, Nicole Gaspriani, Vanja Klepac, Luis Perez-Pardo, Quiling Wang, Scott Rybarczyk, Daniel Collins, Dave Senn and Megan Kogut for their support and encouragement during the last months of thesis writing.

During my six years at MIT I have been fortunate enough to make many good friends. I wish to thank my girlfriends, Maya Farhoud, Alessandra Orsoni, Liina Pylkanen, Danielle Tarraf, Raquel Gimenez, Laila Elias and Corinne Frasson, for making sure that life after work is always full of fun; My Scandinavian friends, Torkel Engeness, Thomas Sunn and Steffen Ernst, for digging out the Scandinavian in me and getting me involved in club organization; James Moran for his good company and good advice.

Finally, I would like to dedicate this thesis to my family: My parents, Svava and Andri, who inspired me to seek the highest degree of learning and explore the world; My sister, Sigrún, who adviced me on how to achieve my goals; My brothers, Thór and Hjalti, who continuously broaden my perspective on life. Without their dedication and support, I would not be where I am today.

Contents

[1] **Published under the title "Thermal mediation by littoral wetlands and impact on lake intrusion depth" in Water Resources Research, Vol. 36, No.3, pages 725-735, March, 2000.**

[2] **Submitted under the name "Thermal mediation in a natural littoral wetland: Measurements and modeling" to Water Resources Research in October 1999.**

List of Figures

List of Tables

Chapter 1

Overview

Wetlands are important transition zones between terrestrial and aquatic systems. Besides being the natural habitat of a wide range of unique wildlife species, including reptiles, amphibians, fish and birds, they also play an important role in stabilizing lakeshores and coasts against erosion, and in controlling floods. Moreover, they can improve downstream water quality by efficiently removing nutrients, suspended sediments, metals and anthropogenic chemicals through sediment settling and various chemical and biological processes. Attempting to harness this filtering capacity, over 300 wetland have been constructed in North-America to provide cheap, low-maintenance wastewater treatment.

The work presented in this thesis tackles three interconnected aspects of wetland physics. The first is wetland water circulation. Water circulation is one of the most important parameter in the design of constructed wetlands because it regulates the residence time distribution, and thus the removal efficiency of the system. The second aspect is thermal mediation, i.e. the temperature modification of the water that flows through wetlands. For a littoral wetland, this change in water temperature can have a significant impact on lake water quality and the management of reservoir use and withdrawals. The third research project tackles exchange flows between littoral wetlands and lakes, and how these exchange flows regulate the flushing of the wetlands and thus modify what role they play in lake water quality.

The outline of this thesis is the following. Chapter 2 describes a theoretical study of wetland thermal mediation. Applying a dead-zone model to a river reach, wetland and lake, we characterize when and why wetland thermal mediation occurs, and how they impact lake

intrusion dynamics. The results suggest that littoral wetlands located in small and forested watersheds can raise the water temperature of the lake inflow during summer enough to create surface inflows when a plunging inflow would otherwise occur. Consequently, more land borne nutrients and chemicals enter the epilimnion where they can enhance eutrophication and the risk of human exposure. Chapter 3 provides field observations that support the findings in chapter 2. In addition, the observations demonstrates that wetland circulation changes from laterally well mixed during low flows to short-circuiting during storms, which in combination with a reduced nominal residence time undermines the wetland potential for removal and thermal mediation during storms. Chapter 4 describes exchange flows between littoral wetlands and lakes during different times of the year. The major result is that wind- and buoyancy-driven exchange flows are often the dominant flushing mechanisms in littoral wetlands during summer when river flows are typically low. These exchange flow can enhance the flushing of the wetland by a factor of ten, thus dramatically impairing their potential for removal and thermal mediation.

Chapter 2

Thermal Mediation: Theoretical Considerations[1]

Lake inflow dynamics can be affected by the thermal mediation provided by shallow littoral regions such as wetlands. In this study, wetland thermal mediation is evaluated using a linearized dead-zone model. Its impact on lake inflow dynamics is then assessed by applying the model sequentially to the river reach, wetland and lake. Our results suggest that littoral wetlands can dramatically alter the inflow dynamics of reservoirs located in small or forested watersheds, *e.g.* by raising the temperature of the inflow during the summer, and creating surface intrusions when a plunging inflow would otherwise exist. Consequently, river-borne nutrients, contaminants and pathogens enter directly into the epilimnion, where they enhance eutrophication and the risk of human exposure. The addition of a littoral wetland has less significant effects in larger watersheds, where the water has already equilibrated with the atmosphere upon reaching the wetland, and sun-shading is less prominent.

[1]**Published under the title "Thermal mediation by littoral wetlands and impact on lake intrusion depth" in Water Resources Research, Vol. 36, No.3, pages 725-735, March, 2000.**

2.1 Introduction

Littoral wetlands are important transition zones between uplands and deep aquatic systems (figure 2-1). Besides having a unique ecosystem, they can improve downstream water quality both through sediment settling and chemical and biological processes [*Johnston et al.*, 1984; *Tchobanoglous*, 1993]. Attempting to harness this filtering capacity, over 300 wetlands have already been constructed in North America to provide cheap, low maintenance wastewater treatment [*Reed and Brown*, 1992; *Bastian and Hammer*, 1993]. In addition to transforming the chemical and particulate composition of the water, wetlands can also alter the water temperature, such that the temperature of the water leaving the wetland, T_W, differs from that of the river that feeds it, T_R (see figure 2-1). This thermal mediation is especially important in littoral wetlands, where it can alter the intrusion dynamics in a lake and ultimately affect lake water quality.

A recent attempt at eutrophication control for Lake McCarrons in Minnesota provides an instructive example of why one must consider thermal mediation when designing a constructed wetland for water quality improvement. A wetland was constructed to reduce nutrient loads to Lake McCarrons. Although effective in reducing nutrient fluxes, the wetland did not improve the lake water quality, partly because it raised the lake inflow temperature sufficiently during summer months to change its intrusion depth. In particular, after the addition of the wetland, contaminant and nutrient fluxes were carried directly into the lake's epilimnion where they were more damaging (*i.e.* $T_W \approx T_L$ on figure 2-1), instead of plunging into the thermocline as they had before the wetland was built (*i.e.* $T_W < T_L$ on figure 2-1) [*Oberts*, 1998; *Metropolitan Council*, 1997]. Because thermal mediation was not considered in the design, the wetland performance was significantly undermined.

Despite the important implications for lake water quality, wetland thermal mediation remains a relatively unstudied process. To the authors knowledge, fundamental questions such as when and why wetland thermal mediation occurs, and how it alters lake intrusion dynamics, have still not been answered. To address these questions, wetland thermal mediation must be considered as a part of an integrated watershed process (figure 2-1): First, the degree of thermal mediation provided by a littoral wetland depends on the temperature of the water delivered from the watershed, *i.e.* the river temperature, T_R. Second, the impact of wetland thermal mediation on lake water quality depends on the temperature of

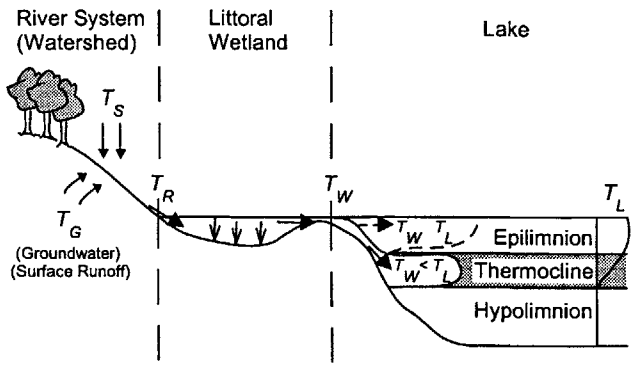

Figure 2-1: Littoral wetlands are transition zones between uplands and deep aquatic systems. The water temperature evolves from its source (T_G or T_S), down the river reach (T_R), through the wetland (T_W) and in the lake (T_L). If thermal mediation occurs within the wetland, *i.e.* $T_W \neq T_R$, the lake intrusion dynamics may be altered. Specifically, if $T_W \approx T_L$ then surface intrusions occur, whereas if $T_W < T_L$ a plunging inflow occurs.

the wetland outflow, T_W, relative to the temperature of the lake epilimnion, T_L [*Fisher et al.*, 1979, p. 209]. Therefore, to fully understand this process requires an analysis of both the local thermal processes within the wetland and the global thermal processes across the watershed, *i.e.* determining groundwater temperature T_G, surface water temperature T_S, as well as T_R, T_W and T_L in figure 2-1.

By considering the watershed scale, the work presented in this paper goes beyond previous thermal analyses aimed at eutrophication control [*e.g. Harleman*, 1982] and cooling water discharge [*e.g. Jirka et al.*, 1978], both of which focused on small sub-sections of the watershed. Furthermore, this paper provides a link between thermal mediation in shallow flow-through systems and differential heating and cooling, a process responsible for diurnal exchange flows between the pelagic region of a lake and its shallow stagnant side-arms [*Monismith et al.*, 1990; *Farrow and Patterson*, 1993]. The differential heating and cooling pattern is generated because rivers and wetlands are shallower and more enclosed than pelagic regions in lakes. As a result, they distribute heat over shorter depths and experience greater sun-shading and wind sheltering, which reduces their exposure to solar, latent and convective heating [*Sinokrot and Stefan*, 1993].

The goal of this paper is to generate a general analytical framework for evaluating the impact of wetland thermal mediation on lake inflow temperature. Building upon cooling pond analysis [*Jirka et al.*, 1978; *Jirka and Watanabe*, 1980; *Adams*, 1982], a simple con-

ceptual model, called the dead-zone model, is introduced to explore the mechanisms behind wetland thermal mediation and river/wetland-lake interactions. The dead-zone model is presented in section 2.2.. The steady and periodic thermal responses predicted by this model are discussed in section 2.3.. Finally, in section 2.4. the model is integrated across different watershed sub-sections, and the results are used to compare the lake intrusion dynamics for systems with and without littoral wetlands. The theoretical results in this paper are verified with field experiments in *Andradóttir and Nepf* [2000].

2.2 Dead-Zone Model

To accurately predict wetland thermal processes a model must properly reflect the wetland circulation. The water circulation controls the skewness and variance of the residence time distribution (RTD), both of which determine how effectively the water is thermally mediated in the system [*Jirka and Watanabe*, 1980]. Wetland circulation is strongly influenced both by the presence of vegetation and meteorological conditions. In particular, natural wetlands receiving unregulated river inflow are often bi-modal, oscillating between two general circulation regimes in response to shifting inflow conditions [*Andradóttir*, 1997; *DePaoli*, 1999]. During low-flows, vegetation drag, wind and buoyancy dominate the water circulation, and the wetland can exhibit a complex 3D flow behavior which varies with the onset and break down of stratification and changing wind conditions. However, the integrated effect of these processes over time is that the wetland behaves as a partially-well-mixed reactor in which the river inflow fills the wetland volume, producing an RTD with a large variance around the nominal residence time, $\bar{t}$ (figure 2-2a). In contrast during high flows, river momentum dominates the circulation and short-circuiting occurs, *i.e.* the river trajectory cuts straight across the wetland, with most flow exiting in much less time than the nominal residence time, $\bar{t}$, producing a skewed RTD (figure 2-2b). Short-circuiting can be enhanced by stationary dead-zones created by vegetation and irregular bathymetry [*e.g.* *Thackston et al.*, 1987].

The dead-zone model is a simple conceptual model, originally developed for river routing and dispersion studies, that accounts for dead-zone trapping by channel irregularities, bedforms and vegetation [*e.g.* *Valentine and Wood*, 1977; *Bencala and Walters*, 1983]. In addition, the model can simulate a wide range of circulation regimes, including both the

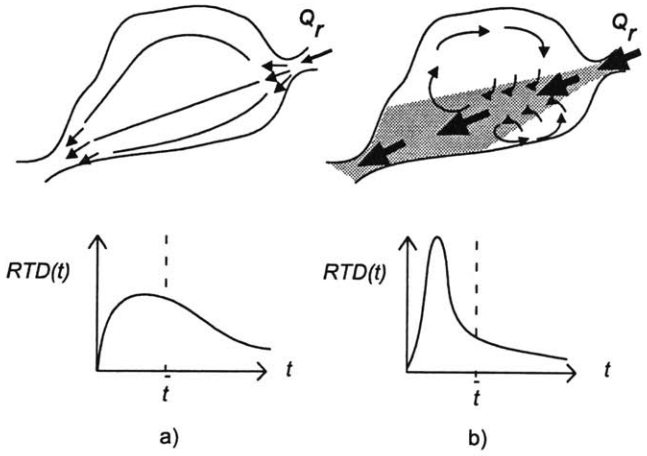

Figure 2-2: Schematic of circulation regimes and residence time distributions (RTD) in free water surface wetlands. a) Water circulation dominated by vegetation drag, wind and buoyancy. The wetland behaves as a partially well mixed reactor, corresponding to an RTD with a large variance around the mean nominal residence time, $\bar{t}$. b) River-dominated circulation with a distinct flow region (dark shaded). Short-circuiting occurs, producing a skewed RTD with much of the flow exiting the wetland in less time than $\bar{t}$.

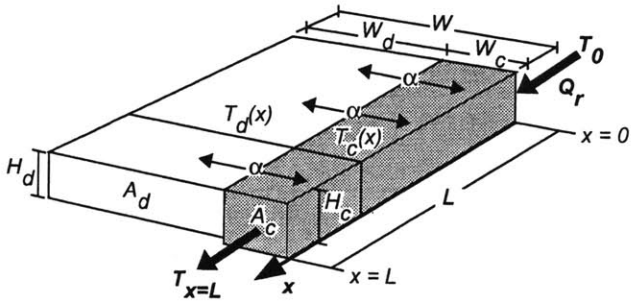

Figure 2-3: Schematic of the dead-zone model. The wetland is divided into a channel or flow zone (shaded) and stationary dead-zone. These two zones communicate with one another through spatially uniform lateral water exchange, α [s^{-1}]. Thermal mediation within the wetland is reflected in $T_{x=L} \neq T_0$.

short-circuiting and well mixed regimes discussed above. For these reasons, the dead-zone model is an appropriate choice and adapted here to wetlands. The schematic of the model is presented in figure 2-3. The wetland is divided into two zones. The first zone is a flow zone (channel) of mean depth, H_c, width, W_c, and cross-sectional area, $A_c = W_c H_c$. This zone receives inflow at temperature, T_0, and flowrate, Q_r, that traverses across the wetland at the mean velocity, $u = Q_r/A_c$, and disperses longitudinally with dispersion coefficient, D_x. The second zone is a stationary ($u = 0$) dead-zone with depth, H_d, width, W_d, and cross-sectional area, $A_d = W_d H_d$. The two zones communicate with one another through a spatially uniform lateral exchange characterized by the lateral exchange coefficient, $\alpha = \Delta Q/(A_c + A_d)L$, where ΔQ is the total lateral exchange rate between the two zones and L the length of the wetland. The governing equation for the depth-averaged temperature in the flow zone, $T_c(x,t)$, is

$$\frac{\partial T_c}{\partial t} + u\frac{\partial T_c}{\partial x} = D_x \frac{\partial^2 T_c}{\partial x^2} + \frac{\alpha}{q}(T_d - T_c) + \frac{\phi}{\rho C_p H_c} \tag{2.1}$$

and for the depth-averaged temperature in the dead zone, $T_d(x,t)$,

$$\frac{\partial T_d}{\partial t} = -\frac{\alpha}{1-q}(T_d - T_c) + \frac{\phi}{\rho C_p H_d}, \tag{2.2}$$

where $q = A_c/(A_c + A_d)$ is the jet areal ratio, $\phi(t)$ is the net surface heat flux per surface area, ρ the density and C_p the specific heat of water. To ensure heat conservation, the boundary conditions are

$$\begin{aligned} uT_c(0,t) - D_x \left.\frac{\partial T_c}{\partial x}\right|_{x=0} &= uT_0(t) \\ \left.\frac{\partial T_c}{\partial x}\right|_{x=L} &= 0. \end{aligned} \tag{2.3}$$

The net surface heating is the sum of five heat fluxes:

$$\phi = (1-R)S + \phi_1 + \phi_2 + \phi_S + \phi_L, \tag{2.4}$$

where S is the incoming solar (short wave) radiation, R the reflection coefficient, ϕ_1 the incoming long wave radiation, ϕ_2 the back-radiation, ϕ_S the sensible (conductive) and ϕ_L the latent (evaporative) heat flux. Many empirical expressions exist for each one of these

terms, and the resulting equation is a nonlinear function of both water temperature and atmospheric conditions such as air temperature, wind speed, relative humidity and cloud cover [*e.g. Fisher et al.*, 1979, p.163]. These heat flux estimates may need to be modified to account for sun-shading and wind-sheltering, which can occur in rivers as well as wetlands due to emergent vegetation, borderline trees and nearby hills.

In order to derive analytical solutions, ϕ can be linearized using the concept of an equilibrium temperature, T_E, defined as the temperature for which the water is at equilibrium with atmospheric conditions such that the net surface heat flux equals to zero [*Edinger and Geyer*, 1965], *i.e.*

$$\frac{\phi}{\rho C_p H} = \frac{K}{H}(T_E - T). \tag{2.5}$$

The surface heat transfer coefficient, K, represents the rate of surface heating and cooling, and varies temporally with meteorological conditions (in particular wind speed) and surface water temperature [*e.g.* Ryan *et al.*, 1974]. This coefficient generally lies between 0.4-1.0 m/day for low winds (less than 2 m/s), increasing to 0.8-2.0 m/day for high winds (8 m/s) [*Ryan et al.*, 1974]. The ratio $t_{heat} = H/K$ is the timescale of vertical heat transfer and represents the thermal inertia of the water column, which is a measure of how rapidly the system responds to changes in atmospheric forcing and how much heat it stores. Shallow systems with low thermal inertia can more readily track changing atmospheric conditions, but store less heat, than deep systems, *i.e.* as $H \to 0$ then $t_{heat} \to 0$, and $T \to T_E$.

Finally, (2.5) is an exact representation of the surface heat flux if the heat transfer coefficient, K, is allowed to vary in time. For mathematical simplicity, however, K will be taken as constant following *Jirka and Watanabe* [1980], and *Adams* [1982]. This is a reasonable approximation except when the water temperature deviates substantially from the equilibrium temperature [*Yotsukura et al.*, 1973], as occurs when the timescale of variation for T_E is short compared to t_{heat}, *e.g.* over synoptic and diurnal timescales.

2.3 Exploration of General Results

Temperature variations in shallow water are driven by meteorological changes that occur predominantly on three timescales, *i.e.* diurnal (P = 1 day), synoptic (P = 1-2 weeks), and seasonal (P = 1 year) [*Adams*, 1982]. To explore these multiple timescales of variations, the meteorological forcing, T_E, and temperature of the wetland inflow (at $x = 0$), T_0, are

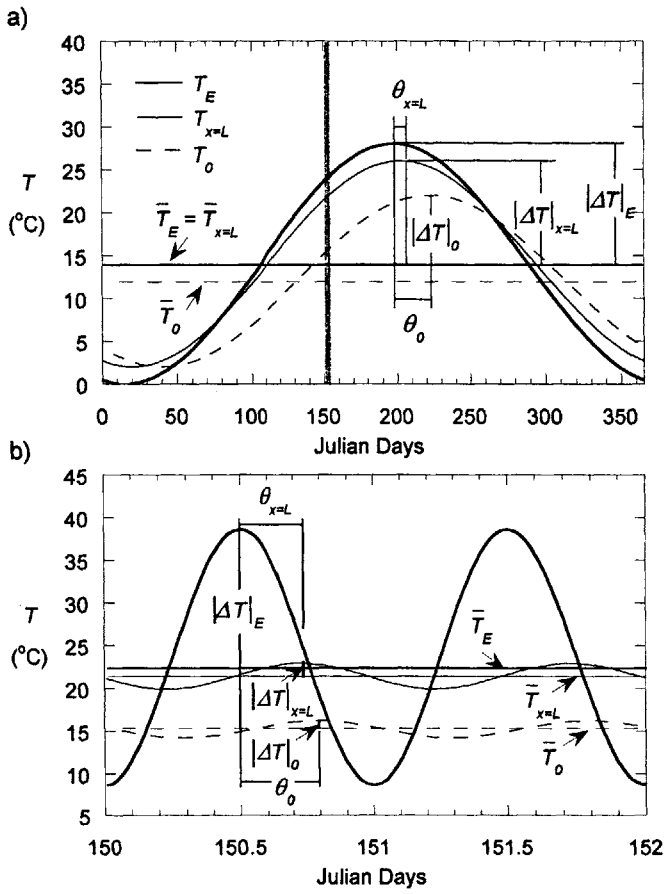

Figure 2-4: Thermal cycles at the inlet, T_0, and outlet, $T_{x=L}$, of a wetland, forced by changes in the equilibrium temperature, T_E. a) Seasonal cycle ($P = 1$ year), and b) diurnal cycle ($P = 1$ day) during early June ($jd = 150 - 152$) in North-America, when the inflow is on average colder than the outflow. Thermal mediation occurs both on seasonal and diurnal timescales.

assumed to be sinusoidal with period P, *i.e.*

$$T_E = \bar{T}_E + \Delta T_E e^{i2\pi t/P}, \tag{2.6}$$

$$T_0 = \bar{T}_0 + \Delta T_0 e^{i2\pi t/P}. \tag{2.7}$$

With this input, the linearized dead-zone model (equations 2.1-2.5) is solved for the water temperature in the wetland channel (c) and dead-zone (d) in the form

$$T_{c,d} = \bar{T}_{c,d} + \Delta T_{c,d} e^{i2\pi t/P}. \tag{2.8}$$

Here, $\bar{T}_i$ represents the steady and ΔT_i the periodic component of these sinusoidal temperature cycles. The periodic component $\Delta T_i = |\Delta T|_i \ \mathrm{e}^{-i\,2\pi\theta_i/P}$ incorporates both the amplitude, $|\Delta T|_i$, and timelag, θ_i, between the water and equilibrium temperatures (*i.e.* $\theta_E = 0$). To get familiar with this notation, consider figure 2-4 which displays typical thermal cycles at the inlet, T_0, and outlet, $T_{x=L}$, of a wetland responding to seasonal and diurnal meteorological forcing (T_E). On seasonal timescales (figure 2-4*a*), the wetland thermally mediates the water temperature, such that $T_{x=L} \neq T_0$. Specifically, the timelag is reduced (*i.e.* $\theta_{x=L} < \theta_0$), and the amplitude of thermal oscillation is increased (*i.e.* $|\Delta T|_{x=L} > |\Delta T|_0$). On a day-to-day basis (figure 2-4*b*), this seasonal thermal mediation appears as a difference in the mean temperature between the inlet (15^oC) and the outlet (21^oC) water of the wetland. Notice that although the wetland also mediates the diurnal thermal response, *i.e.* $|\Delta T|_{x=L} > |\Delta T|_0$ and $\theta_{x=L} < \theta_0$ on figure 2-4*b*, this diurnal thermal mediation does not significantly add to the seasonal thermal mediation, which dominates during large portions of the year (*e.g.* *jd* 50-250 and 300-365 on figure 2-4*a*). Finally, figure 2-4*b* illustrates that the wetland water is unable to track the diurnal meteorological changes (*i.e.* $\Delta T_E >> |\Delta T|_{x=L}$ and $\theta_{x=L} \approx 6$ hrs $= P/4$), which leads to differential heating and cooling as will be discussed in more detail in section 2.3.2.. To summarize, figure 2-4 demonstrates that to fully understand the impact of wetlands, both diurnal and seasonal responses must be considered.

2.3.1 Steady Response

The steady state response of the wetland is found by solving the governing equations (2.1) and (2.2) with $\partial T_{c,d}/\partial t = 0$. Assuming u, D_x, K and α are constant in space and time, the solution for the flow zone temperature can be written as

$$\frac{\bar{T}_c - \bar{T}_0}{\bar{T}_E - \bar{T}_0} = 1 - 2 \cdot \frac{(1-a)\cdot\exp(\frac{1}{2E^*}(1+a)\frac{x}{L}) \quad - \quad (1+a)\cdot\exp(\frac{a}{E^*}+\frac{1}{2E^*}(1-a)\frac{x}{L})}{(1-a)^2 \quad - \quad (1+a)^2\cdot\exp(\frac{a}{E^*})}, \tag{2.9}$$

where $a = \sqrt{1+4E^*b_S}$ and

$$b_S = r\left(\frac{\alpha^*(1-w)}{\alpha^* \quad + \quad (1-w)r} \quad + \quad w\right). \tag{2.10}$$

Here b_S represents the effective thermal capacity of the wetland, the details of which are discussed later in this section. The solution for the dead-zone temperature is

$$\frac{\bar{T}_d}{\bar{T}_E} = \frac{\alpha^*\frac{\bar{T}_c}{\bar{T}_E} \quad + \quad (1-w)r}{\alpha^* \quad + \quad (1-w)r}. \tag{2.11}$$

The steady response of the wetland is thus governed by 4 non-dimensional parameters:

$r = \bar{t}/\bar{t}_{heat} = KWL/Q_r$	Nominal thermal capacity.
$E^* = D_x/uL$	Dispersion number (or inverse Peclet number).
$\alpha^* = \alpha\cdot\bar{t} = \Delta Q/Q_r$	Non-dimensional lateral exchange coefficient.
$w = W_c/W$	Width ratio.

The thermal capacity, r, reflects the heating/cooling potential of the system. It is defined as the ratio between the nominal residence time, $\bar{t} = (A_c + A_d)L/Q_r$, and nominal thermal inertia, $\bar{t}_{heat} = K/H$, where H is the average wetland depth. Notice that although both $\bar{t}$ and $\bar{t}_{heat}$ are functions of depth, the thermal capacity $r = \bar{t}/\bar{t}_{heat}$ is not. The three remaining parameters, E^*, α^* and w, define the hydraulic or circulation regime within the wetland, and control the shape of the residence time distribution RTD (see figure 2-2). The dispersion number, E^*, describes the relative importance of longitudinal dispersion and advection. The lateral exchange coefficient, α^*, represents the fractional water exchange between the flow and dead-zone (*i.e.* $\Delta Q/Q_r$) and describes the relative importance of lateral exchange and advection. The width ratio, w, describes the size of the flow zone relative to the total wetland and is related to the jet areal ratio, *i.e.* $w = q/(H_c/H)$. If the wetland has uniform water depth, *i.e.* $H = H_c = H_d$, then $w = q$.

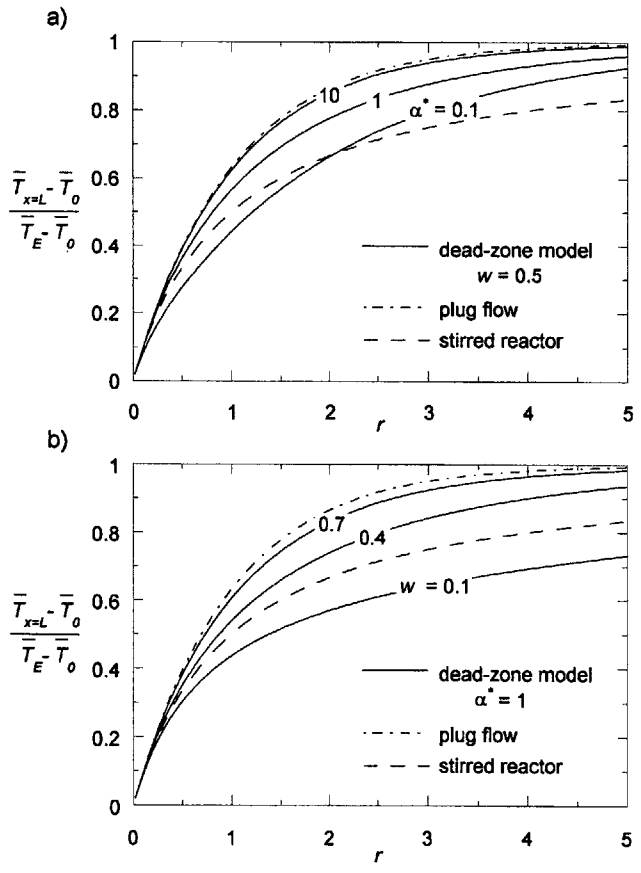

Figure 2-5: Steady dead-zone model results as a function of thermal capacity r for $E^* = 0$. a) Variable α^* with $w = 0.5$, and b) variable w with $\alpha^* = 1$. Increasing α^* and/or w improves the thermal efficiency, *i.e.* more thermal mediation $(\bar{T}_{x=L} - \bar{T}_0)/(\bar{T}_E - \bar{T}_0)$ is achieved at any given r.

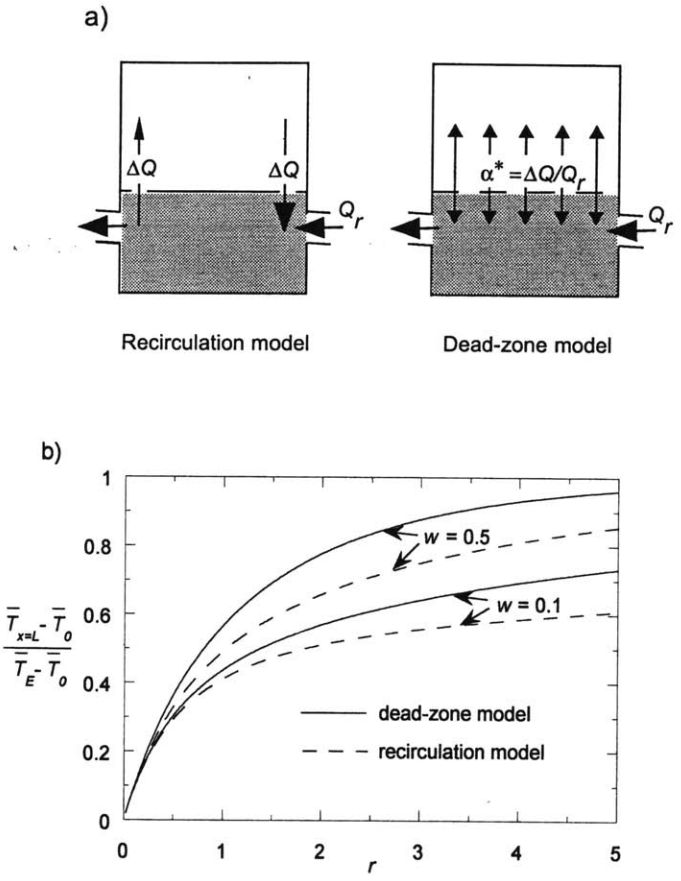

Figure 2-6: Comparison between short-circuiting predicted by the dead-zone model and the recirculation model [*Jirka and Watanabe*, 1980]. a) Schematic of both models. b) Steady thermal mediation with respect to w and r ($\Delta Q/Q_r = 1$ and $E^* = 0$). The recirculation model predicts consistently less thermal mediation than the dead-zone model.

The dependence of the steady solution (2.9) with respect to E^* is the same as the 1-D, longitudinal dispersion model. In general, increasing the longitudinal dispersion, E^*, reduces the degree of thermal mediation within the system. A more detailed description of this dependence is given by *e.g. Jirka and Watanabe* [1980] and will not be repeated here. Instead, for simplicity, we assume $E^* = 0$ and use this sub-case to explore the remaining governing parameters and their effect on wetland thermal mediation. This simplification does not strictly limit the model, as short-circuiting, shear flow dispersion and plug flow can all be represented with $E^* = 0$ (see Appendix A, section 2.6.), and the general trends described here apply for $E^* \neq 0$ as well.

The dependence of the steady solution (2.9) on the parameters, r, α^*, and, w is illustrated in figure 2-5 for $E^* = 0$. The degree of thermal mediation is given by the ratio $(\bar{T}_{x=L} - \bar{T}_0)/(\bar{T}_E - \bar{T}_0)$, which represents the actual change in temperature between the inlet and outlet of the wetland, $\bar{T}_{x=L} - \bar{T}_0$, relative to the maximum potential change, $\bar{T}_E - \bar{T}_0$, which would occur if thermal equilibrium with the atmosphere were reached. As shown on figure 2-5, the thermal capacity, r, controls the degree of thermal mediation provided by a wetland. For $r << 1$, the residence time limits the heat capture and no thermal mediation occurs, *i.e.* $\bar{T}_{x=L} = \bar{T}_0$. For $r >> 1$, however, the residence time is not limiting, and the outflow temperature reaches equilibrium with atmospheric conditions, *i.e.* $(\bar{T}_{x=L} - \bar{T}_0)/(\bar{T}_E - \bar{T}_0) = 1$. The rate with respect to r at which the thermal mediation curves approach equilibrium is described as the *thermal efficiency* and depends on the hydraulic parameters α^* and w. The most efficient flow regime is plug flow (dot-dashed line on figure 2-5), which is equivalent to $\alpha^* \to \infty$ given $E^* = 0$, and for which $b_S = r$. For other flow regimes, the *effective* thermal capacity of the wetland, b_S, is smaller than the *nominal* thermal capacity, r. In particular, (2.10) shows that

$$w \cdot r|_{\alpha^*=0} \quad \leq \quad b_S \quad \leq \quad r|_{\alpha^* \to \infty},$$

which indicates that a large dead-zone (small w) and a small exchange flow (small α^*) both reduce the effective thermal capacity of the wetland such that $b_S << r$. Such systems have low thermal efficiency, *i.e.* produce less thermal mediation at any value of r (figures 2-5*a* and 2-5*b*), because only a fraction of the nominal thermal capacity, r, is utilized to mediate the water temperatures. As either α^* or w increase, $b_S \to r$ because the dead-

zone contributes more actively to the thermal mediation. Such systems are more laterally homogeneous, *i.e.* $\bar{T}_c \rightarrow \bar{T}_d$, and have higher thermal efficiency, *i.e.* produce more thermal mediation at any value of r (figures 2-5a and 2-5b). As a result of this dependence on α^* and w, both short-circuiting flow ($\alpha^* \cdot w < H/H_c$) and stirred reactor type flow (dashed line on figure 2-5) are less efficient than shear-flow with dispersion ($\alpha^* \cdot w > H/H_c$). This is in agreement with previous analysis of steady cooling pond performance [*Jirka and Watanabe*, 1980].

Finally, the impact of short-circuiting based on a dead-zone model with a uniformly distributed lateral exchange, as presented here, differs from previous recirculation models of short-circuiting [*Jirka and Watanabe*, 1980], which assume that the exchange flow, ΔQ, enters the channel at a discrete location near the entrance of the wetland and recirculates back to the dead-zone near the outlet (see figure 2-6a). The steady state solutions from both models are compared on figure 2-6b. For a given exchange flow ratio $\Delta Q/Q_r$, and jet areal ratio w (or q), the recirculation model consistently predicts less thermal mediation than the dead-zone model. Actual wetlands will tend to fall between these two models, displaying a combination of lateral exchange and basin scale recirculation. In particular, sparsely vegetated wetlands with a large length-to-width ratio (figure 2-2b) are likely to contain some degree of recirculation [*Jirka et al.*, 1978; *Thackston et al.*, 1987]. This tendency to recirculate is reduced by uniform vegetation drag [*Wu and Tsanis*, 1994], which exerts a stabilizing effect on large scale eddies [*Babarutsi et al.*, 1989], and uneven vegetation which generates preferential flow paths. Consequently, the dead-zone model is expected to realistically capture short-circuiting in densely/unevenly vegetated wetlands, but may slightly overpredict thermal mediation in sparsely vegetated wetlands.

2.3.2 Periodic Response

The periodic response is considered relative to the equilibrium temperature, *i.e.*

$$\Gamma_j = \frac{\Delta T_j}{\Delta T_E} = |\Gamma|_j \, e^{-i\,2\pi\theta_j/P}, \qquad j = c, d, 0$$

where Γ_j incorporates the relative amplitude, $|\Gamma|_j$, and timelag, θ_j, between the water and equilibrium temperature. Both $|\Gamma|_j$ and θ_j reflect the degree to which equilibrium with the atmosphere is reached (see figure 2-4). The analytical solution of (2.1)-(2.5) for the wetland

flow zone is

$$\frac{\Gamma_c - \Gamma_0}{\Gamma^* - \Gamma_0} = 1 - 2 \cdot \frac{(1-a)\cdot \exp(\frac{1}{2E^*}(1+a)\frac{x}{L}) \quad - \quad (1+a)\cdot \exp(\frac{a}{E^*} + \frac{1}{2E^*}(1-a)\frac{x}{L})}{(1-a)^2 \quad - \quad (1+a)^2 \cdot \exp(\frac{a}{E^*})}, \quad (2.12)$$

where $a = \sqrt{1 + 4E^* b_P}$,

$$b_P = \frac{\alpha^* r \left((1-w) + i2\pi(1 - w\frac{H_c}{H})\frac{\bar{t}_{heat}}{P}\right)}{\alpha^* + r\left((1-w) + i2\pi(1-w\frac{H_c}{H})\frac{\bar{t}_{heat}}{P}\right)} + wr\left(1 + i2\pi\frac{H_c}{H}\frac{\bar{t}_{heat}}{P}\right) \quad (2.13)$$

$$= r\left(1 + i2\pi\frac{\bar{t}_{heat}}{P}\right)\cdot\left(w + \frac{\alpha^*(1-w)}{\alpha^* + r(1-w)\left(1 + i2\pi\frac{\bar{t}_{heat}}{P}\right)}\right) for \frac{H_c}{H} = 1, \quad (2.14)$$

and

$$\Gamma^* = \frac{\alpha^* \quad + \quad wr\left((1-w) + i2\pi(1-w\frac{H_c}{H})\frac{\bar{t}_{heat}}{P}\right)}{\alpha^*\left(1 + i2\pi\frac{\bar{t}_{heat}}{P}\right) \quad + \quad wr\left(1 + i2\pi\frac{H_c}{H}\frac{\bar{t}_{heat}}{P}\right)\cdot\left((1-w) + i2\pi(1-w\frac{H_c}{H})\frac{\bar{t}_{heat}}{P}\right)} \quad (2.15)$$

$$= \frac{1}{1 + i2\pi\frac{\bar{t}_{heat}}{P}} for \frac{H_c}{H} = 1. \quad (2.16)$$

Here Γ^* represents the asymptotic state under periodic forcing, *i.e.* $\Gamma_c \to \Gamma^*$ as $r >> 1$. The periodic solution for the dead-zone is

$$\Gamma_d = \frac{\alpha^*\Gamma_c \quad + \quad (1-w)r}{\alpha^* \quad + \quad r\left((1-w) + i2\pi(1-w\frac{H_c}{H})\frac{\bar{t}_{heat}}{P}\right)}. \quad (2.17)$$

The periodic solution has the same form as the steady solution, as seen by comparing (2.12) to (2.9). As with the steady response, thermal mediation generally increases as r, α^* and w increase. The important difference between the periodic and steady solutions arises from the additional dependence on the timescale ratio $\left[\frac{H_c}{H}\bar{t}_{heat}\right]/P$ appearing in (2.13), (2.15) and (2.17), which compares the thermal inertia of the channel,

$$t_{heat,ch} = \frac{H_c}{H}\bar{t}_{heat} = \frac{H_c}{K},$$

to the period of the forcing, P. This timescale ratio controls the degree to which the periodic heat capture of a wetland is limited by the thermal inertia of the flow zone, $t_{heat,ch}$. This dependence is illustrated on figure 2-7, which displays the periodic thermal mediation with respect to r for different values of $t_{heat,ch}/P$. For simplicity, the solution assumes a constant

inflow temperature, $\Gamma_0 = 0$, and $E^* = 0$. Figure 2-7 shows that as r increases, the wetland response loses its dependency on r and approaches the state of a stationary water body [*Adams*, 1982], *i.e.*

$$|\Gamma|_{x=L} \overset{r>>1}{\longrightarrow} \frac{1}{\sqrt{(2\pi \cdot t_{heat,ch}/P)^2 + 1}} \tag{2.18}$$

and

$$\theta_{x=L} \overset{r>>1}{\longrightarrow} \frac{\tan^{-1}(2\pi \cdot t_{heat,ch}/P)}{2\pi/P}. \tag{2.19}$$

Consequently, the periodic thermal mediation for $r >> 1$ is solely determined by $t_{heat,ch}/P$. When $t_{heat,ch}/P$ is large, the wetland is unable to track the atmospheric forcing, because the forcing varies more rapidly than the wetland can respond. This results in decreasing values of $|\Gamma|_{x=L}$ and $\theta_{x=L}/t_{heat,ch}$ as seen on figure 2-7. Furthermore, for large $t_{heat,ch}/P$, the timescale ratio $wr\frac{H_c}{H}\bar{t}_{heat}/P = [wrt_{heat,ch}]/P$ that appears in (2.13) also becomes large. As a result, the residence time in the channel, $wrt_{heat,ch}$, limits the fraction of the heating cycle the wetland captures, producing oscillations in $|\Gamma|_{x=L}$ and $\theta_{x=L}$ relative to r (see figure 2-7, $t_{heat,ch}/P = 1, 5$). Finally for small $t_{heat,ch}/P$, the thermal inertia is not limiting and the wetland is at quasi-steady state with the forcing. Consequently, if r is large enough, the wetland tracks the atmospheric fluctuations, *i.e.* $|\Gamma|_{x=L} \to 1$, but with a lag, *i.e.* $\theta_{x=L} \to t_{heat,ch}$.

The dependence of the periodic thermal response on $t_{heat,ch}/P$ has two important implications. First, in a given water system the seasonal response ($P = 365$ days) will significantly differ from both the synoptic ($P = 7 - 14$ days) and diurnal ($P = 1$ day) responses. For example, the seasonal response can be at equilibrium with atmospheric conditions (*e.g.* $|\Gamma|_{x=L} \approx 1$ for $r >> 1$), while the synoptic response is partially dampened (*e.g.* $0.25 < |\Gamma|_{x=L} < 0.85$ for $r > 1$), and the diurnal response severely dampened (*e.g.* $|\Gamma|_{x=L} < 0.25$). The system portrayed on figure 2-4 demonstrates this difference in seasonal and diurnal response. The second implication is that for a given P, the thermal response of shallow (small $t_{heat,ch}$) and deep (large $t_{heat,ch}$) systems can vary significantly, potentially producing intrusion depth variability and exchange flows. This process is generally referred to as differential heating and cooling (see section 2.1.). For example, consider a 1 m deep wetland ($t_{heat,ch} = 2$ days) and a 10 m deep lake ($t_{heat,ch} = 20$ days) with negligible inflow (*i.e.* $r >> 1$). On synoptic timescales ($P = 10$ days) the amplitude response of the wetland, $|\Gamma_W| \approx 0.6$, is much larger than that of the lake, $|\Gamma_L| \approx 0.1$ (see figure 2-7*a*). However, the

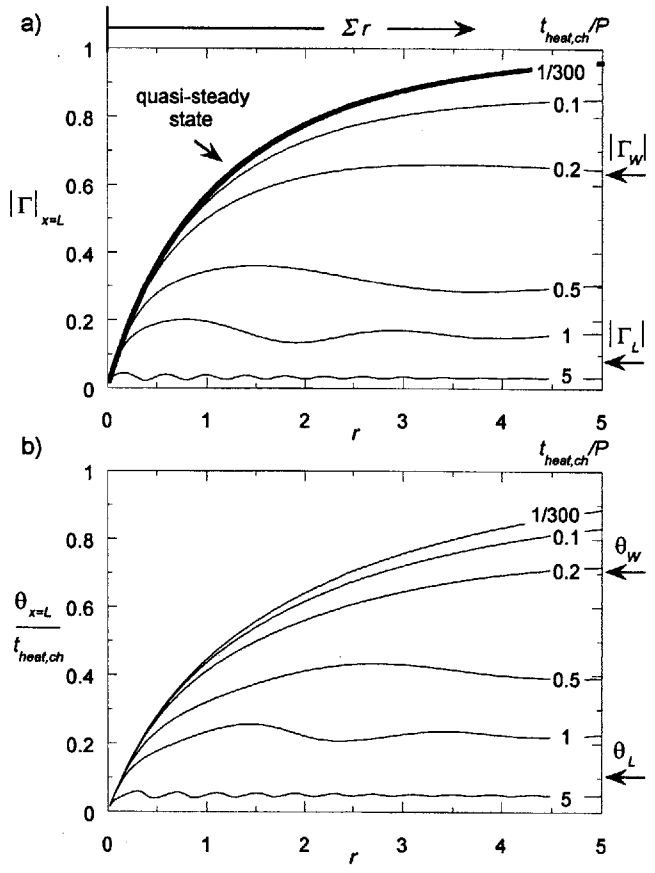

Figure 2-7: Periodic dead-zone model results as a function of r and $t_{heat,ch}/P$ with $E^* = 0$, $\alpha^* = 1$, $w = 0.5$, $H_c/H = 1$ and $\Gamma_0 = 0$. a) Non-dimensionalized amplitude $|\Gamma|_{x=L}$, and b) timelag $\theta_{x=L}/t_{heat,ch}$, between the outlet and equilibrium temperature. The periodic thermal response becomes more damped as $t_{heat,ch}/P$ increases.

timelag between the water and equilibrium temperatures is on the same order of magnitude in both systems, *i.e.* $\theta_W = 0.7 \cdot t_{heat,ch} = 1.4$ day and $\theta_L = 0.1 \cdot t_{heat,ch} = 2$ days (see figure 2-7*b*). Similar trends occur on diurnal timescales ($P = 1$ day), *i.e.* $|\Gamma_W| \approx 0.1$, $|\Gamma_L| \approx 0.01$, and a timelag of 6 hrs. Consequently, the water in the wetland warms more over the day and synoptic heating periods, and cools more at night and during synoptic cooling. This differential heating/cooling will affect the intrusion depth variability, as discussed later in section 2.4.2., and may also produce exchange flows, as described by *Monismith et al.* [1990] and *Farrow and Patterson* [1993]. While the dead-zone model can predict when these exchange flows occur, it does not account for their effect on wetland thermal mediation. Finally, on seasonal timescales ($P = 365$ days), both the wetland and lake are at quasi-steady state with the forcing, *i.e.* $|\Gamma_W| \approx |\Gamma_L| \approx 1$. However, the lake lags the wetland due to its larger thermal inertia, producing another form of differential heating/cooling.

2.4 Wetland Impact on Lake Inflow

To understand the impact of littoral wetlands on lake water quality, the wetland response must be considered in the context of the thermal processes in the watershed. This watershed scale analysis involves tracing the thermal evolution of the water starting at its source, along the river reach, through the wetland and into the lake (see figure 2-1). In section 2.4.2. this analysis is used to determine when a wetland can significantly impact lake intrusion dynamics.

2.4.1 Watershed Scale Analysis

The watershed scale analysis consists of four steps. First, the thermal properties of the water source must be defined. During non-storm conditions, the water in the river usually originates from groundwater recharge. Because of the thermal inertia of the ground, the seasonal temperature variations of groundwater are severely damped, $|\Gamma_G| \approx 0.2 - 0.4$, and can lag the equilibrium temperature by 2-4 months [*e.g.* based upon *Gu et al.*, 1996]. Shorter timescale variations (*e.g.* diurnal and synoptic) are even more dampened such that $|\Gamma_G| \approx 0$. During storms, however, river water originates predominantly from surface runoff, which typically is close to equilibrium with both seasonal and synoptic atmospheric cycles.

Second, the equilibrium temperature T_E must be defined. The equilibrium temperature

is a function of both incoming solar radiation and wind. During the summer when leaf cover is peaking, narrow rivers and wetlands experience sun-shading and wind sheltering that can give them a different equilibrium temperature than open water (*e.g.* lakes). While the two processes have a counteracting effect, *i.e.* sun-shading reduces T_E but wind sheltering increases T_E, the sun-shading effect is generally more pronounced [*Sinokrot and Stefan*, 1993], yielding lower equilibrium temperature for narrow systems than for open water.

Third, the model parameters, $\bar{t}$, $\bar{t}_{heat}$, E^*, α^* and q must be determined for each sub-section of the watershed. These parameters are site-specific, and depend upon the system's size and shape, the amount and type of vegetation, and the meteorological conditions. The hydraulic parameters E^*, α^* and q are generally evaluated by conducting dye experiments [*Kadlec*, 1994; *Bencala and Walters*, 1983], whereas the nominal parameters $\bar{t} = WHL/Q_r$ and $\bar{t}_{heat} = H/K$ can be estimated from maps and flow-measurements. For a river system which is fed by groundwater/surface runoff throughout its entire reach, the river network residence time can be estimated from the river catchment area, A_W, and the river discharge at the wetland/lake, Q_r. Assuming that the average travel length in the river scales on $\sqrt{A_W}$, and the spatially averaged flow along the reach is $Q_r/2$, then $\bar{t} \approx 2WK\sqrt{A_W}/Q_r$. A representative range for these input parameters under non-storm conditions is given in table 2.1 for each watershed sub-section. The parameter values indicate that wetlands are transition zones between the upland and deep aquatic systems, with a small thermal inertia, $t_{heat,ch}$, like rivers, but a large thermal capacity, r, like lakes.

	$\bar{t}$	H (m)	E^*	α^*	q	t_{heat} (days)	r
R	hrs - month [1]	0.1-10 [1]	0.005-0.08 [2,3]	0.1-0.8 [2]	0.25-0.95 [2,4]	0.1-20	1-5
W	days - month [5,6]	0.1-2 [6,7]	-	0-4 [5]	0.5-0.7 [5]	0.1-2	2-20
L	week-years [8]	2-100 [9]	-	-	-	2-100	2-20

Table 2.1: Typical ranges of dead-zone model parameters for rivers (R), wetlands (W) and surface layers of lakes (L) under non-storm conditions. Adapted from 1) Leopold et al. [1992, p. 142, 240-2], 2) Bencala and Walters [1983], 3) Day [1975], 4) Yu and Wenzhi [1989], 5) Kadlec [1994], 6) Wood [1995], 7) Mitsch and Gosselink [1993, p. 620], 8) Fisher et al. [1979, p. 148], 9) Hutchinson [1957, p. 460].

Finally, with the appropriate choice of input parameters, the dead-zone model solutions (2.12)-(2.16) can be applied sequentially to each watershed sub-section. As shown on figure 2-8, the outflow temperature from the previous sub-section becomes the inflow temperature for the next sub-section, that allows tracing the thermal evolution of the surface water from

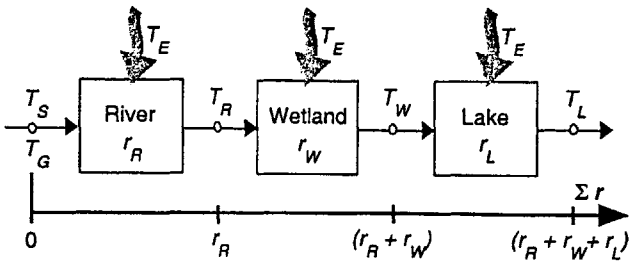

Figure 2-8: Schematic of the watershed scale analysis. The dead-zone model is applied to each sub-section of a watershed, using the outflow temperature of the previous sub-section as the inflow temperature for the next sub-section.

its source, T_G or T_S, to the end of the river reach, T_R, to the wetland outflow, T_W, and into the lake epilimnion, T_L. For simplicity, the vertical heat transfer between the epilimnion and hypolimnion of a lake is neglected. Since this heat transfer is a slow process occurring over months, this assumption introduces errors only at the seasonal timescale, but not on the shorter timescales.

2.4.2 Wetland Impact Scenarios

The thermal evolution presented in figure 2-8 depends upon three factors: First, the equilibrium temperature, T_E, and second the thermal inertia of the water, $t_{heat,ch}$, which together determine the asymptotic thermal state of surface water. This state may differ across the watershed due to sun-shading and wind-sheltering and variable water depth. Third, the cumulative thermal capacity, Σr, which represents the total time that the surface water has been exposed to atmospheric heating relative to the thermal inertia. As Σr increases, the surface water approaches its asymptotic state. In the following, we consider the impact of a wetland on lake intrusion dynamics first during low-flow conditions, when the river is predominantly groundwater fed. Then we consider a storm scenario, when the river is predominantly fed by surface runoff. For simplicity, the effects of suspended sediments and salinity on lake intrusion dynamics are neglected.

Non-Storm Scenario 1

First consider a system where the thermal capacity of the river alone is not large enough for it to reach its asymptotic state, *i.e.* $r_R \approx 2WK\sqrt{A_W}/Q_r < 3$ (figure 2-7), or where sun-shading and wind-sheltering are prominent. This generally applies to small watersheds (small A_W) with a high annual discharge (large Q_r), or narrow rivers obstructed by trees or hills. In both cases, the water temperature at the end of the river reach, T_R, will differ from that in the wetland, T_W, and lake, T_L. Figure 2-9 illustrates simulated thermal cycles in one such system with $r_R = 1$ and $r_W = r_L = 2$. For simplicity, the equilibrium temperature of the river, wetland and lake are assumed to be the same. First consider the system without a littoral wetland. On seasonal timescales ($P = 365$ days), figure 2-9a shows that the river water retains the attenuated amplitude and lag ($|\Delta T_R| \approx 9.5^oC$ and $\theta_R = 11$ days) originating from the damped groundwater source (see sectoin 2.4.1.). In contrast, the lake epilimnion with its long cumulative thermal capacity $\Sigma r > 3$, is almost at equilibrium with the seasonal cycle ($|\Delta T_L| \approx |\Delta T_E| = 15^oC$ and $\theta_L = 9$ days). Consequently, the river water is colder than the surface waters of the lake during the summer ($T_R < T_L$ for $jd = 100 - 280$) and warmer in winter ($T_R > T_L$ for $jd = 0 - 100$ and $280 - 365$). On diurnal and synoptic timescales ($P = 1, 10$ days), figure 2-9b shows that the thermal response of the shallower river ($t_{heat,ch} = 1$ day) is more pronounced than that of the lake ($t_{heat,ch} = 10$ days). However, this differential heating and cooling does not produce variability in intrusion depth during the summer period shown because of the large seasonal difference between the river and lake, *i.e.* $T_R < T_L$ in spite of the diurnal and synoptic river temperature fluctuations. Thus in the absence of a littoral wetland, the lake intrusion depth varies predominantly on seasonal timescales, the inflow plunging into the hypolimnion during summer and inserting at the surface during winter.

Next consider the impact of adding a littoral wetland to this system. The wetland provides extra thermal capacity allowing the water to reach its asymptotic state. The amplitude of the seasonal temperature cycle of the lake inflow increases from $|\Delta T_R| \approx 9.5^oC$ to $|\Delta T_W| \approx 15^oC$, as the cumulative thermal capacity increases from $\Sigma r = r_R = 1$ to $\Sigma r = (r_R + r_W) = 3$. Consequently the wetland outflow, T_W, tracks the seasonal temperature cycle in the lake, T_L, more closely than the river does, reducing the seasonal variability in intrusion depth (figure 2-9a). On diurnal and synoptic timescales (figure 2-9b), the wetland

heats and cools more rapidly, and thus has larger temperature oscillations than the lake, *i.e.* $|\Delta T_W| >> |\Delta T_L|$. With the seasonal temperature difference reduced, this process now produces diurnal and synoptic variability in the lake intrusion depth, that is $T_W > T_L$ over the day and $T_W < T_L$ at night during periods of synoptic heating ($jd = 202 - 207$ and $212 - 217$).

To summarize, the introduction of a littoral wetland to a watershed where the thermal capacity of the river is small or sun-shading/wind-sheltering are prominent, can drastically change the lake inflow dynamics. Specifically, the variability in intrusion depth is shifted from being predominantly seasonal (no wetland), to occurring predominantly on diurnal and synoptic timescales. Consequently, during the summer more inflow will be directed towards the lake surface, potentially degrading the lake water quality. This is the scenario that undermined the wetland project at Lake McCarrons, discussed in section 2.1. [*Oberts*, 1998; *Metropolitan Council*, 1997].

Non-Storm Scenario 2

Next consider a system where the river has a sufficiently long residence time to reach its asymptotic state, *i.e.* $r_R \approx 2WK\sqrt{A_W}/Q_r \geq 3$ (see figure 2-7), and sun-shading and wind-sheltering are less prominent. These conditions are satisfied in large watersheds (large A_W) with a low annual discharge (small Q_r), and a wide river unobstructed by emergent vegetation, borderline trees or hills. Unlike the previous scenario, a littoral wetland in such systems can produce little or no additional thermal mediation. Figure 2-10 illustrates the thermal cycles in one such system with $r_R = 3$. As shown on figure 2-10*a*, the seasonal thermal cycles in the river, wetland and lake are all at equilibrium with the atmosphere ($|\Delta T_i| \approx |\Delta T_E| = 15^oC$, $i = R, W, L$). However since $\theta \rightarrow t_{heat,ch}$ in the limit $r >> 1$ and $t_{heat,ch} << 1$ (see eq. 2.19), the lake ($t_{heat,ch} = 20$ days) lags the shallower river and wetland ($t_{heat,ch} = 1 - 2$ days) by 16-18 days. This produces a seasonal variation in intrusion depth, with the river and wetland inflow predominantly entering at the surface during $jd = 20 - 200$ when $T_R, T_W > T_L$, but otherwise plunging. On diurnal and synoptic timescales (figure 2-10*b*), the river and wetland heat and cool more rapidly than the lake, *i.e.* $|\Delta T_W|, |\Delta T_R| >> |\Delta T_L|$. For the river with $t_{heat,ch} = 2$ days, the combined diurnal and synoptic temperature fluctuations are not large enough to produce variability in intrusion depth during a large fraction of the year, *e.g.* $T_R < T_L$ throughout the time period on

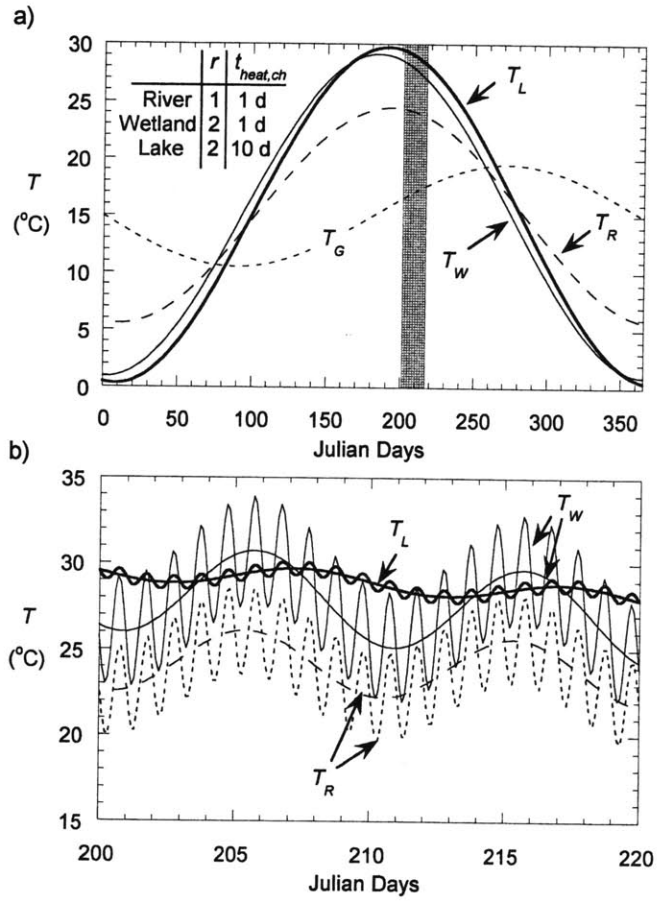

Figure 2-9: Non-storm wetland impact scenario 1: $r_R = 1$. Dead-zone model solutions for a river, T_R, wetland, T_W, and lake epilimnion, T_L, originating from groundwater with the seasonal cycle $\bar{T}_G = 15^oC$, $|T_G| = 5^oC$ and $\theta_G = 3$ months [*Gu et al.*, 1996]. a) Seasonal ($P = 365$ days), b) synoptic ($P = 10$ days) and diurnal ($P = 1$ day) responses. The addition of a littoral wetland can drastically change the lake intrusion dynamics, shifting the variation from predominantly seasonal to predominantly diurnal/synoptic.

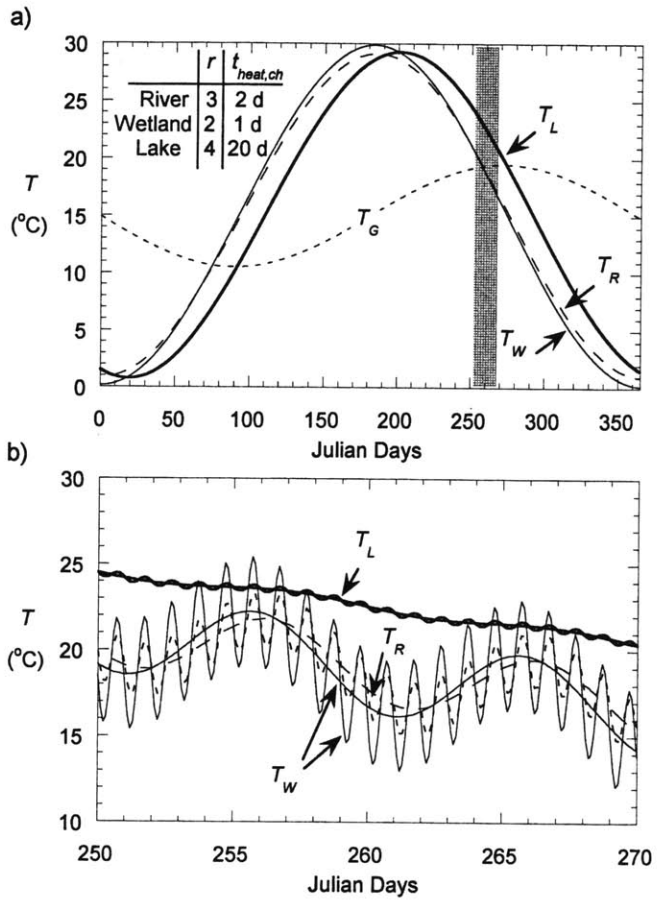

Figure 2-10: Non-storm wetland impact scenario 2: $r_R = 3$. Dead-zone model solutions for a river, T_R, wetland, T_W, and lake epilimnion, T_L, originating from groundwater with the seasonal cycle $\bar{T}_G = 15^oC$, $|T_G| = 5^oC$ and $\theta_G = 3$ months [*Gu et al.*, 1996]. a) Seasonal ($P = 365$ days), b) synoptic ($P = 10$ days) and diurnal ($P = 1$ day) responses. The addition of a littoral wetland does little to change the lake intrusion dynamics.

figure 2-10*b*. For the wetland with $t_{heat,ch} = 1$ day, the larger amplitude response (*i.e.* $|\Delta T_W| > |\Delta T_R|$) produces some variability in intrusion depth, *e.g.* on $jd = 254 - 257$ and $264 - 267$, during the 20 day period illustrated on figure 2-10*b*. Despite this difference, the intrusion depth dynamics of the river and the wetland are predominantly characterized by the seasonal variability, which is the same for both systems.

To summarize, a littoral wetland is less likely to alter the lake inflow dynamics in a watershed where the thermal capacity of the river system alone is sufficient to bring the water to its asymptotic state, and where sun-shading and wind-sheltering are less prominent. The lake intrusion depth in such systems can vary on seasonal, synoptic, and/or diurnal timescales depending upon the specific system configurations.

Episodic Events - Storms

Lake intrusion dynamics are of particular interest during storms, when nutrient and contaminant loads are peaking. Under these conditions the thermal evolution of surface water through the watershed differs significantly from the low-flow conditions described in the two previous sections. First, the source of river water switches from groundwater to surface runoff, which more closely reflects the current synoptic and seasonal atmospheric conditions. Second, the residence time in the river and the wetland drops significantly with the increased flowrates. This decreases their thermal capacity such that r_R and $r_W < 1$. Third, the wetland circulation becomes jet-dominated, and the associated short-circuiting further reduces its effective thermal capacity (see section 2.3.1.). As a result, little thermal mediation occurs in the river or the wetland, and the temperature of the water reaching the lake reflects the prevailing synoptic meteorological conditions. In contrast, the lake does not respond to these short-term meteorological fluctuations because of its larger thermal inertia (recall from figure 2-7, $|\Gamma|_{x=L} < 0.2$ for $t_{heat,ch}/P > 1$) but retains its balance with the seasonal conditions. Therefore, during storms, the intrusion depth is governed by the prevailing meteorological conditions, which dictate the temperature of the lake inflow, and whether the prevailing conditions are warmer or colder than the seasonal conditions, which dictate the lake temperature. This result is useful in predicting the impact of storm contaminant fluxes on lake water quality, since it provides a simple tool for assessing whether the inflow plunges (conditions are colder than seasonal average), or enters directly into the surface water (warmer than seasonal average).

2.5 Conclusions

Thermal mediation is a process through which shallow littoral regions such as wetlands, forebays or side-arms, can control the initial fate of river-borne nutrient and contaminant fluxes within a lake or reservoir. As a river traverses these systems, the water temperature is modified through atmospheric heat exchange. The change in temperature can affect the intrusion depth, and thus impact the lake water quality.

This paper provides a simple framework for evaluating the impact of these shallow littoral regions on the thermal characteristics of lake inflow. The dead-zone model, previously used for river routing and dispersion problems, is adapted to wetlands to predict thermal mediation under different meteorological conditions. The impact of the wetlands on lake inflow dynamics is then evaluated by integrating the wetland model into a watershed scale analysis of surface water temperature, tracing the thermal evolution of the water from its source (runoff and/or groundwater), along the river reach, through the wetland and finally within the lake. This watershed scale perspective is a new approach necessary to study the interaction between the river, wetland and lake. In addition, this approach for the first time describes the link between thermal mediation in shallow flow through systems and the previously studied process of differential heating and cooling.

Our analysis suggests that littoral wetlands can provide significant thermal mediation in watersheds, where the river water has not had enough time to equilibrate with the atmosphere, or sun-shading produces a different equilibrium temperature for the river than the lake. In such a system, a wetland prolongs the time for heating/cooling during non-storm conditions, reducing the seasonal temperature differences between the wetland outflow and lake. This makes the intrusion depth more sensitive to diurnal and synoptic meteorological fluctuations. Specifically in summer, the wetland can sufficiently raise the temperature of the lake inflow to produce a surface intrusion during the day, causing more river-borne nutrients and contaminants to enter directly into the epilimnion where they can potentially enhance eutrophication and human exposure to pathogens. This scenario was observed at Lake McCarrons, discussed in section 2.1. [*Oberts*, 1998; *Metropolitan Council*, 1997], and the Mystic Lake in Massachusetts [*Andradóttir and Nepf*, 2000]. A littoral wetland has less impact on lake intrusion dynamics in watersheds, where sun-shading and wind-sheltering are less prominent, and the water has already reached thermal equilibrium with

the atmosphere before reaching the wetland. Finally, nutrient and contaminant loads often peak during storms, making such events of particular interest to lake water quality. Our analysis suggest that during storms, wetland thermal mediation is less important, and the intrusion depth is governed by the difference between current and seasonal meteorological conditions.

2.6 Appendix A

The dead-zone model with $E^* = 0$ mimics a range of wetland circulation and thus does not limit the generality of the results presented in this paper. This can be seen by considering the product of the lateral exchange coefficient, α^*, and the jet areal ratio, q,

$$\alpha^* \cdot q = \frac{\Delta Q}{(A_c + A_d)L} \cdot \frac{A_c L}{Q_r} = \frac{q\bar{t}}{(A_c + A_d)L/\Delta Q} = \frac{t_{advection}}{t_{exchange}}.$$

For $\alpha^* \cdot q < 1$, very little lateral exchange occurs in the timescale of advection producing short-circuiting (figure 2-2*b*). However if $\alpha^* \cdot q > 1$, lateral exchange occurs at the same timescale as advection, and the balanced combination of differential advection (flow zone *vs.* dead-zone) and the lateral exchange creates longitudinal shear dispersion even if $E^* = 0$ [*e.g. Taylor*, 1954; *Chikwendu and Ojiakor*, 1985]. Finally, if $\alpha^* \cdot q >> 1$, lateral exchange is much faster than advection, and the dead zone is no longer distinct from the flow zone, effectively producing plug flow through the entire area $(A_c + A_d)$.

2.7 Acknowledgments

This work was funded by the National Institute of Environmental Health Sciences, Superfund Basic Research Program, Grant No. P42-ES04675. The authors would like to thank Dr. Eric Adams for his valuable feedback throughout the development of this work; and Dr. Chin Wu for his technical suggestions.

Bibliography

[1] Adams, E. E., The transient response of cooling ponds, *Water Resour. Res., 18*(5), 1469-1478, 1982.

[2] Andradóttir, H. Ó., Circulation and mixing in the upper forebay of the Mystic Lake system, Winchester, Massachusetts, Master's thesis, Mass. Inst. of Technology, 1997.

[3] Andradóttir, H. Ó., and H. M. Nepf, Thermal mediation in a natural littoral wetland: Measurements and modeling, *Water Resour. Res.,* 2000 (in prep.). Also chapter 3 in this thesis.

[4] Babarutsi, S., J. Ganoulis, and V. H. Chu, Experimental investigation of shallow recirculating flows, *J. Hydraul. Eng., 115*(7), 906-924, 1989.

[5] Bastian, R. K., and D. A. Hammer, The use of constructed wetlands for wastewater treatment and recycling, in *Constructed wetlands for water quality improvement*, Ed. G.A. Moshiri, Lewis Publishers, 1993.

[6] Bencala, K. E., and R. A. Walters, Simulation of solute transport in a mountain pool-and-riffle stream: A transient storage model, *Water Resour. Res., 19*(3), 718-724, 1983.

[7] Chikwendu S. C., and G. U. Ojiakor, Slow-zone model for longitudinal dispersion in two-dimensional shear flows, *J. Fluid Mech., 152*, 15-38, 1985.

[8] Day, T. J., Longitudinal dispersion in natural channels, *Water Resour. Res., 11*, 909-918, 1975.

[9] DePaoli, L. L., Numerical modelling of wetland hydrodynamics, Master's thesis, Mass. Inst. of Technology, 1999.

[10] Edinger, J. E., and J. C. Geyer, Heat exchange in the environment, *Publ. 65-902*, Edison Electr. Inst., New York, 1965.

[11] Farrow, D. E., and J. C. Patterson, On the response of a reservoir sidearm to diurnal heating and cooling, *J. Fluid Mech., 246*, 143-161, 1993.

[12] Fisher, H. B., E. J. List, R. C. Y. Koh, J. Imberger, and N. H. Brooks, *Mixing in inland and coastal waters*, Academic Press, Inc., London, 1979.

[13] Gu, R., F. N. Luck, and H. G. Stefan, Water quality stratification in shallow wastewater stabilization ponds, *Water Resour. Bull., 32*(4), 831-844, 1996.

[14] Harleman, D. R. F., Hydrothermal analysis of lakes and reservoirs, *J. Hydraul. Div. ASCE, 108*(HY3), 302-325, 1982.

[15] Hutchinson, G. E., *A treatise on limnology*, John Wiley & Sons, New York, 1957.

[16] Jirka, G. H., M. Watanabe, K. H. Octavio, C. F. Cerco, and D. R. F. Harleman, Mathematical predictive models for cooling ponds and lakes, Part A: Model development and design considerations, *Tech. Rep. 238*, Ralph M. Parsons Lab. for Water Resour. and Hydrodyn., Mass. Inst. of Technology, 1978.

[17] Jirka, G. H., and M. Watanabe, Steady-state estimation of cooling pond performance, *J. Hydraul. Div. ASCE, 106*(HY6), 1116-1123, 1980.

[18] Johnston, C. A., G. D. Bubenzer, G. B. Lee, F. W. Madison, and J. R. Mc Henry, Nutrient trapping by sediment deposition in a seasonally flooded lakeside wetland, *J. Environ. Qual., 13*(2), 283-290, 1984.

[19] Kadlec, R. H., Detention and mixing in free water wetlands, *Ecological Engineering, 3*, 345-380, 1994.

[20] Leopold, L. B., M. G. Wolman, and J. P. Miller, *Fluvial processes in geomorphology*, Dover publications, Inc., New York, 1992.

[21] Metropolitan Council, Lake McCarrons wetland treatment system-phase III study report, *publ. No. 32-97-026*, Metropolitan Council, City of Roseville, Minnesota, 1997.

[22] Mitsch, W. J., and J. G. Gosselink, *Wetlands*, Van Nostrand Reinhold, New York, 1993.

[23] Monismith, S. G., J. Imberger, and M. L. Morison, Convective motions in the sidearm of a small reservoir, *Limnol. Oceanogr., 35*(8), 1676-1702, 1990.

[24] Oberts, G. L., Long-term reductions in removal effectiveness: Lake McCarrons wetland treatment system, presentation at ASCE Wetlands Engineering and River Restoration Conference, Denver, Colorado, 1998.

[25] Reed, S. C., and D. S. Brown, Constructed wetland design-the first generation, *Water Environ. Res., 64*(6), 776-781, 1992.

[26] Ryan, P. J., D. R. F. Harleman, and K. D. Stolzenbach, Surface heat loss from cooling ponds, *Water Resour. Res., 10*(5), 930-938, 1974.

[27] Sinokrot, B. A., and H. G. Stefan, Stream temperature dynamics: Measurements and modeling, *Water Resour. Res., 29*(7), 2299-2312, 1993.

[28] Taylor, G. I., Dispersion of soluble matter in solvent flowing slowly through a tube, *Proc. of the Royal Soc. of London, 223*(A), 446-468, 1954.

[29] Tchobanoglous, G., Constructed wetlands and aquatic plant systems: Research, design, operational and monitoring issues, in *Constructed wetlands for water quality improvement*, Ed. G.A. Moshiri, Lewis Publishers, 1993.

[30] Thackston, E. L., F. D. Jr. Shields, and P. R. Schroeder, Residence time distributions of shallow basins, *J. Environ. Eng., 113*(6), 1319-1332, 1987.

[31] Valentine, E. M, and I. R.Wood, Longitudinal dispersion with dead zones, *J. Hydraul. Div. ASCE, 103*(HY9), 975-990, 1977.

[32] Wu, J., and I. K. Tsanis, Pollutant transport and residence time in a distorted scale model and numerical model, *J. Hydraul. Res., 32*(4), 583-598, 1994.

[33] Wood, A., Constructed wetlands in water pollution control: Fundamentals to their understanding, *Wat. Sci. Tech., 32*(3), 21-29,1995.

[34] Yotsukura, N., A. P. Jackman, and C. R. Faust. Approximation of heat exchange at the air-water interface, *Water Resour. Res., 9*(1):118-128, 1973.

[35] Yu, Y. S., and L. Wenzhi, Longitudinal dispersion in rivers: A dead-zone model solution, *Wat. Resour. Bull., 25*(2), 319-325, 1989.

Chapter 3

Thermal Mediation: Measurements and Modeling[1]

As a river flows through shallow littoral regions such as wetlands, forebays and side-arms, the temperature of the water is modified through atmospheric heat exchange. This process, which we call thermal mediation, can control the initial fate of river-borne nutrient and contaminant fluxes within a lake or reservoir. This paper presents temperature observations that demonstrate the occurrence of thermal mediation and directly support the theoretical results derived by *Andradóttir and Nepf* [2000]. The measurements show that the wetland warms the river inflow by approximately 1-3^{o}C during summer and fall non-storm conditions. Less thermal mediation occurs during storms, both because the residence time is significantly reduced and because the wetland circulation shifts from laterally-well-mixed (low flows) to short-circuiting (storms). The dead-zone model can simulate both these regimes and the transition between the regimes, and is therefore a good choice for wetland modeling.

[1]**Submitted under the name "Thermal mediation in a natural littoral wetland: Measurements and modeling" to Water Resources Research in October 1999.**

3.1 Introduction

Wetlands can play an important role in improving downstream water quality. Numerous mass balance studies have shown that suspended sediments, nutrients, metals and anthropogenic chemicals are efficiently removed in natural and constructed wetlands through a variety of sink mechanisms, such as bacterial conversion, sorption, sedimentation, natural decay, volatilization, and chemical reactions [*Tchobanoglous*, 1993]. Yet other studies have shown that wetlands may also act as a temporal source of nutrients and pollutants as they release stored materials [*Mitsch and Gosselink*, 1993, p. 157]. To date, extensive research has been conducted to understand the chemical, biological and physical processes underlying the removal performance of these complex ecosystems.

One process that so far has received little attention is thermal mediation, *i.e.* the temperature modification of the water flowing through the wetland. For littoral wetlands, the outflow temperature determines the lake intrusion depth which in turn affects the initial fate of nutrients/contaminants in the lake, as well as the residence time and mixing dynamics within the lake. Using a dead-zone model, *Andradóttir and Nepf* [2000] showed that wetland thermal mediation can shift the timescales of lake intrusion depth variability, from being predominantly seasonal to occurring on synoptic and diurnal timescales. Moreover, wetlands can prolong surface intrusions during summer, which can lead to increased human exposure to river-born contaminants. Similarly, the increased nutrient supply to the epilimnion during the growing season can accelerate lake eutrophication [*Carmack et al.*, 1986; *Metropolitan Council*, 1997]. On the other hand, more surface intrusions lead to quicker flushing, thus reducing the long-term deposits of nutrients and contaminants in the lake. Wetland thermal mediation can therefore have complex short- and long-term effects on lake water quality.

This chapter presents the first detailed observations of thermal mediation in a natural wetland that receives unregulated river inflow. The major contributions of the paper are to: 1) Demonstrate through field observation that wetland thermal mediation occurs in a small watershed, and how it is affected by flow conditions. 2) Compare wetland thermal structure and circulation during low-flows and storms. 3) Validate the use of the dead-zone model in wetlands, both by confirming the analytical dead-zone model results derived by *Andradóttir and Nepf* [2000], and by showing that the model simulates well wetland thermal behavior during variable flow conditions. 4) Demonstrate the effect of wetland thermal mediation on

lake intrusion dynamics. This paper is the observational counterpart to the theory presented by *Andradóttir and Nepf* [2000].

3.2 Theoretical Background

Thermal mediation is a well-known process in cooling ponds, in which atmospheric heat exchange is exploited to attenuate the waste heat from power plants. *Andradóttir and Nepf* [2000] showed that thermal mediation is also an important process in littoral wetlands, when the river inflow follows a different seasonal temperature cycle than the wetland water. This condition is met in small or forested watersheds, where the river follows a damped seasonal cycle because of groundwater recharge [*Gu et al.*, 1996] and/or sun-shading [*Sinokrot and Stefan*, 1993]. While the inflow condition sets the potential for wetland thermal mediation, the degree of thermal mediation actually occurring is governed by the residence time distribution (RTD) within the wetland and the thermal inertia of the water, t_{heat}. The thermal inertia represents the heating timescale of the water column and is defined as the ratio of the water depth, H, and the surface heat transfer coefficient, K, *i.e.* $t_{heat} = H/K$. Under "ideal" (plug) flow conditions, the thermal capacity

$$r = \frac{\bar{t}}{t_{heat}} \tag{3.1}$$

or the ratio between the nominal residence time and the thermal inertia, is the major factor controlling how much thermal mediation occurs: $r = 0$ produces no thermal mediation, whereas $r > 3$ produces over 90% of the maximum thermal mediation possible in the system [*e.g. Jirka and Watanabe*, 1980]. Wetland flow regimes, however, are rarely ideal [*Kadlec*, 1994], and water circulation, which governs both the skewness and variance of the RTD, will generally modify how efficiently the wetland mediates the water temperatures.

Wetland water circulation depends on vegetation drag and meteorological forces such as wind, river buoyancy and river inertia. The relative importance of vegetation drag, wind and water buoyancy to the river inertia can be summarized by the following three non-dimensional parameters:

$$\Lambda = \frac{C_f}{2}\frac{L}{H} \quad Vegetation\ drag\ parameter [DePaoli, 1999]. \tag{3.2}$$

$$\Omega = \frac{\bar{\tau}_w}{\rho U_0^2}\frac{L}{H} \quad Wind\ parameter. \tag{3.3}$$

$$Fi^{-2} = \frac{|\Delta\rho/\rho|gH}{U_0^2} \quad (Internal\ Froude\ number)^{-2}. \tag{3.4}$$

Here C_f is the friction factor, $\bar{\tau}_w$ the mean wind shear stress, $\Delta\rho$ the density anomaly between the inflow and wetland water, ρ the water density, g the acceleration of gravity, L the length of the wetland, and H the water depth. The river inertia is characterized by the inflow velocity, $U_0 = Q_r/A_r$, where Q_r is the flow rate and A_r the cross-sectional area of the river. Notice that since both Ω and $Fi^{-2} \propto U_0^{-2}$ then the influence of wind and buoyancy on water circulation changes with flow conditions. Similarly, Λ is indirectly related to U_0 through the friction factor C_f, which depends strongly on water depth and velocity, as well as vegetation type and density [*Petryk and Bosmajian III*, 1975; *Chen*, 1976; *Shih and Rahi*, 1982]. In particular, Λ can decrease drastically during storms, as a result of increased water depths and stem pronation. This is shown by the characteristic values of C_f given in table 3.1. Water circulation is therefore expected to change between low flows and storms [*DePaoli*, 1999; *Andradóttir*, 1997]: During low flows, vegetation drag, wind and buoyancy dominate the water circulation ($\Lambda, \Omega, Fi^{-2} >> 1$). Uniform vegetation drag will distribute the river flow over the width of the wetland [*Wu and Tsanis*, 1994], and wind will enhance lateral and vertical mixing. Consequently, the wetland often behaves as a partially-well-mixed reactor where the RTD has a large variance around the mean nominal residence time $\bar{t}$ (figure 3-1*a*) [*Kadlec*, 1994]. During high flows, however, the circulation often becomes inertia- or jet-dominated ($\Lambda, \Omega, Fi^{-2} < 1$), and substantial short-circuiting occurs, *i.e.* a large portion of the river flow exits the wetland in much less time than the nominal residence time $\bar{t}$ (figure 3-1*b*). Both these regimes, and especially the short-circuiting regime, produce less thermal mediation than the ideal plug flow [*Andradóttir and Nepf*, 2000].

Vegetation	Flow	$Re = \frac{UH}{\nu}$	C_f	Λ
yes	Low	$O(10^3)$	0.2-2 [1,2]	28-280
yes	High	$O(10^5)$	0.008-0.02 [2,3]	1.1-2.8
no	High	$O(10^5)$	0.004 [4]	0.55

Table 3.1: Vegetation drag estimates in the upper forebay adapted from 1) Kadlec and Knight (1996, p. 201); 2) Chen (1976); 3) Dunn et al (1996, p. 54); 4) Andradottir (1997, p. 69, 74). Bed drag decreases significantly during storms because of increased water depths and pronation of vegetation stem.

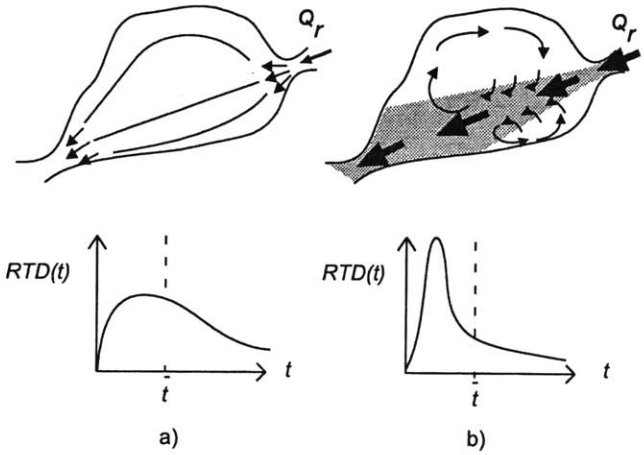

Figure 3-1: Bi-modal circulation in free surface wetlands. a) Under low flows, drag, wind and/or buoyancy dominate the circulation ($\Lambda, \Omega, Fi^{-2} >> 1$), the wetland is laterally well mixed producing a relatively symmetric RTD around the nominal residence time $\bar{t}$. b) During high flows, the circulation is river dominated ($\Lambda, \Omega, Fi^{-2} < 1$), short-circuiting occurs producing a skewed RTD with much of the flow exiting the wetland in much shorter time than $\bar{t}$.

3.3 Methods

3.3.1 Site Description

The Aberjona watershed is a medium-size watershed (65 km^2 surface area) located in suburban Boston, Massachusetts. Due to long term industrial activities, the watershed is heavily contaminated with heavy metals such as arsenic and lead which are routinely transported downstream by the Aberjona river until they are finally deposited in the Upper Mystic Lake [*Solo-Gabriele*, 1995; *Aurilio et al.*, 1994]. Before entering the lake, the river flows through two littoral wetlands, first the larger upper forebay, and then the smaller lower forebay (figure 3-2*a*). Both wetlands are vegetated with water lilies and submerged coontail, and their mean water depth ranges between 1.3 m to 2.0 m depending upon season. In comparison, the lake epilimnion is approximately 5 m deep and the thermocline 5 m wide during the summer.

In this paper, we focus predominantly on the thermal mediation occurring in the upper forebay shown on figure 3-2*b*. Due to its larger size, the residence time in this wetland is longer than in the lower forebay thus allowing more thermal alterations. Furthermore, only limited exchange flow occurs at the neck between the upper and lower forebay, justifying the

use of a uni-directional, depth-averaged model such as the dead-zone model. In contrast, the thermal dynamics of the lower forebay are largely determined by the exchange flow occurring through the wide inlet connecting the wetland to the lake (figure 3-2*a*). The enhanced flushing associated with this exchange flow reduces the residence time in the lower forebay such that little or no thermal mediation occurs. The outflow temperature of the upper forebay is thus representative of the temperature of the inflow to the lake.

3.3.2 Field Observations

Water temperatures were monitored every 5 min at different locations in the Upper Mystic Lake system from July to November in 1997 and 1998. Temperature measurements were made 10-20 cm below the surface and 10-20 cm above the bed at each site in the upper forebay shown on figure 3-2*b* using Onset temperature loggers with 0.2 ^{o}C resolution. In 1997, the temperature loggers at the outlet of the wetland were repeatedly stolen so the following year, the measurements were repeated with additional loggers deployed at the outlet and in the shallow vegetated zone. Lake water temperatures were measured in 1997 at 1-1.5 m depth intervals within the surface mixed layer and thermocline (1.8-10.9 m depth) at the locations shown on figure 3-2*a* using thermistor chains with 0.1 ^{o}C resolution [*Fricker and Nepf*, 1999]. Lake intrusion depth with and without the wetlands was estimated by matching the average of the near-surface and near-bed wetland channel temperature, and the river bed temperature, respectively, to the lake thermistor data. Surface intrusions within the top 2 m in the lake were not resolved because no thermistor was located there. Changes in suspended sediment levels did not significantly affect the water density and were neglected in the calculations.

Wind speed and direction were measured 10 m above ground at the southern end of the lake at 10 min intervals in 1997 and 1998 (figure 3-2*a*). Hourly Aberjona river flow was measured by USGS approximately 800 m upstream of the inlet to the upper forebay. In addition, air temperature, relative humidity and solar radiation were monitored every 5 min during 1997 (figure 3-2*a*). Cloud cover was measured at 3 hrs interval at the Boston Logan Airport located 15 km east of the study site.

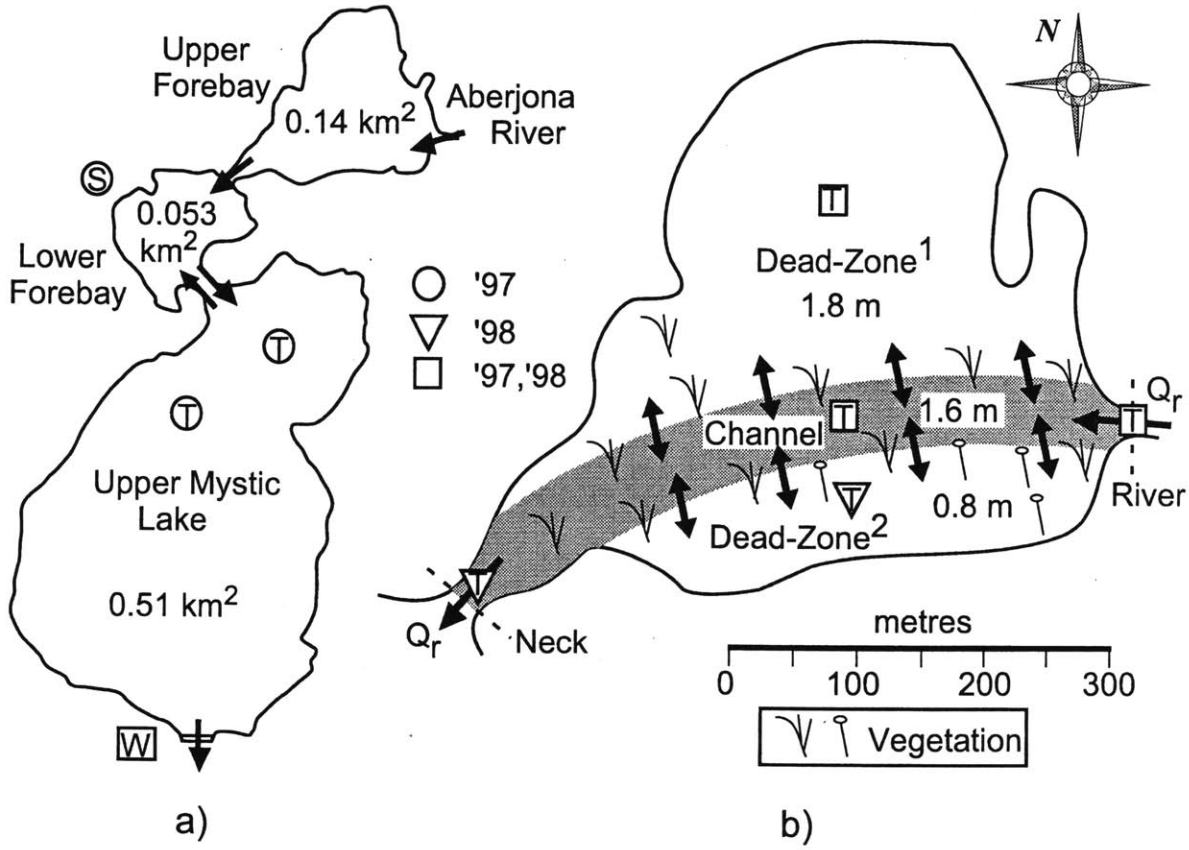

Figure 3-2: Monitoring program in the Upper Mystic Lake system, Winchester, Massachusetts. a) Site overview and surface areas. b) Detailed map of the upper forebay with mean water depths during the 1998 monitoring period. Thermistor locations are denoted by T, the anemometer by W and the weather station by S.

3.3.3 Dead-Zone Model Application

Model Formulation. The dead-zone model was described in detail by *Andradóttir and Nepf* [2000]. In short, the wetland area is divided into two zones, a flow zone (or channel) with cross-sectional area, A_c, and a stationary dead-zone with cross-sectional area, A_d. As shown on figure 3-2*b*, while the river traverses the wetland channel (dark shaded area), it exchanges continuously with two stationary dead-zones on either side of the channel. Notice that the southern dead-zone is smaller, shallower and more vegetated than the northern dead-zone. The circulation regime in the wetland is described by the areal ratio, $q = A_c/(A_c + A_d)$, and the non-dimensional lateral exchange coefficient, $\alpha^* = \Delta Q/Q_r$, where ΔQ is the total lateral exchange rate between the channel and dead-zones and Q_r the inflow flowrate. Neglecting longitudinal dispersion ($D_x = 0$), the simplified governing equations for the depth-averaged water temperature in the channel, $\bar{T}_c(x,t)$, and dead-zone, $\bar{T}_d(x,t)$, are

$$\frac{\partial \bar{T}_c}{\partial t} + u\frac{\partial \bar{T}_c}{\partial x} = \frac{\alpha^* u}{L}\left(\bar{T}_d - \bar{T}_c\right) + \frac{\phi}{\rho C_p H_c} \tag{3.5}$$

$$\frac{\partial \bar{T}_d}{\partial t} = -\frac{\alpha^* u}{L}\frac{q}{1-q}\left(\bar{T}_d - \bar{T}_c\right) + \frac{\phi}{\rho C_p H_d}. \tag{3.6}$$

The boundary conditions at the inlet ($x = 0$) and outlet ($x = L$) are

$$\bar{T}_c(0,t) = \bar{T}_0(t) \tag{3.7}$$

$$\left.\frac{\partial \bar{T}_c}{\partial x}\right|_{x=L} = 0. \tag{3.8}$$

Here $u = Q_r(t)/A_c$ is the average speed in the channel, L the length of the wetland, $\bar{T}_0$ the wetland inflow temperature, ϕ the net surface heat flux per surface area and C_p the specific heat of water.

The parameters q and α^* are site-dependent and are typically evaluated by conducting dye experiments [*e.g. Bencala and Walters*, 1983]. For preliminary design and assessment,

however, it is useful to derive independent expressions based upon the inflow and site geometry alone. First consider the river-dominated circulation regime, for which lateral exchange may be scaled on turbulent entrainment (figure 3-1*b*). The model parameters q and α^* can thus be determined from 2-D jet theory. Laboratory experiments suggest that the jet areal ratio is solely dependent on a constant spreading coefficient, $\beta \approx 0.1$, and the length-to-width ratio L/W [*Chu and Baines*, 1989], *i.e.*

$$q = \beta \frac{L}{W} \leq 1. \tag{3.9}$$

This is consistent with the observation that dead-zone effects (or short-circuiting) are principally correlated to the aspect ratio L/W, with longer, narrower wetlands having proportionally smaller dead-zones [*Thackston et al.*, 1987]. For the upper forebay, (3.9) yields $q \simeq 0.22$ which is in agreement with observations (see section 3.4.).

Similarly, an estimate for the lateral exchange coefficient can be found by adapting the results of *Chu and Baines* [1989] for 2-D jets confined by two boundaries to open channel flows with only one boundary, yielding

$$\alpha^* \approx \frac{\Delta Q}{Q_r} = \sqrt{3.02\beta L/B_o}\exp(-\Lambda/2) - 1 \quad for\ \Lambda < 0.96, \tag{3.10}$$

where Λ is the vegetation drag parameter (3.2) and B_o the initial jet width taken as the width of the inlet. (3.10) indicates that the lateral exchange coefficient is sensitive to vegetation drag, and that α^* decreases as Λ increases. Notice that this relationship is only appropriate for situations when the momentum of the jet has not been significantly eroded by bed drag, *i.e.* $\Lambda < 1$. For the storms occurring in the upper forebay, $\Lambda = 0.6 - 3$ (table 3.1) which suggests that a jet structure will not always be present. However, for the larger storms when the jet condition is satisfied, (3.10) yields $\alpha^* = 1 - 1.5$.

Finally, consider low flows when the wetland circulation is dominated by wind, buoyancy and drag. Under these conditions, the river jet is no longer distinct, and $q = 1$. For this value of q, the simplified dead-zone model can only predict the ideal plug flow regime. To incorporate longitudinal dispersion neglected in (3.5), q can be set by the jet-dominated condition (3.9), and α^* adjusted to produce an adequate mixing [*Andradóttir and Nepf*, 2000]. Thus a single model configuration (fixed q) can be used for both high and low flows,

with changes in water circulation represented by changes in α^*. We later show that thermal simulations in wetlands during low flows are not sensitive to the selection of α^*.

Numerical Simulations. The dead-zone model equations (3.5) to (3.8) were solved using a backwards difference numerical scheme, the measured inflow temperature, $\bar{T}_0(t)$, and flowrate, $Q_r(t)$. For simplicity, $Q_r(t)$ was assumed to adjust instantaneously across the wetland, and the mean water depth was taken to be constant in space and time, $H_c = H_d$. The model was run for both low flows and storms using $q = 0.22\frac{x}{L}$, where x/L accounts for the linear spreading of the river jet (figure 3-1*b*). The transition criteria between the two flow conditions was taken as

$$\alpha^* \simeq \begin{cases} 1 & Fi^{-2} < \mu_1 \text{ and } \Omega < \mu_2, \\ 10 & Fi^{-2} \geq \mu_1 \text{ or } \Omega \geq \mu_2, \end{cases}$$

where $\alpha^* \simeq 1$ corresponds to short-circuiting flow and $\alpha^* \simeq 10$ to laterally mixed flow [*Andradóttir and Nepf*, 2000]. The threshold value for the buoyancy forcing was taken as $\mu_1 = 2$, corresponding to the inter-annual mean flow in the Aberjona river $Q_r = 0.8$ m^3/s given the typical density difference occurring between the river and wetland water during summer and fall. The threshold for the wind forcing was taken as $\mu_2 = 0.5$ based upon observations. A value $\mu_2 < 1$ is consistent with the fact that the wind stress acts on a larger surface than the channel (*i.e.* $q \simeq 0.22$ in the upper forebay).

Finally, the net surface heat flux $\phi(t)$ was estimated as

$$\phi = (1 - R)S + \phi_1 + \phi_2 + \phi_S + \phi_L.$$

Here, the incoming solar (short wave) radiation, S, was measured directly, and the amount of reflected short wave radiation was estimated according to the reflection coefficient $R = 0.07$ [*Bras*, 1990, p. 38]. The other four terms, the incoming long wave radiation, ϕ_1, the back-radiation, ϕ_2, the sensible (conductive), ϕ_S, and the latent (evaporative) heat flux, ϕ_L, were all estimated from the weather data measured at the site and/or Boston International airport using established empirical relationships [*Fisher et al.*, 1979, p. 163; *Bras*, 1990, p. 190]. The diffusive heat flux terms (ϕ_S and ϕ_L) included both forced and free convection following *Ryan and Harleman* [1973]. Heat input from direct rain over the wetland was

small compared to the river input and was neglected.

3.4 Results and Discussion

3.4.1 Thermal Mediation

In this section, water temperatures recorded in the Upper Mystic Lake system during the typical flow year of 1997, when the Aberjona river had an annual mean flow of $Q_r = 0.7$ m^3/s, are used to demonstrate that thermal mediation occurs, and that the degree of thermal mediation is affected by flow conditions. For simplicity, the temperature records summarized on figure 3-3 have been low-pass filtered using a 2nd order Butterworth filter to remove diurnal fluctuations. We will start by considering the prevailing low-flow conditions (unshaded areas on figure 3-3), and then focus on the episodic storm events (shaded areas).

Low Flows

Figure 3-3*a* compares the water temperature in the river entering the wetland, T_R, and in the middle of the wetland channel, T_c. Since the river is consistently colder than the wetland water throughout summer and early fall, the wetland mediates the temperature of the lake inflow, warming up the water on the average by 2.2 ± 1.4^oC during this period. The degree of thermal mediation varies seasonally, and is more prominent in summer (4^oC), than in late fall (1^oC). These observations are in agreement with the analytical results derived from the dead-zone model presented by *Andradóttir and Nepf* [2000]. According to the model, thermal mediation occurs in the upper forebay for two reasons. First, the Aberjona river follows a damped seasonal cycle compared to the wetland, which makes it consistently colder through summer and early fall, as shown. Since the thermal capacity of the river, $r_R > 3$ (table 3.2), is large enough for the river to reach atmospheric equilibrium, this seasonal damping is mostly generated by sun-shading which produces a lower equilibrium state for the narrow river than the wide open wetland, and to a lesser extent by groundwater recharge. The second reason for the thermal mediation is that the wetland provides the thermal capacity, $r_W > 3$ (table 3.2), needed to erase the thermal signature of the river inflow, and bring the water to a new atmospheric equilibrium.

Next consider figure 3-3*b*, which compares the water temperature in the middle of the wetland channel and at the base of the lake epilimnion (at 5.8 m depth). The wetland

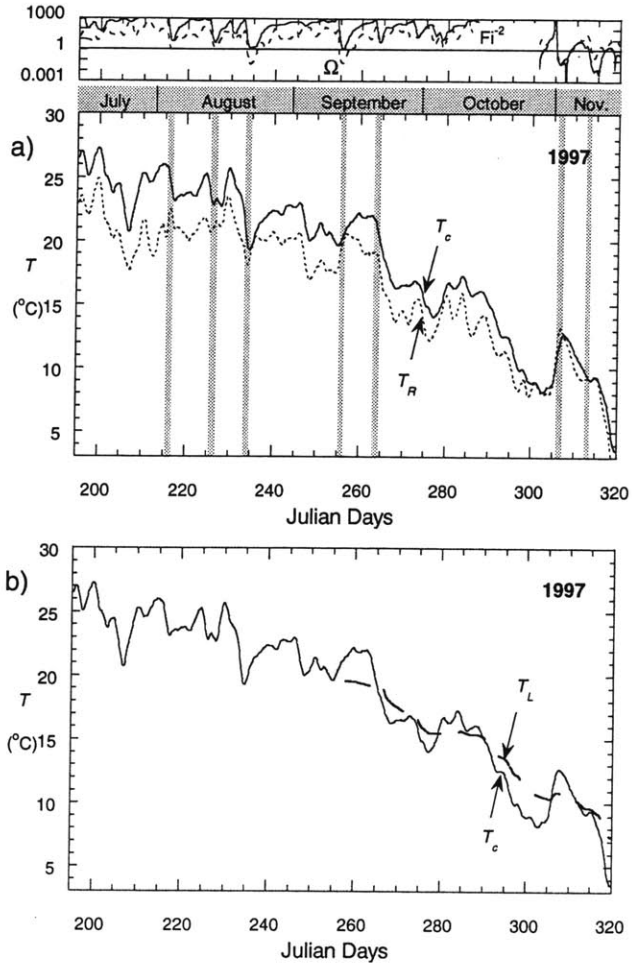

Figure 3-3: Comparison between the near-bed temperature in the river, T_R, the average of the near-surface and near-bed temperatures in the wetland channel, T_c, and the temperature at the base of the lake epilimnion, T_L, in 1997. Notice that the thermistors in the lake were deployed 60 days later than the wetland thermistors. a) Thermal mediation occurs, *i.e.* $T_R < T_c$. b) Differential heating and cooling occurs between the 1.6 m deep wetland and the 5.8 m deep surface mixed layer in the lake.

	r			$\bar{t}_{heat}$
	annual	summer/fall	storms	(days)
River	1	3 - 9	0.2 - 1	1.6 ± 0.4
Wetland	1	3 - 8	0.2 - 1	3.0 ± 0.6
Lake	4	10 - 30	0.7 - 4	11 ± 2

Table 3.2: Thermal capacity, r, and thermal inertia, $\bar{t}_{heat}$, in the Upper Mystic Lake system in 1997. Wetland thermal capacity is sufficiently large during low flows to produce significant thermal mediation as opposed to storms, when the residence time is not long enough for thermal mediation to occur. Differential heating and cooling occurs on synoptic and diurnal timescales between the wetland (low thermal inertia) and lake (large thermal inertia).

water temperature follows closely the seasonal trend of the lake epilimnion as opposed to the river, which follows a damped seasonal cycle. Wetland thermal mediation thus reduces the seasonal temperature difference between the lake and its inflow. On synoptic timescales (1-2 weeks), however, the wetland water oscillates from being warmer and cooler than the lake epilimnion. This trend is even more prominent on diurnal timescales not illustrated on figure 3-3. Both are a reflection of differential heating and cooling which occurs between systems of different thermal inertia, *i.e.* a shallow wetland (small thermal inertia) responds more rapidly to short-term meteorological fluctuations than a deep lake (large thermal inertia, see table 3.2). The combined effect of thermal mediation and differential heating-cooling is to shift the timescale of intrusion depth variability, as will be discussed in more detail in section 3.4.4..

Storms

The shaded regions on figure 3-3*a* show that the temperature difference between the river and wetland is reduced during storms, indicating that less thermal mediation is occurring in the wetland. This is in agreement with the analytical results from the dead-zone model, which show that the potential for thermal mediation is reduced with increased flowrates, largely because the residence time (time available for thermal mediation to occur) is decreased *Andradóttir and Nepf* [2000]. This is reflected in the thermal capacity of the wetland, r_W, which drops significantly during storms, *i.e.* $r_W < 1$ in table 3.2. In addition, the circulation becomes jet-dominated. As we will show later, this leads to short-circuiting, which further diminishes the effective thermal capacity of the wetland.

3.4.2 Wetland Circulation

Water circulation affects both how efficiently a wetland can mediate the temperature of the lake inflow, and how much particle removal/water purification occurs in a wetland. As discussed in section 3.2., the water circulation is expected to change between low flows and storms, as the relative importance of river buoyancy, wind and vegetation drag drops with increasing flowrates. In the following, we consider the detailed temperature signals in the upper forebay during both flow conditions, and discuss what they imply about the wetland circulation.

Low Flows

The non-shaded areas on figure 3-4 illustrate the temperature variations during low flows at different locations inside the upper forebay in the wet year of 1998, when the Aberjona river flow was $Q_r = 1.5$ m^3/s, or approximately twice the inter-annual mean. The heavy line represents the near-surface temperature, which does not vary significantly (0.1^oC) between the channel and dead-zones of the wetland suggesting that sun-shading due to emergent water lilies is not important in this wetland. Notice that the wetland surface water exhibits strong diurnal temperature fluctuations ($\pm 2^oC$ in late summer, $\pm 0.5^oC$ in fall) in response to the diurnal heating cycle. The light lines on figure 3-4 represent the near-bed temperatures in the channel and two dead-zones. The difference between the near-surface and near-bed temperatures indicates whether the water is stratified (large difference) or vertically well mixed (no difference). Figure 3-4 thus shows that the water in the shallow, densely vegetated southern dead-zone (T_{d1}) is weakly stratified and mixes over depth at night. In comparison, the water in the deeper channel (T_c) and northern dead-zone (T_{d2}) is stratified during most of the summer and early fall except during periods of strong winds (*e.g.* jd 222-224 on figure 3-4*a*). Progressing into late fall (figure 3-4*b*), the wetland stratification breaks down as a result of the increased convective cooling, which also generates the rapid drop in wetland temperature, from 20^oC in early October to 7^oC in late November. Finally, notice that at several times the near-bed channel water is colder than the near-bed water in the slightly deeper, northern dead-zone (jd 226, 249, 257, 262, 268, 273 and 280). These events all occur when the wind blows from South and is sufficiently strong to produce downwelling of warm surface water in the northern dead-zone based upon the Wedderburn # criteria [*e.g.*

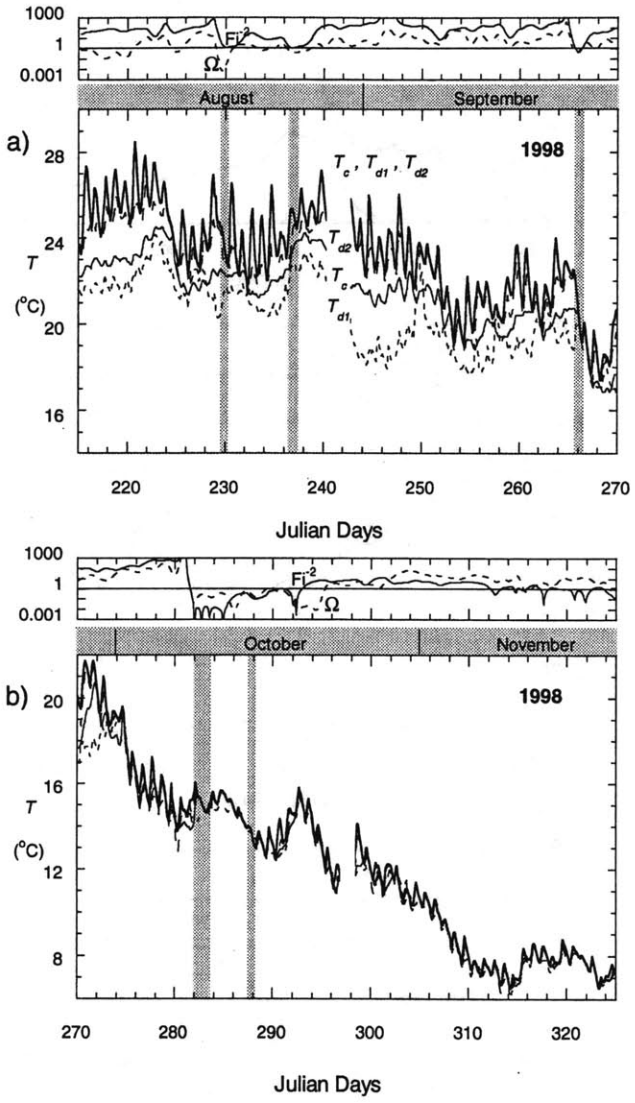

Figure 3-4: Wetland water temperatures, buoyancy, Fi^{-2}, and wind, Ω, parameters during a) early and b) late fall 1998. Shaded areas denote large storm occurrences where $Q_r > 1$ m^3/s. Wetland stratification and diurnal surface temperature fluctuations decrease progressing into the fall due to convective cooling and increasing winds.

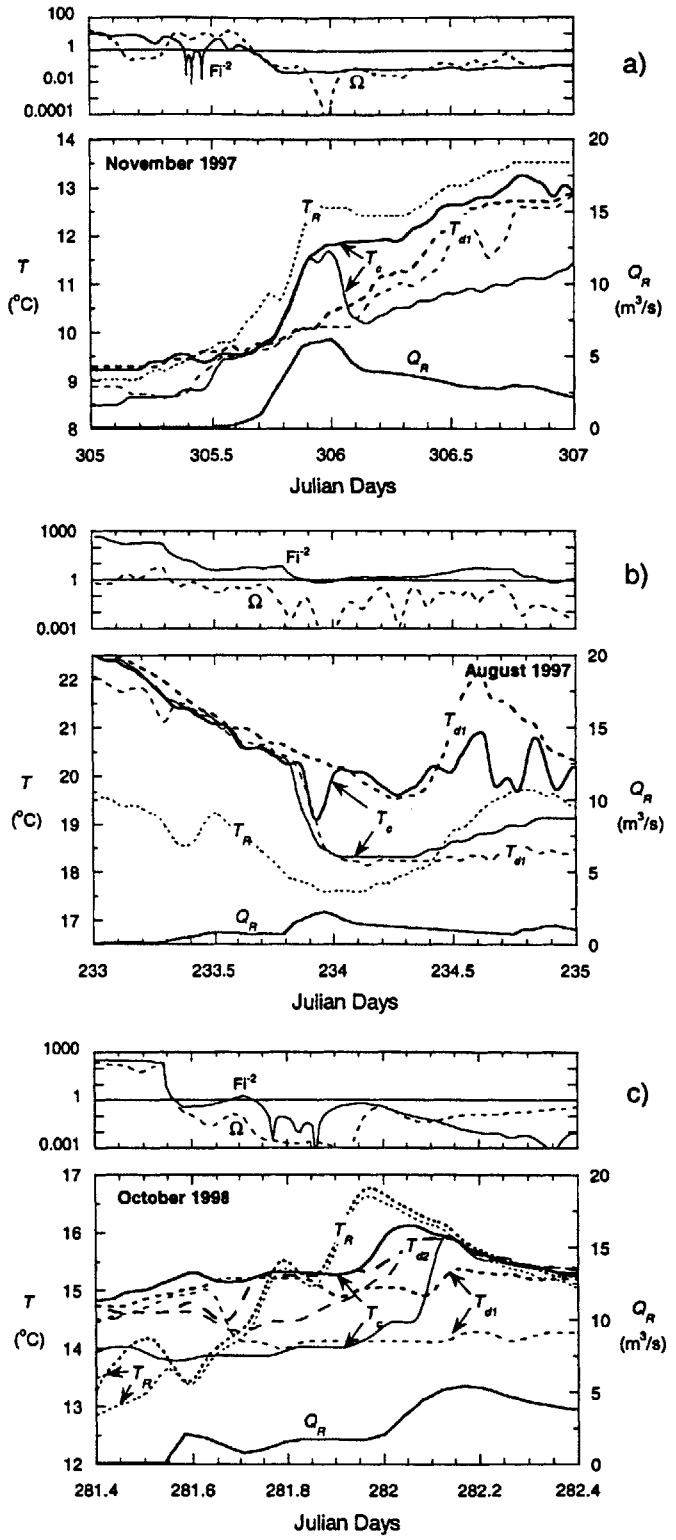

Figure 3-5: River and wetland water temperatures at $x = 0.4L$ during large storms in a) November 1997, b) August 1997 and c) October 1998. Heavy lines depict near-surface temperatures and light lines near-bed temperatures.

Imberger, 1985].

The above discussion of the temperature records in the upper forebay suggests that episodes of stratification, wind mixing and wind-driven internal circulation occur alternatively during low flows, in agreement with Fi^{-2} and Ω ranging from 10-1000 (figure 3-3 and 3-4). Under these conditions, the wetland can exhibit a complex, transient, 3-D flow behavior. Since Λ ranges from 30-300 (table 3.1), vegetation drag is also expected to play an important role in distributing the river laterally [*DePaoli*, 1999]. Dye experiments show that the integrated effect of all these processes over the residence time in the wetland (¿ 3 weeks) is that the wetland behaves as a partially-well-mixed reactor [*Andradóttir*, 1997]. This supports the use of a simple 1-D model such as the dead-zone model for low flow simulations, even though the instantaneous circulation may be far from 1-D.

Storms

The shaded areas on figure 3-4 show that the diurnal thermal fluctuations are reduced or erased during storms (*e.g.* jd 229, 265 and 282) as the wetland heat budget is more strongly influenced by the river inflow than atmospheric fluxes. Furthermore, the buoyancy and wind parameters drop by 1-3 orders of magnitude during storms, *i.e.* $Fi^{-2}, \Omega < 2$ (figure 3-3 & 3-4), and similarly the drag parameter reduces significantly, *i.e.* $\Lambda < 2$ (table 3.1). With this dramatic shift in forcing, the wetland circulation changes.

Figure 3-5 illustrates the thermal responses during three large storms in the 1997 and 1998 monitoring periods. First consider the largest storm in 1997, portrayed on figure 3-5*a*. As is typical for late fall storms, the river is a source of warm water to the wetland. Unlike low-flow conditions, the water temperatures in the channel and dead-zone deviate from one another. In particular, during the initial stage of the storm (jd 305.7-306), the water temperature in the channel increases abruptly, whereas the water temperature in the dead-zone rises more gradually. This is consistent with *short-circuiting* in which the river inflow approaches a jet-like structure (figure 3-1*b*) and a large portion of the river advects rapidly through the wetland channel while the remainder mixes slowly with the dead-zones. The time lag between the temperature increase in the river and wetland channel (1 hr) matches the advective timescale estimated for a river jet [*e.g. Chu and Baines*, 1989]. Another noteworthy feature of this storm is that the water column in the flow zone is well mixed during the rising limb of the hydrograph, as expected when the river inertia dominates

buoyancy and wind effects ($Fi^{-2}, \Omega < 0.5$). However, this one-layer channel flow structure breaks down on the receding limb shortly after the onset of a southerly wind (see the rapid increase in Ω at jd 306). The colder water that appears at the channel bed is thus likely advected from the northern dead-zone by the sub-surface return flow associated with the wind setup.

Next consider the August storm illustrated on figure 3-5*b*. In the beginning of the storm, the river is a source of cold water to the wetland, the reverse of the previous storm. Short-circuiting is again observed as the channel temperature drops more abruptly than the dead-zone temperature around jd 234.0. Furthermore, the water column is well mixed on the rising limb of the storm, but becomes stratified on the receding limb. Unlike the previous storm, this transition cannot be easily explained based upon the available data, because it does not coincide with wind setup, nor a significant increase in buoyancy forcing. After jd 234.0, the colder river flows through the wetland as an underflow until around jd 234.4, when the river becomes warmer than the wetland water. The river then switches to an overflow that appears to be short-circuiting, indicated by the sudden drop in the near-surface temperature in the channel that is not mirrored in the dead-zone around jd 234.7.

Finally, consider the largest storm episode in 1998, depicted on figure 3-5*c*. The wetland thermal response is very complicated, both because this event consists of a series of storms and because it occurs on windy days (0-7 m/s). In the first storm (jd 281.6), the river is colder than the wetland water and the wind is blowing from South (>3 m/s). The bed water temperature in the channel is consistently colder than in both dead-zones, likely because of sustained upwelling of cold water from the northern dead-zone associated with the wind setup. Since the temperature signature is masked by an internal wind driven circulation, it is inconclusive about whether the river is short-circuiting through the wetland. In the second storm (jd 282.2), the river is warmer than the wetland water. Furthermore, the wind, still strong (>4 m/s), has changed direction and is now blowing from North which produces less interference with the jet-structure, likely because the wetland is better sheltered from the North by hills and large homes. The temperature records on the rising limb of this storm show the warm river pulse moving through the wetland as an overflow, reaching the channel station more rapidly than both the northern and southern dead-zones. This is in agreement with the conceptual picture of short-circuiting portrayed on figure 3-2*b* in which

the channel cuts through the middle of the wetland. The river continues to short-circuit on the receding limb of the second storm (jd > 282.2), as seen by the fact that the water in the channel is significantly warmer than that in the northern dead-zone. Furthermore, in contrast to the storms on figures 3-5*a* & *b*, the flow is stratified on the rising limb of the storm, but well mixed on the receding limb.

To summarize, despite the temperature records of storm events are quite complex, they consistently demonstrate that the river short-circuits through the wetland (figure 3-1*b*). Our observations thus support the hypothesis that wetland circulation and thermal regime change during storms, from partially well mixed to short-circuiting. In addition, the upper forebay exhibits vertical structure both during low-flows and storms. This suggests that the use of a depth-averaged dead-zone model is at times an oversimplification, especially during storms. This will be investigated in greater detail in the following section.

3.4.3 Dead-Zone Model Simulations

As discussed in section 3.4.1., the observations of thermal mediation in the Upper Mystic Lake wetland agree with the linearized dead-zone model predictions [*Andradóttir and Nepf*, 2000]. To further validate the application of the dead-zone model, we now consider how well the model simulates the thermal response within the upper forebay during both low-flows and storms.

Low Flows

Figure 3-6 illustrates model simulations for a 10 day period in 1997, when the Aberjona river flowrate was 0.1 m^3/s. The simulated depth-averaged temperatures in the middle of the wetland channel and dead-zone on figure 3-6*a* show that the wetland water is laterally well mixed, $\bar{T}_c = \bar{T}_d$, in agreement with observations [*Andradóttir*, 1997]. Furthermore, the simulations lie between the observed near-surface and near-bed temperatures in the channel, indicating that the dead-zone model simulates well the diurnal temperature variations in the wetland during low-flows. The fact that the model temperatures are colder than observed on the windy days (jd 246-8) is likely because the model overpredicts convective cooling as it does not account for wind sheltering. Finally, during this low-flow period the residence time in the wetland is so long, $r_W \approx 8$, that the upper forebay has reached the limit of being a *stationary water body* [*Andradóttir and Nepf*, 2000]. At this limit, the thermal

budget is predominantly governed by the surface heat flux and not the river inflow, and the actual circulation regime in the wetland is not so important in predicting thermal mediation. This is demonstrated by the fact that both the stirred reactor and the dead-zone models predict very similar wetland outflow temperatures (figure 3-6*b*). However, the wetland circulation is still important for predicting chemical or solid removal [*Thackston et al.*, 1987]. Since wetlands/ponds tend to behave like partially mixed reactors with some degree of short-circuiting even during low-flows [*e.g. Kadlec*, 1994], the dead-zone model is generally expected to perform better than a stirred reactor model for river source materials unaffected by atmospheric exchange.

Storms

Figure 3-7 summarizes model simulations during the three large storms in 1997 and 1998 previously discussed in section 3.4.2.. First consider the 1997 November storm, which has the strongest signature of short-circuiting. Figure 3-7*a* shows that the dead-zone model predicts well the propagation of the warm river front to the middle of the wetland channel ($x = 0.4L$). Even when the flow is no longer 1-D (jd > 306), the model continues to capture well the movement of the warm, short-circuiting surface flow in the channel. The model, however, slightly underpredicts the water temperature in the Northern dead-zone, probably because it does not account for lateral exchange generated by wind driven circulation. For the 1997 August storm portrayed on figure 3-7*b*, the model again simulates well the channel and dead-zone temperatures in the middle of the wetland ($x = 0.4L$). Similarly, figure 3-7*c* shows that the dead-zone model does a good job predicting the movement of the thermal front along the wetland channel both at $x = 0.4L$ and $x = L$ during the 1998 October storm. Recall that the resolution of the thermistor probes is 0.2^oC, and the difference between the observed and simulated water temperatures (0.2-0.3^oC) is therefore not significant. These three simulations thus demonstrate that the 1-D, quasi-steady, dead-zone model gives reliable predictions of short-circuiting and the transition between short-circuiting and laterally-well-mixed flow during storms, even in systems such as the Upper Mystic Lake forebays which exhibit vertical structure (*i.e.* non 1-D behavior).

Finally, the comparison between the dead-zone and stirred reactor model simulations on the three bottom plots on figure 3-7 highlights the strength of the dead-zone model relative to the stirred reactor model. As expected, the dead-zone model captures the sharp

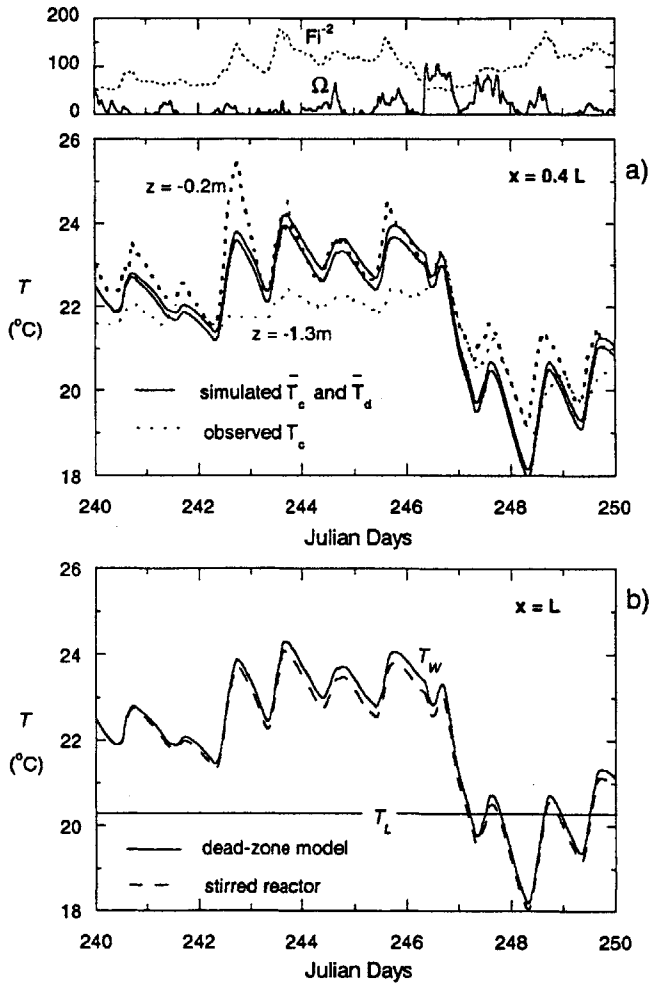

Figure 3-6: Low-flow model simulations. a) Comparison between dead-zone model simulations and field measurements at $x = 0.4L$. b) Wetland outflow temperature predicted by the dead-zone and stirred reactor models. Observation resolution is $\pm 0.2^o$C.

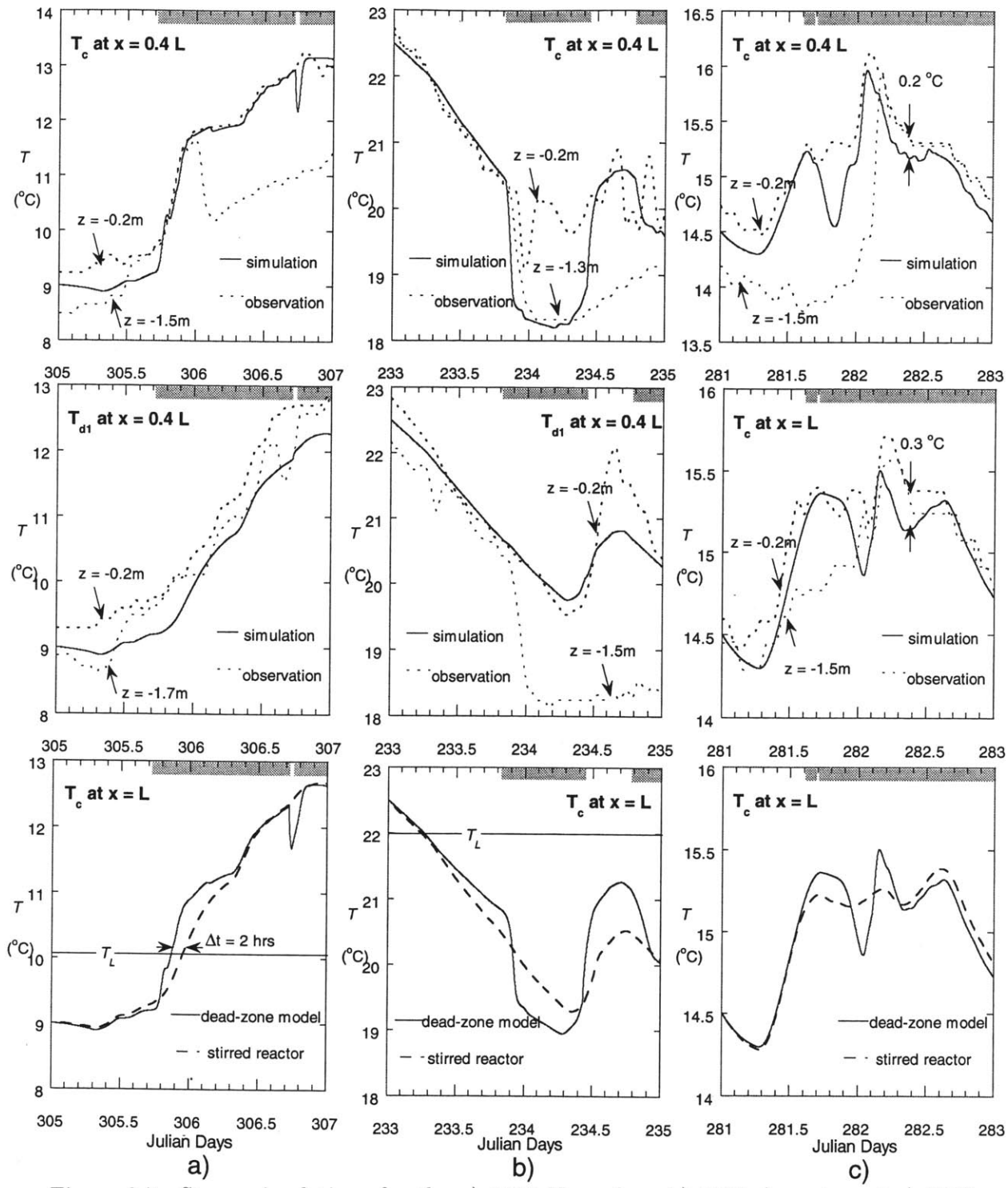

Figure 3-7: Storm simulations for the a) 1997 November, b) 1997 August, and c) 1998 October storms. Dead-zone model simulations (solid), are compared with observations (dotted) and stirred reactor simulations (dashed) at different locations within the wetland. The shaded areas across the top indicate the periods when the flow is jet-dominated, *i.e.* $Fi^{-2} < 2$ and $\Omega < 0.5$. Observation resolution is $\pm 0.2^o$C.

rises/drops in water temperature associated with short-circuiting, whereas the stirred reactor model predicts a diffused front because it assumes that the river mixes instantaneously throughout the wetland. This in turn can affect the lake intrusion depth predictions. For example, during the 1997 November storm on figure 3-7*a*, the stirred reactor model predicts a 2 hrs delay in surface intrusions ($T_{x=L} > T_L$) during the peak flow rates. Since the highest concentrations typically occur during the rising limb of a storm, the stirred reactor model will underpredict the contaminant/nutrient transport to the lake surface, which can have important implications on human health and reservoir management as will be discussed in greater detail in the following section.

3.4.4 Lake Intrusion Dynamics and Water Quality

Wetland thermal mediation is an important physical process in part because it can alter lake intrusion dynamics which in turn impact downstream water quality. Figure 3-8 describes the expected intrusion depth in the Upper Mystic Lake with and without the upper forebay based on the water temperature measurements in 1997, as discussed in section 3.3.2.. The seasonal and synoptic trends presented in figure 3-8*a* show that in the absence of the wetland, the colder river water would plunge when entering the lake throughout the fall except for a few days of short-term heating (*e.g.* jd 284 and 305-310). But with the littoral wetland present, episodes of surface intrusion are prolonged and occur during 28 days or 40% of the monitoring period (*e.g.* jd 256-265, 279-291 and 306-312). Therefore, substantially more river-borne fluxes are delivered into the surface water of the lake with the wetland present, which in turn has a high impact on the nutrient and chemical budgets of the lake as discussed in section 3.1.. A close-up on diurnal timescales (figure 3-8*b*) shows that the intrusion depth can also vary significantly over the course of a day, especially during synoptic heating periods when the inflow inserts into the lake epilimnion. During these times, a small temperature variation can lead to a large change in intrusion depth because of the low thermal gradient in the lake surface layer. In the Upper Mystic Lake these variations can be as large as 4-6 m. Overall, the temperature measurements in the Upper Mystic Lake system suggest that the presence of a littoral wetland shifts the timescale of lake intrusion depth variability, from predominantly seasonal (no wetland) to synoptic and diurnal timescales (with wetland). A similar result was predicted by the linearized dead-zone model [*Andradóttir and Nepf*, 2000]. The shift in intrusion depth variability can impact

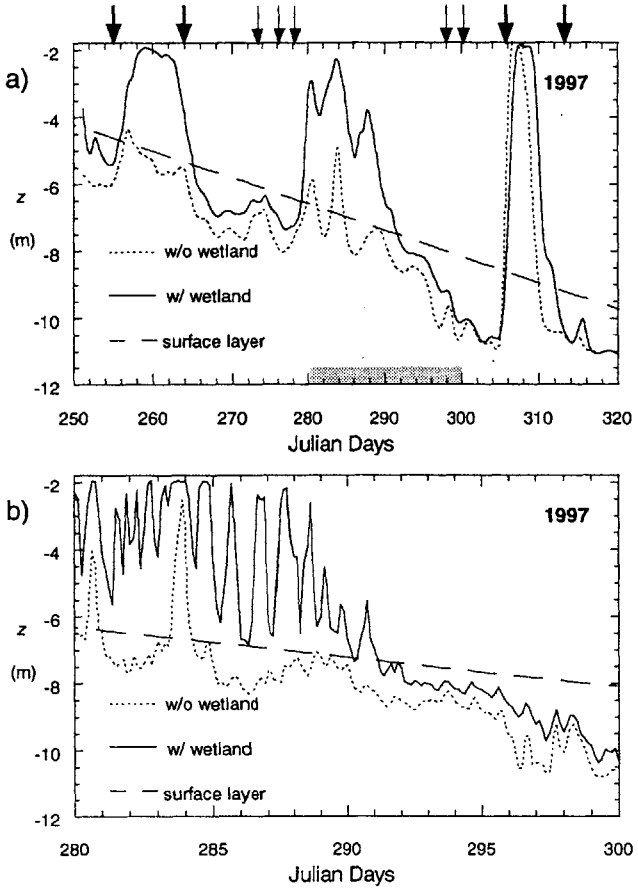

Figure 3-8: Intrusion depth with and w/o a wetland in 1997. Wetland thermal mediation increases a) synoptic, and b) diurnal intrusion depth variability. Heavy arrows depict large ($Q_r > 1$ m^3/s) storm occurrences, and light arrows small ($Q_r < 1$ m^3/s) storm occurrences. Uncertainty is ± 0.8 m for surface intrusions and ± 0.3 m for intrusions into the thermocline.

lake water quality. For example, nutrients and contaminants may be more homogeneously distributed over depth as the river inflow covers a larger vertical domain in the lake. In addition, lateral and vertical transport processes in the lake can be enhanced. Both of these will affect the management of reservoir use and withdrawals.

The intrusion depth during storms is of particular importance for lake water quality. Due to surface runoff and remobilization of channel sediments, river nutrient and contaminant concentrations usually increase during storms. For example, storms account for 30-60% of the total annual fluxes of heavy metals such as arsenic, chromium, iron and copper to the Upper Mystic Lake [*Solo-Gabriele*, 1995]. Furthermore, sewage overflow during storms can introduce high concentrations of E-coli and Cryptosporidium into surface water, both of which can make people sick after only short-term exposure. The arrows on figure 3-8*a* depict the storm occurrences in the Upper Mystic lake system during fall 1997. As expected from the previous discussion, the presence of a wetland does not significantly modify the lake intrusion depth during storms because of the low effective thermal capacity associated with the high flowrates. Furthermore, the dead-zone model predicts that whether storms enter the lake surface or insert at depth depends upon the water temperature of the surface runoff (which reflects synoptic conditions) relative to the lake water temperature (which reflects the seasonal conditions) [*Andradóttir and Nepf*, 2000]. Figure 3-3*a* shows that storms during late summer and early fall are generally a source of cold water to the wetland and coincide with synoptic cooling, whereas storms in late fall are often a source of warm water and coincide with synoptic warming. Figure 3-8*a* shows that the majority of the storms follow this trend, *e.g.* late summer early fall storms produce intrusions in the thermocline whereas late fall storms produces surface intrusions, in agreement with the theory.

3.5 Conclusions

Thermal mediation in littoral wetlands is an important process that can alter the intrusion depth in lakes and thus can determine the downstream fate of land-borne nutrients and contaminants. Measurements in the Upper Mystic Lake system in Massachusetts during summer and fall 1997-8 demonstrate that thermal mediation occurs in natural littoral wetlands, and that it is affected by flow conditions. During low flows, the wetland raises the temperature of the lake inflow by approximately 1-3^{o}C, which is sufficient to change the

lake intrusion depth by 1-6 m and shift the timescale of lake intrusion depth variability from seasonal (no wetland) to synoptic and diurnal (with wetland). In contrast, during storms almost no thermal mediation occurs. These observations are both in agreement with the theory presented by *Andradóttir and Nepf* [2000]. This difference in thermal response with flow conditions can partially be explained by a shift in wetland circulation: During low flows, the river inflow fills the entire wetland volume and the wetland behaves like a partially-well-mixed reactor. During storms, however, the temperature records demonstrate that the river short-circuits across the wetland, and thus only a fraction of the wetland volume is available to produce thermal mediation. A simple 1-D, quasi-steady, dead-zone model can give reliable predictions of thermal mediation during both regimes, and predicts well the transition between short-circuiting and laterally-well-mixed flow.

3.6 Acknowledgments

This work was funded by the National Institute of Environmental Health Sciences, Superfund Basic Research Program, Grant No. P42-ES04675. Special thanks to the Winchester boat-club for their interest in our research and for allowing us to launch our boats from their docks, and to the Medford boat-club for providing a pole for our anemometer. The authors would also like to thank Dr. Eric Adams for his insight and feedback on this work, and Laura DePaoli, for her comments on the manuscript.

3.7 Appendix

The net surface heat flux $\phi(t)$ was estimated as a sum of five heat flux terms, i.e.

$$\phi = (1 - R)S + \phi_1 + \phi_2 + \phi_S + \phi_L.$$

The incoming solar (short wave) radiation, S, was measured directly at the site. The amount of short wave radiation absorbed in the water was adjusted by the term $(1 - R)$, where the reflection coefficient R was chosen as 0.07 based on the solar altitude of the Upper Mystic Lake [*Bras*, 1990, p. 38]. The other four heat flux terms were estimated from the weather measurements using established empirical relationships [*Fisher et al.*, 1979, p. 163; *Bras*,

1990, p. 190]. The incoming long wave radiation, ϕ_1, was taken as

$$\phi_1 = 5.18 \cdot 10^{-13}(1 + 0.17C^2)(T_a + 273)^6 \tag{3.11}$$

where C is the cloud cover fraction measured at the Boston International airport, and T_a the air temperature (in ^{o}C) over the Upper Mystic Lake. Similarly, the back-radiation, ϕ_2, was taken as

$$\phi_2 = -5.5 \cdot 10^{-8}(T + 273)^4 \tag{3.12}$$

where T is the water temperature. The latent (evaporative) heat flux, ϕ_L, included both free [*Fisher et al.*, 1979, p. 163] and forced [*Ryan and Harleman*, 1973] convection, i.e.

$$\phi_L = \left\{1.5 \cdot 10^{-3}\rho_a L_w W_{10} + 2.7\frac{P}{0.622}(\Delta T_V)^{1/3}\right\}(q_a - q). \tag{3.13}$$

Here $\rho_a = 1.2$ kg/m^3 is the density of air, $L_w = 2.5 \cdot 10^6$ J/kg the latent heat of evaporation, W_{10} the wind speed (m/s) at 10 m above the water surface, P the atmospheric pressure (mb), ΔT_V the virtual temperature difference that generates free convection, q_a the specific humidity of air, and q the saturation specific humidity at the air-water interface. The virtual temperature difference is defined as

$$\Delta T_V = \frac{T}{1 - 0.608q} - \frac{T_a}{1 - 0.608q_a}$$

for $T > T_a$, but is otherwise zero. The specific humidity is related to the vapor pressure, e, and thus air temperature, pressure, and relative humidity, RH, through the following relationship

$$\begin{aligned} q(T, P, RH) &= \frac{0.622}{P}e(T, P, RH) \\ &= \frac{0.622}{P}RH \cdot 6.11\ mb \cdot \exp\left(\frac{L_w}{R_v}\left(\frac{1}{273} - \frac{1}{273 + T}\right)\right). \end{aligned}$$

where $R_v = 461$ J/(kg^{o}K) is the vapor gas constant. Consequently, $q_a = q(T_a, P, RH)$ and $q = q(T, P, 1)$. Lastly, with the latent heat flux determined, the sensible (conductive) heat

flux, ϕ_S, was estimated using the Bowen ratio, i.e.

$$Bowen\ Ratio = \frac{\phi_S}{\phi_L} = 3.8 \cdot 10^{-4} \frac{T_a - T}{q_a - q}. \tag{3.14}$$

Bibliography

[1] Andradóttir, H. Ó., Circulation and mixing in the upper forebay of the Mystic Lake system, Winchester, Massachusetts, Master's thesis, Mass. Inst. of Technology, 1997.

[2] Andradóttir, H. Ó., and H. M. Nepf, Thermal mediation by littoral wetlands and impact on lake intrusion depth, *Water Resour. Res., 36*(3), 725-735, 2000. Also chapter 2 in this thesis.

[3] Aurilio, A. C., R. P. Mason, and H. F. Hemond, Speciation and fate of arsenic in three lakes of the Aberjona Watershed, *Environ. Sci. Technol., 28*, 577-585, 1994.

[4] Bencala, K. E., and R. A. Walters, Simulation of solute transport in a mountain pool-and-riffle stream: A transient storage model, *Water Resour. Res., 19*(3), 718-724, 1983.

[5] Bras, R. L., *Hydrology, an introduction to hydrologic science*, Addison-Wesley Publishing Company, Reading, Massachusetts, 1990.

[6] Carmack, E. C., R. C. Wiegand, R. J. Daley, C. B. J. Gray, S. Jasper, and C. H. Pharo, Mechanisms influencing the circulation and distribution of water mass in a medium residence-time lake, *Limnol. Oceanogr., 31*(2), 249-265, 1986.

[7] Chen, C., Flow resistance in broad shallow grassed channels, *J. Hydraul. Div. ASCE, 102*(HY3), 307-322, 1976.

[8] Chu, V. H., and W. D. Baines, Entrainment by buoyant jet between confined walls, *J. Hydraul. Eng., 115*(4), 1989.

[9] DePaoli, L. L., Numerical modelling of wetland hydrodynamics, Master's thesis, Mass. Inst. of Technology, 1999.

[10] Dunn, C., F. Lopez, and M. Garcia, Mean flow and turbulence in a laboratory channel with simulated vegetation, *Civil Engineering Studies: Hydraulic Engineering Studies, 51*, 1996.

[11] Fisher, H. B., E. J. List, R. C. Y. Koh, J. Imberger, and N. H. Brooks, *Mixing in inland and coastal waters*, Academic Press, Inc., London, 1979.

[12] Fricker, P. D., and H. M. Nepf, Bathymtery, stratification, and internal seiche structure, *J. Geophysical Res.*, 1999 (in press).

[13] Gu, R., F. N. Luck, and H. G. Stefan, Water quality stratification in shallow wastewater stabilization ponds, *Water Resour. Bull., 32*(4), 831-844, 1996.

[14] Imberger, J., Thermal characteristics of standing waters: an illustration of dynamic processes, *Hydrobiologia, 125*, 7-29, 1985.

[15] Jirka, G. H., and M. Watanabe, Steady-state estimation of cooling pond performance, *J. Hydraul. Div. ASCE, 106*(HY6), 1116-1123, 1980.

[16] Kadlec, R. H., Detention and mixing in free water wetlands, *Ecological Engineering, 3*, 345-380, 1994.

[17] Kadlec, R. H., and R. L. Knight, *Treatment wetlands*, CRC Press Inc., Boca Raton FL, 1996.

[18] Metropolitan Council, Lake McCarrons wetland treatment system-phase III study report, *publ. No. 32-97-026*, Metropolitan Council, City of Roseville, Minnesota, 1997.

[19] Mitsch, W. J., and J. G. Gosselink, *Wetlands*, Van Nostrand Reinhold, New York, 1993.

[20] Petryk, S., and G. Bosmajian III, Analysis of flow through vegetation, *J. Hydraul. Div. ASCE, 101*(HY7), 871-884, 1975.

[21] Ryan, P. J.,and D. R. F. Harleman, An analytical and experimental study of transient cooling pond behaviour, *Tech. Rep. 161*, R. M. Parsons Lab for Water Res. and Hydrod., Mass. Inst. of Technology, 1973.

[22] Shih, S. F., and G. S. Rahi, Seasonal variations of Manning's roughness coefficient in a subtropical marsh, *Transactions of the ASAE, 25*(1), 116-119, 1982.

[23] Sinokrot, B. A., and H. G. Stefan, Stream temperature dynamics: Measurements and modeling, *Water Resour. Res., 29*(7), 2299-2312, 1993.

[24] Solo-Gabriele, H., Metal transport in the aberjona river system: monitoring, modelling, and mechanisms. PhD thesis, Mass. Inst. of Technology, 1995.

[25] Tchobanoglous, G., Constructed wetlands and aquatic plant systems: Research, design, operational and monitoring issues, in *Constructed wetlands for water quality improvement*, Ed. G.A. Moshiri, Lewis Publishers, 1993.

[26] Thackston, E. L., F. D. Jr. Shields, and P. R. Schroeder, Residence time distributions of shallow basins, *J. Environ. Eng., 113*(6), 1319-1332, 1987.

[27] Wu, J., and I. K. Tsanis, Pollutant transport and residence time in a distorted scale model and numerical model, *J. Hydraul. Res., 32*(4), 583-598, 1994.

Chapter 4

Exchange Flows between Littoral Wetlands and Lakes

4.1 Introduction

Exchange flows are an important transport mechanism both in estuaries and lakes. In estuaries, the quasi-steady baroclinic circulation generated by the fresh-salt water density gradient (figure 4-1a) efficiently removes river borne contaminants from the headwaters to the open sea [*Nunes Vaz et al.*, 1989]. Similarly, freshwater exchange flows generated by differential heating and cooling between regions of different depth or optical clarity (figure 4-1b) can contribute significantly to the transport of nutrients and other chemicals from littoral to pelagic regions of lakes [*James and Barko*, 1991], to the heat dissipation in cooling lakes [*Jain*, 1980], and to enhanced flushing in littoral regions [*Horsch and Stefan*, 1988; *Sturman et al.*, 1999].

To date, freshwater exchange flows have mostly been studied by performing lab experiments and numerical modeling of natural convection in shallow cavities. The earliest of such studies focus on the steady circulation generated for example in sidearms of cooling lakes [*e.g. Brocard and Harleman*, 1980], while the most recent work characterizes the time variability and mixing properties in natural sidearms [*Farrow and Patterson*, 1993; *Sturman et al.*, 1996; *Sturman and Ivey*, 1998]. Only a few of these studies have been supplemented by field experiments, especially in shallow (< 2 m deep) sidearms such as littoral wetlands. In addition, few studies have evaluated the influence of wind on freshwater exchange flows.

Freshwater exchange flows are typically shallower and have a much smaller density gradient than estuarine flows. Consequently, wind effects are expected to have greater impact there than in estuaries. Wind can modify the baroclinic exchange in several ways. For example, the onset of a wind-driven circulation can surpress or promote the baroclinic circulation depending upon the wind direction. *Geyer* [1997] found that in shallow estuaries, such wind effects can increase the flushing by a factor of three. In addition, wind generated surface and internal seiches have been observed to drive barotropic and baroclinic exchange flows between enclosed bays and large lakes such as Lake Biwa in Japan and Lake Ontario [*Hamblin*, 1998]. Wind stirring is also a major source of turbulence, which will smooth out vertical inhomogeneities, resulting in a reduced baroclinic transport [*Linden and Simpson*, 1986]. In addition to the wind, topographic features such as contractions and sills can exert a hydraulic control on the exchange flow [*Armi and Farmer*, 1986; *Farmer and Armi*, 1986]. *Adams and Wells* [1984] found that constrictions formed by highway bridge abutments can significantly impair sidearm heat loss performance in cooling lakes.

This chapter provides a description of field observations of exchange flows between a shallow littoral wetland and lake. The goals of this work is to characterize the exchange between littoral wetlands and lakes on both diurnal and seasonal timescales, and to evaluate its influence on wetland flushing, removal and thermal mediation. Building upon previous sidearm work, here we additionally consider the influence of wind, river entrainment and topographic constraints on freshwater exchange flows, and describe the relative importance of baroclinic exchange and barotropic river flow during different times of the year. The outline of the chapter is the following. The site and study methods are introduced in sections 4.2 and 4.3. The field observations of the exchange flow and wetland circulation are summarized in section 4.4. Finally, the effect of wind on the exchange flows, and the impact of exchange on wetland flushing, lake transport and lake heating are discussed in section 4.5.

4.2 Site Description

The Upper Mystic Lake is a dimictic lake located in suburban Boston, Massachusetts, which is heavily used for recreational sailing, fishing and swimming in the summertimee (figure 4-2a). Due to long term industrial activities in this region, this lake receives high loads of

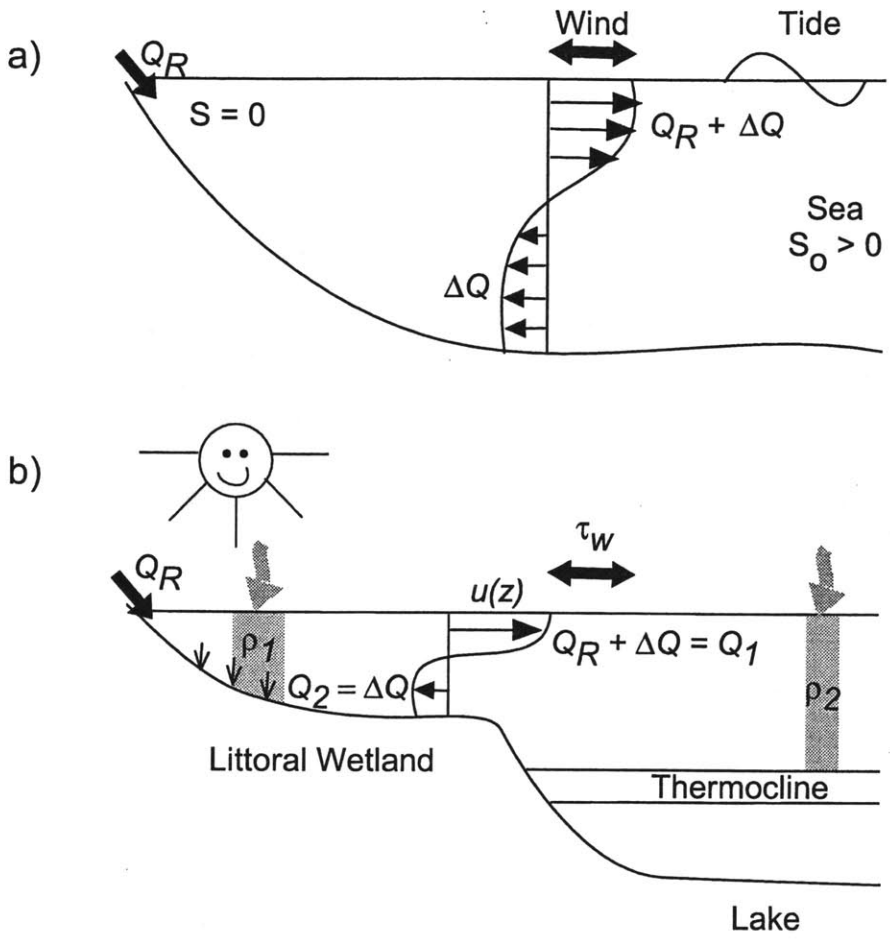

Figure 4-1: Schematic of a) estuarine, and b) freshwater exchange flows.

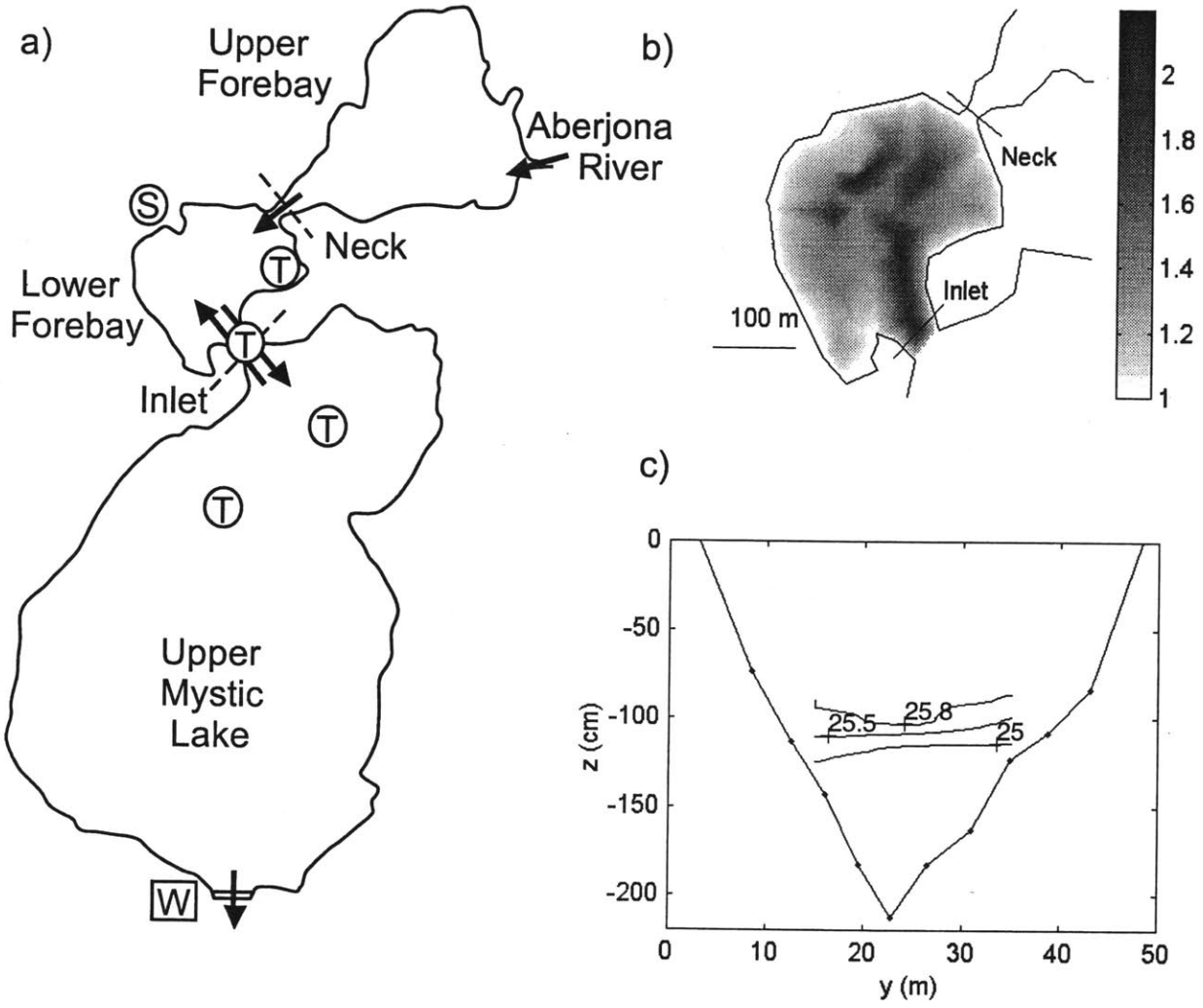

Figure 4-2: Field site characteristics. a) Overview of the Upper Mystic Lake system. Locations of water temperature probes are denoted by T, anemometer by W and the weather station by S. b) Bathymetry map (m) of the lower forebay in May 1997. c) Inlet cross section and typical water temperatures (July 30 1997, 6pm).

	H (m)	A_{surf} (10^4 m^2)	W (m)	L (m)
UFB	1.3-1.7	14.0 $\pm$ 0.3	255	550
LFB	1.5-1.9	5.2 $\pm$ 0.2	250	210
Inlet	1.4-1.7	0.35 $\pm$ 0.05	60	60
Lake	15	50.9 $\pm$0.7	530	960

Table 4.1: Upper Mystic Lake system dimensions. H represents the mean water depth, A_{surf}, the surface area, L, length from the inlet to the outlet, and $W = A_{surf}/L$ the mean width.

heavy metals such as arsenic and lead from the Aberjona river [*Solo-Gabriele*, 1995]. Before entering the lake, the river flows through two littoral wetlands, first the larger upper forebay (UFB), and then the smaller lower forebay (LFB). In this paper, we investigate the exchange flow between the lower forebay and the lake that occurs through the 60 m wide channel which we call the inlet. The lower forebay is a relatively flat bay with the exception of a 2 m deep channel that runs from the neck towards the lake inlet, which has an approximately parabolic cross section (figure 4-2b and c). Other relevant dimensions of this wetland-lake system are summarized in table 4.1. The ranges in mean water depth represent the seasonal variability, where the higher bound corresponds to early spring when the Aberjona river flow is typically high because of snowmelt and surface runoff, and the lower bound to late summer, when the river flowrates are typically low (figure 4-3a). Similarly, the wind over the lake follows a seasonal cycle, with winds blowing from the South during the summer months, and from the North in fall and winter at 1.5-3 m/s speed (figure 4-3c and d). The maximum wind recorded during the 1994-1998 interval was 12.5 m/s and occurred in November of 1997 (see table 4.6 in Appendix 4.8.1). Finally, the Upper Mystic Lake begins to stratify in April, and remains stratified until it overturns in November [*Aurilio et al.*, 1994]. The peak stratification occurs in the summer, when the 22-27 ^{o}C surface water is separated from the 4-7 ^{o}C hypolimnetic water by a thermocline typically located at 5-6 m depth.

4.3 Methods

Two field studies were conducted during 1997, the first one in April (high flows) and the second in July (low flows). The water velocities were monitored at the narrowest section of the inlet and several other locations in the lower forebay at regular depth intervals using a

Sontek ADV with a resolution of 0.1 mm/s. The ADV was deployed from a boat anchored on both ends in April, and from a free-standing rod stuck into the wetland sediments in July. Tracer experiments were also conducted in which Rhodamine WT dye was released across the width of the neck between the upper and lower forebays either instantaneously (April and July) or continuously (April). The dye was tracked as it traversed the wetland by taking vertical profiles of dye and temperature with a fluorometer-CTD system with a vertical resolution of 2-5 cm. A DGPS (Differential Global Positioning System) provided 1 m accuracy on spatial position. The dye leaving the wetland was monitored by regularly sampling water from 70 cm depth at the center of the lake inlet with an autosampler. More details about the field data collection and the meteorological conditions during each day of the studies are summarized in table 4.2.

Date	ADV Loc.	Dye Release at Neck		Dye Profiling	$\bar{W}_{10}$	wind	T_{air}
		Time	Mass (g)	Time	(m/s)	dir.	(^{o}C)
4/14	Inlet	—	—	—	5.3 ± 2.1	NW	15
4/15	Inlet	—	—	—	2.7 ± 1.6	NW	17
4/16	LFB	*Continuous* $10:40-13:15$	675 ± 1	$10:45-14:45$	1.8 ± 0.8	SW	19
4/17	All	*Instantaneous* $10:20 \pm 7$ *min*	25 ± 1	$11:00-15:05$	0.8 ± 0.5	S	15
7/25	All	—	—	—	5.1 ± 1.3	NE	21
7/30	All	*Instantaneous* $12:35 \pm 10$ *min*	38.9	$13:15-20:12$	2.9 ± 1.1	N	29
7/31	All	—	—	$11:40-13:15$ $17:40-18:35$	1.7 ± 0.8	NW	31
8/01	None	—	—	$16:15-17:15$	2.3 ± 0.8	W	32

Table 4.2: Overview of field experiments and meteorological conditions during the 1997 April and July studies.

In addition to the two extensive field programs in 1997, water temperatures were monitored continuously every 5 min from late July to November in the lower forebay both 10-20 cm below the surface and 10-20 cm above the bed using Onset temperature loggers with 0.2 ^{o}C resolution. Water temperatures were also measured in the shallower northern region of the lake during fall 1997 every 1 m starting from 1.8 m depth using thermistor chains with 0.1 ^{o}C resolution [*Fricker and Nepf*, 2000]. The locations of the thermistors are shown on figure 4-2a. Furthermore, air temperature, relative humidity and solar radiation were monitored every 5 min in the lower forebay from April through November 1997. Wind speed

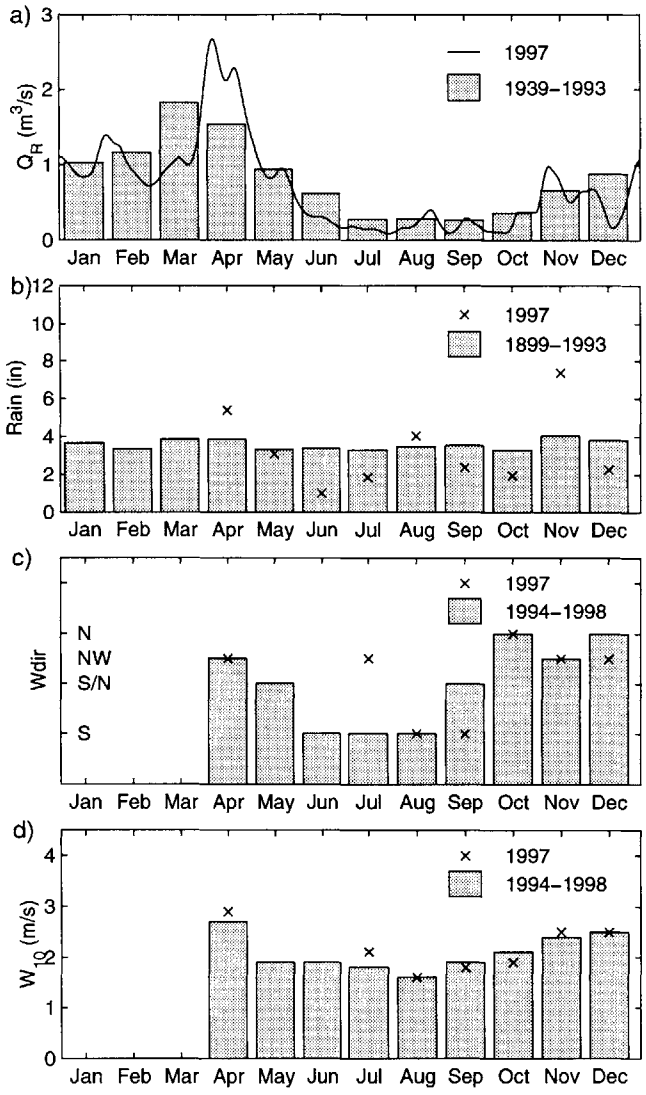

Figure 4-3: Monthly mean meteorological conditions in the Upper Mystic Lake system. a) Aberjona river flow rates, b) rainfall in Reading, c) prevalent wind direction and d) mean wind speed.

and direction were measured 10 m above ground at the southern end of the lake at 10 min intervals regularly during 1994-1998. Cloud cover was measured at 3 hrs intervals at the Boston Logan Airport located 15 km east of the study site. Hourly Aberjona river flow was measured by USGS approximately 800 m upstream of the entrance to the upper forebay. To account for the additional drainage area between the USGS station and the lower forebay, the reported flowrates were multiplied by a factor of 1.06. Finally, rainfall was measured by Climatologist R. Lautzenheizer in the town of Reading located approximately 10 km north of the study site.

4.4 Observations

4.4.1 Exchange Flow

Figure 4-4 summarizes the flow and water temperatures at the inlet on three different days during the April study. A positive water speed on figure 4-4a corresponds to wetland outflow to the lake, and a negative speed to return flow from the lake into the wetland. The temperature profiles illustrated on figure 4-4b show that the wetland and lake surface water are heating approximately 0.5-1 ^{o}C per day during this spring period, consistent with the net heat fluxes over the wetland (see table 4.4 in section 4.5.3). In addition, the wetland is persistently 1-1.7 ^{o}C warmer than the lake surface water, until on April 17 when it started raining. The net heat fluxes over the lake during this synoptic heating period suggest that the wetland even remains warmer than the lake overnight, such that no flow reversal occurs. The velocity profiles at the inlet in figure 4-4a reveal a persistent two-layer flow pattern, where the surface water leaves the wetland and the bottom water enters the wetland from the lake. The horizontal bars depict the standard deviation in the flow measurements excluding the variations generated by boat sway, and thus represents the water turbulence. The large horizontal bars on April 14 (approximately 3 cm/s) are a result of strong winds (see table 4.2). In comparison, the horizontal bars are less than 0.7 cm/s on the calm April 17.

In contrast to the steady exchange observed in April, figure 4-5 illustrates that the water temperatures and flow along the inlet in July vary significantly over the course of the day. In the morning of July 30, the near bed wetland water is colder than the surface layer in the lake, whereas the wetland surface water is slightly warmer than that in the lake. The

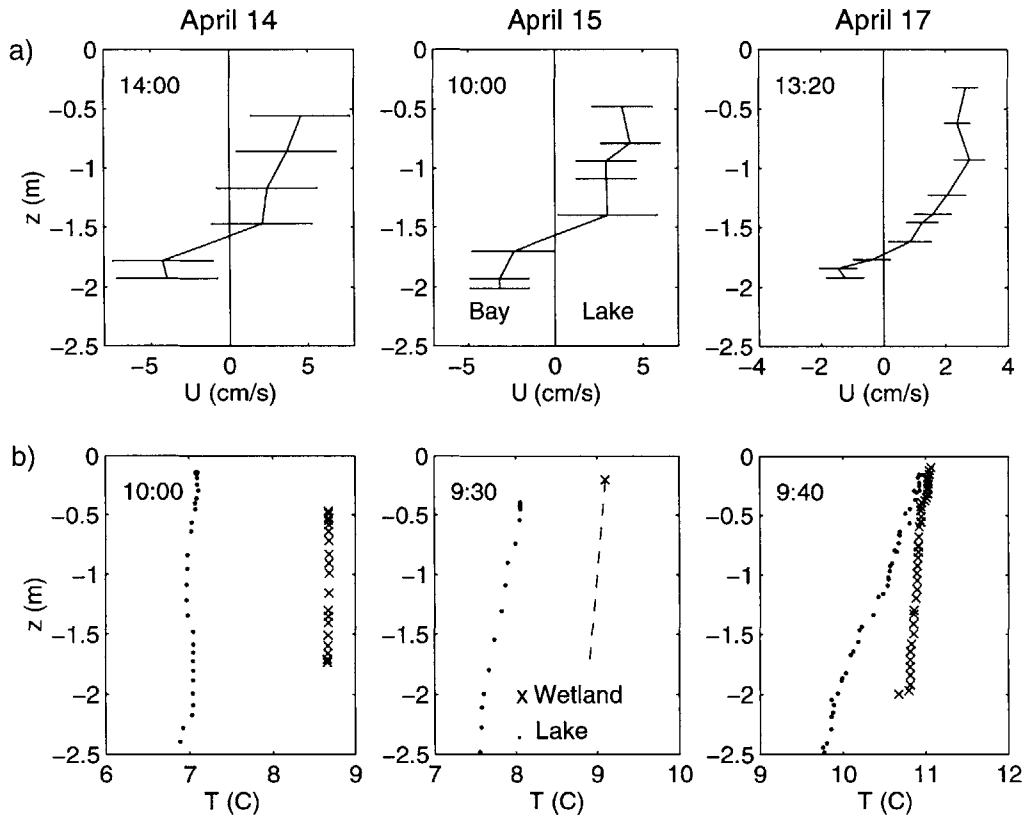

Figure 4-4: Exchange flow characteristics in spring 1997. a) Water speeds at the lake inlet. b) Temperature profiles along the inlet axis, (x) in the wetland and (.) lake.

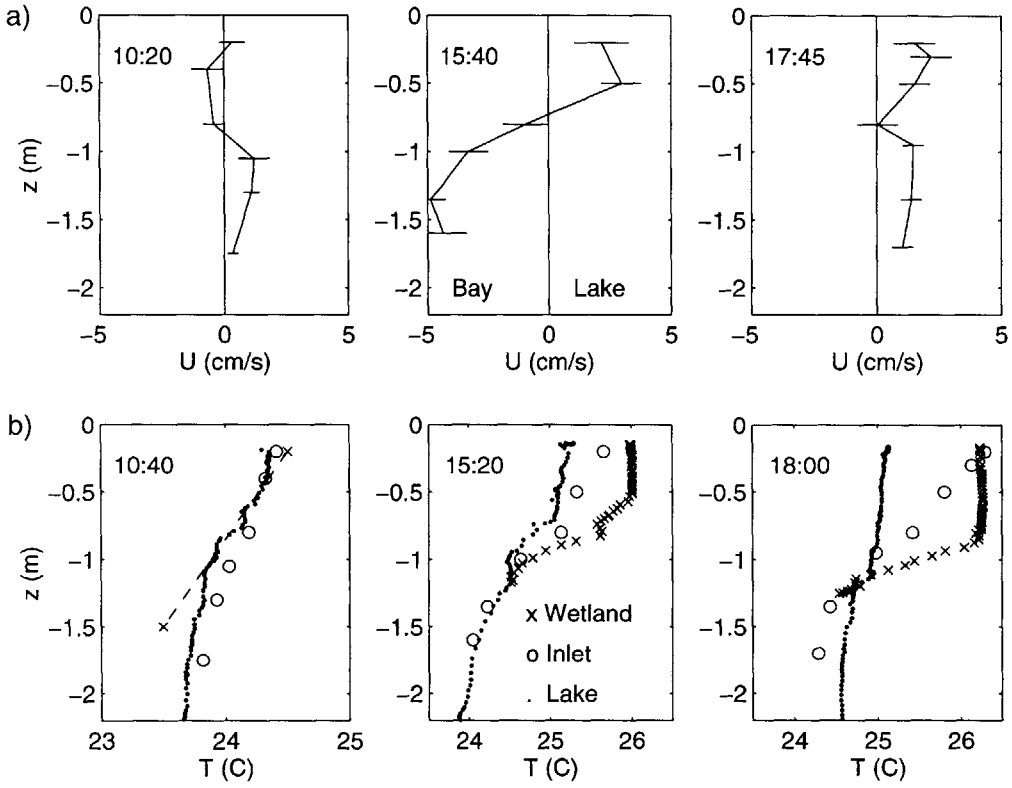

Figure 4-5: Exchange flow characteristics in the morning, mid-afternoon and late afternoon on July 30, 1997. a) Water speeds at the lake inlet. b) Temperature profiles along the inlet axis (x) in wetland, (o) at inlet, (.) in lake.

flow at the inlet at this time is weak (< 1.5 cm/s) and two-layered, with the bottom layer leaving the wetland and a surface intrusion from the lake. In the mid afternoon that same day, the wetland water has become 0.8 °C warmer than the lake water. The corresponding flow is strong (> 4 cm/s), two-layered and of reverse direction, where the surface water flows from the wetland to the lake and the bed water flows from the lake into the wetland. This diurnal flow reversal is consistent with differential heating and cooling, the process by which a shallow littoral region warms up more during the day and cools more at night than a deep pelagic region. At 17:45 that same afternoon, an interesting flow feature is observed. Figure 4-5a shows that the surface water, still significantly warmer in the wetland than in the lake, flows out of the wetland. The near bed water, however, now colder in the wetland than in the lake, has reversed direction and is also flowing out of the wetland. One possible explanation for this feature is that inflow from the lake is pushed in on one or both sides of the inlet, i.e. a lateral circulation is taking place at the inlet. However, this is not likely given that the isotherms across the inlet region are consistently horizontal throughout this study, as shown on figure 4-2c. Although not fully understood, this flow reversal is likely a result of internal seiching in the wetland and lake after the wind stops blowing at 5 pm, as discussed in more detail in section 4.5.1.

Next take a closer look at the characteristics of the flow at the inlet, summarized in table 4.3. First, the flow in the upper and lower layers, Q_1 and Q_2 schematically shown on figure 4-1, are estimated by extrapolating the velocity measurements at the inlet (figure 4-4a and 4-5a) to the surface and bed, then linearly interpolating them over depth, and lastly, integrating them over the upper and lower layer cross-sections, A_1 and A_2. The positive sign in table 4.3 corresponds to the wetland outflow to the lake, and the negative sign to the return flow from the lake into the wetland. The accuracy of these estimates is 25%, which incorporates the uncertainty in the flow profile (15-25%), cross section (5%) and the direction between the cross section and flow component (2%). Spatial flow measurements across the inlet on July 31 indicate that flowrates estimated from just a center velocity profile are only overestimated by 10%. Next, the inlet flow is decomposed into a barotropic river flow, Q_R, and baroclinic exchange flow, ΔQ, by substracting the river flowrates measured by USGS from the outflow to the lake, *i.e.*

$$\Delta Q_i = Q_i - \begin{cases} Q_R & if\ Q_i > 0 \\ 0 & if Q_i < 0 \end{cases} \quad i = 1, 2. \tag{4.1}$$

This analysis thus gives two independent estimates for the exchange flow, ΔQ_1 and ΔQ_2, based upon the flowrates in the upper and lower layer as shown on figure 4-1. The general agreement between ΔQ_1 and ΔQ_2 in table 4.3 is an indication of good measurement accuracy. The relative importance of the exchange flow is then assessed by calculating the ratio $\Delta Q/Q_R$.

In order to compare the relative importance of inertial and buoyancy forces on the flow, the composite internal Froude number is evaluated following *Dalziel* [1992] as

$$G^2 = F_1^2 + F_2^2 = \frac{u_1^2}{g' A_1/w} + \frac{u_2^2}{g' A_2/w}, \tag{4.2}$$

where $u_i = Q_i/A_i$ is the mean water velocity in the upper ($i = 1$) and lower ($i = 2$) layer, and w is the width of the interface between the two layers. In addition, the topographic constraints on the exchange flow are determined by calculating the maximal flowrates that could occur in the upper and lower layers at the inlet, *i.e.*

$$Q_{i,\max} = c_i \sqrt{g' H_{\max}} A \tag{4.3}$$

where $g' = g\,|\rho_2 - \rho_1|\,/\rho$ is the reduced gravity based upon the density in the upper and lower layers, ρ_1 and ρ_2, $H_{\max}$ the maximum water depth and $A = A_1 + A_2$ the cross-sectional area at the constriction. Lastly, c_i is a constant that incorporates both the shape of the channel and the barotropic river forcing following *Dalziel's* [1992] hydraulic control theory. In the absence of barotropic flow ($Q_R = 0$), $c_1 = c_2 = 0.25, 0.23, 0.21$ for rectangular, parabolic and triangular cross-sections, respectively. With a barotropic flow present ($Q_R \neq 0$), $c_1 \neq c_2$ and is no longer a constant but a function of the non-dimensional barotropic flow $Q_R/\sqrt{g' H_{\max}} A$. In the limit $Q_R > 0.5\sqrt{g' H_{\max}} A$, the barotropic flow arrests the exchange, such that $Q_{i,\max} = Q_R$ in the layer leaving the wetland and $Q_{\max} = 0$ in the other layer.

The analysis summarized in table 4.3 shows that the exchange flow is on the same order of magnitude during both the April and July studies. The river flowrates, however, vary drastically between the spring and summer, producing two different flow regimes in the wetland. In the spring, when the river flowrates are high due to snow melt (figure 4-3a),

Date	Q_1 (m^3/s)	Q_2 (m^3/s)	ΔQ_1 (m^3/s)	ΔQ_2 (m^3/s)	Q_R (m^3/s)	$\Delta Q/Q_R$	G^2	$Q_{1,max}$ (m^3/s)	$Q_{2,max}$ (m^3/s)
4/14	2.4	-0.4	0.2	0.4	2.2	0.1-0.2	3	2.2	0.0
4/15	2.2	-0.3	0.4	0.3	1.8	0.2	3	1.7±0.1	-0.1±0.1
4/17	1.5	-0.1	0	0.1	1.5	0.1	6	1.3±0.1	-0.2±0.1
7/25	-0.2	0.3	0.2	0.2	0.09	2	0.3	-0.8±0.2	0.8±0.2
7/30	-0.1	0.2	0.1	0.1	0.06	2	0.0	-0.7±0.1	0.7±0.1
7/30	0.6	-0.9	0.5	0.9	0.06	8-15	0.7	1.0±0.2	-1.0±0.2
7/31	0.9	-0.8	0.8	0.8	0.06	13	0.7	1.1±0.2	-1.1±0.2

Table 4.3: Exchange flow summary 1997.

then the wetland flow regime is river-dominated, i.e. $\Delta Q/Q_R < 1$. In this season, the flow at the inlet varies synoptically with changing river flow. In addition, the flow is super-critical, as indicated by $G^2 > 1$ in table 4.3, which suggests that inertial forces dominate buoyancy forces. Furthermore, hydraulic control theory predicts that the exchange flow at the inlet is severely constrained and even fully arrested by the high spring river flowrates, as indicated by the small maximal exchange flowrates $Q_{2,\max} = \Delta Q_{\max} < 0.1$ m^3/s in table 4.3. In comparison, (4.3) predicts $Q_{1,2\,\max} = \Delta Q_{\max} = 0.7 - 1$ m^3/s if there were no river inflow to the wetland. Notice that the observed flowrates at the inlet, Q_1 and Q_2, do not fully match the predicted maximal layer flowrates, $Q_{1,\max}$ and $Q_{2,\max}$, in table 4.3. In particular, hydraulic theory predicts a fully arrested flow on April 14 when an exchange flow is observed. This discrepancy may be attributed to the fact that the hydraulic control theory does not account for wind, which creates barotropic pressure gradients.

The relative importance of wind to inertial forces can be described by the following dimensionless parameter,

$$\Omega = \frac{\bar{\tau}_w}{\rho U_0^2} \frac{L}{H}, \tag{4.4}$$

which is derived from the Navier-Stokes equations. Here $\bar{\tau}_w$ represents the mean wind shear stress, which is related to the air density, ρ_a, the wind drag coefficient $C_{10} = 10^{-3}$ [*Hicks et al.*, 1974], and the wind speed at 10 m height, W_{10}, by

$$\bar{\tau}_w = \rho_a C_{10} W_{10}^2, \tag{4.5}$$

while ρ is the water density, U_0 the water velocity scale, and L/H the length-to-depth ratio of the wetland. In small systems, wind sheltering and directionality can be important as

is discussed in more detail in section 4.5.1. For the Upper Mystic Lake spring flows with $U_0 = 4$ cm/s, (4.4) suggests that the wind can significantly influence the exchange flows if

$$W_{10} > \sqrt{0.8 \cdot 10^6 U_0^2 \frac{H}{L}} \approx 3.5 \ m/s, \tag{4.6}$$

which is satisfied on the windy April 14.

Next consider the flow characteristics in summer, when the river flowrates are low (figure 4-3a). Table 4.3 shows that during this dry period, the flow in the wetland is exchange-dominated, $\Delta Q/Q_R > 1$. At this time, the flow at the inlet is sub-critical, $G^2 < 1$, indicating that the buoyancy forces dominate river inertia, and varies diurnally as a result of differential heating and cooling between the wetland and lake. In addition, the flow is sub-maximal, $Q_i < Q_{i,\max}$, suggesting that the exchange between the wetland and lake is not constrained by the width of the inlet.

This seasonal transition from river-dominated to exchange-dominated flow regime is not unique to the Upper Mystic Lake system, since many systems exhibit the same seasonal trends in atmospheric heating and river flowrates. The role of topography in constraining the exchange flows, however, depends on the geometry and the river inflows at each particular site. In the following section, the water circulation during these two different flow regimes is considered. The seasonal interplay between wind and buoyancy forcing in generating the exchange is covered in section 4.5.1. Lastly, the effect of the exchange flow on wetland flushing and transport of material to the lake is discussed in section 4.5.2.

4.4.2 Wetland Circulation

River-Dominated Regime, $\Delta Q/Q_R < 1$

In spring, when the river flowrates are high and the exchange flow is low, inertial forces dominate both the water buoyancy, seen by $G^2 > 1$ in table 4.3, and wind, since the mean spring winds (figure 4-3d) are typically less than the critical wind speed of 3.5 m/s determined by (4.6) for spring flow conditions. Consequently, the river inflow behaves like a jet, which independent of the wind takes the shortest path across the wetland. A schematic of this jet-dominated flow structure in the lower forebay is illustrated on figure 4-6a. As the jet flows through the wetland, it entrains water. *Chu and Baines'* [1989] laboratory experiments and theoretical analysis on two-dimensional shallow jets affected by

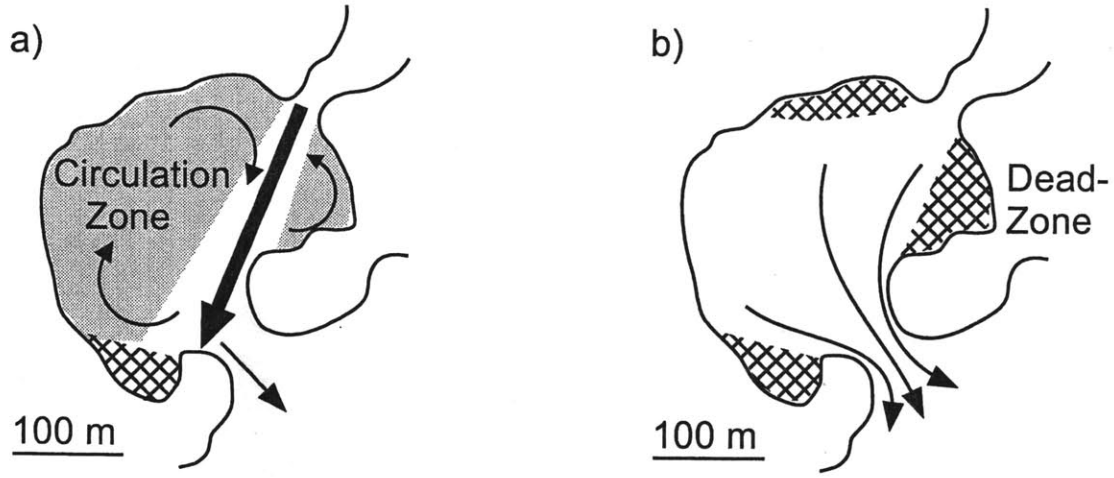

Figure 4-6: Schematic of wetland circulation a) river dominated regime, $\Delta Q/Q_R < 1$, and b) exchange dominated flow regime, $\Delta Q/Q_R > 1$.

wall friction predicts that once the jet reaches the lake inlet, it has doubled its volumetric rate via entrainment, i.e.

$$\frac{Q_{entrain}}{Q_R} = \sqrt{3.02\beta L/W_o + 1}\exp(-\Lambda/2) - 1 \approx 1 \tag{4.7}$$

where $\beta = 0.1$ is the spreading coefficient, $\Lambda = \frac{C_f}{2}\frac{L}{H} = 0.002(250/1.5) = 0.33$ is the vegetation drag parameter of the wetland and $W_o = 15$ m the initial jet width at the neck. The flow observations at the inlet (table 4.3), however, only show a 10-20% increase in wetland outflow, which suggests that 70-80% of the entrained jet water is recirculated within in the wetland as portrayed on figure 4-6a.

The results from the April 1997 dye studies, summarized on figure 4-7, are consistent with this hypothesis. Figure 4-7a shows the areal distribution of dye during the first 1.5 hrs of the 2.5 hrs long continuous release. The dye advects much faster than it disperses laterally, suggesting that the inflow short-circuits through the wetland, which is in agreement with jet flow. Consequently, a significant portion of the inflow will exit the wetland in a much shorter time than the nominal residence time, defined as

$$\bar{t} = \frac{AH}{Q_R + \Delta Q} = \frac{52,000 \cdot 1.9\ m^3}{1.5\ m^3/s} = 18\ hrs. \tag{4.8}$$

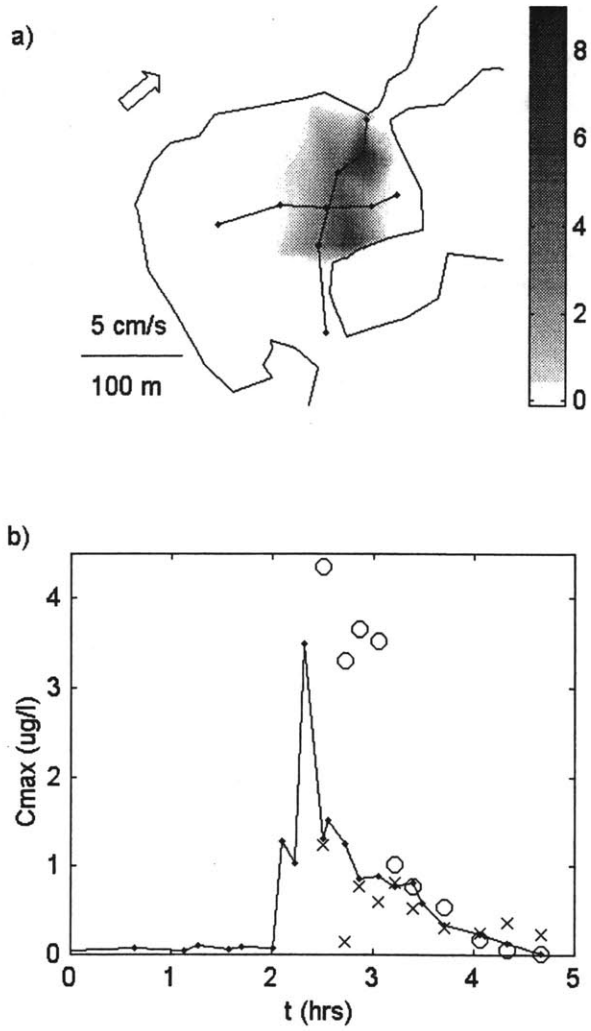

Figure 4-7 (caption on opposite page).

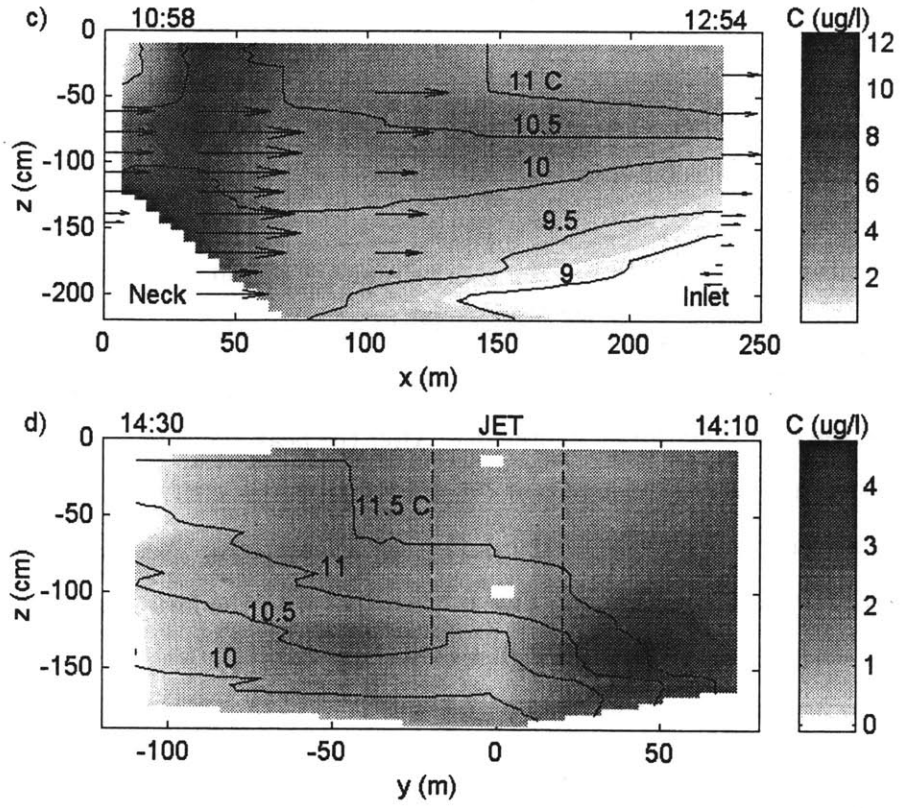

Figure 4-7: Dye study results in April 1997. a) Depth averaged concentrations during the initial stage of a continuous release on April 16 (10:50-12:20). b) Maximum dye concentrations at the west (o), center (-) and east (x) side of the inlet after instantaneous dye release on April 17. c) Longitudinal temperature and dye transect from the neck to the inlet on April 16 with flow measurements from April 17 (8 am - 2 pm). d) Lateral temperature and dye transect 100 m from the neck 1 hr after the continuous dye release ended on April 16.

Notice that both the river and exchange flow contribute to the wetland flushing and are therefore included in (4.8). This short-circuiting is apparent when following a slug of dye through the wetland. Figure 4-7b shows that a portion of a dye released over 15 min at the neck exits the wetland in only 2.5 $\pm$ 0.3 hrs, which is much faster than if the inflow mixes over the entire wetland given by (4.8). The observed short-circuiting time matches the mean travel time of the jet, t_{jet}. This can be seen from *Chu and Baines'* [1989] analysis of Gaussian, linearly spreading jets. In order to account for 92% of the jet flow, the width of the jet is defined as $W_{jet} = W_0 + 3\beta x$, which yields

$$\begin{aligned} t_{jet} &= \int_0^L \frac{W_{jet}(x)}{Q_{jet}/H_{jet}} dx = \frac{H_{jet}}{Q_R} \int_0^L \frac{W_0 + 3\beta x}{\sqrt{3.02\beta x/W_o + 1}} \exp(\frac{\Lambda}{2}\frac{x}{L}) dx \\ &\approx 2.1 \pm 0.2 \; hrs. \end{aligned} \tag{4.9}$$

Figure 4-7b also shows that during the short-circuiting period, the dye concentrations on the western side of the lake inlet are consistently higher than those at the center and eastern side. This distribution is consistent with a linear jet trajectory between the entrance of the wetland and the lake as shown on figure 4-6a. After the peak concentrations associated with short-circuiting has passed through (i.e. $t > 4.5$ hrs on figure 4-7b), the dye concentrations at the middle and western side of the outlet are almost zero. Yet, at least 40% of the injected dye remains in the wetland. This is consistent with the fact that some of the water that the jet entrains as it flows through the wetland does not leave the wetland because of the flow constriction at the wetland outlet, but is recirculated within the two side zones next to the jet (figure 4-6b). This dye is eventually flushed out of the wetland following the flushing timescales in these two zones. Based upon the sidezone volumes and the rate of entrainment, the side zone flushing timescales are

$$t_{sidezone} = \frac{AH|_{sidezone}}{(Q_{entrain})/2} = \begin{cases} 5 \pm 1 \; hrs & east \\ 1 \; day & west \end{cases} . \tag{4.10}$$

Since both of these timescales are longer than the monitoring period, the dye concentrations at the wetland outlet are expected to exhibit secondary peaks after a delay given by (4.10).

Next consider in greater detail the spatial structure of the flow during the continuous release on April 16. The longitudinal dye and water temperature transect on figure 4-7c

shows that the jet is is mostly confined within the top 1.5 m of the water column and moving at 3-5 cm/s along its 240 $\pm$ 10 m long travel path through the wetland. The 1 ^{o}C warming of the surface water from the neck to the inlet corresponds to the atmospheric heating over the two hours during which the transect was taken (see figure 4-7a). The return flow from the lake, characterized by the low water temperatures and dye concentrations near the bed, only extends halfway up into the wetland until it is arrested by the jet. Recall from section 4.4.1, the flow structure at the inlet is steady over the course of several days, suggesting that the velocity profiles shown on this longitudinal transect portray the long-term flow structure in the wetland.

Figure 4-7d depicts the lateral dye and temperature transect 100 m downstream of the neck 1 hr after the continuous dye release ended. The jet is now replaced by clear water, and is characterized by the low concentrations at $y = (-20, 20)$ m. The dye on both sides of the jet is evidence of the trapping and recirculation of dye in the eastern and western side zones as illustrated on the schematic figure 4-6a. Perhaps the most interesting feature of this transect is the lateral temperature gradient in the wetland, specifically the observation that the water in the eastern side zone has warmed up to a greater extent than other parts of the wetland. This is a consistent feature observed both during the April and July studies in the wetland, and is likely due to varying depth as well as differential heat absorption, which will be discussed in more detail in the following section.

Exchange-Dominated Regime, $\Delta Q/Q_R > 1$

In summer, when the river flows are very low, the main driving forces to the flow are buoyancy and wind. Since the buoyancy forcing is generated by differential heating and cooling between the shallow wetland and deeper lake, it is a global force, as opposed to the inflow jet which acts only on a selected portion of the wetland. Consequently, the wetland circulation is no longer expected to be jet-dominated, but rather a point sink flow where the water is drawn from all directions as illustrated on the schematic figure 4-6b.

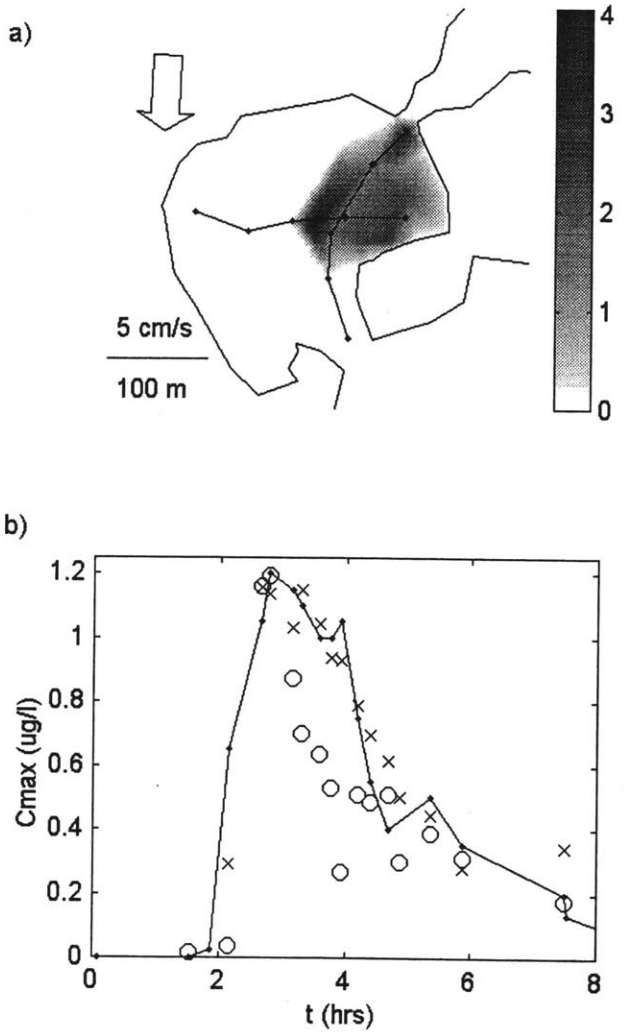

Figure 4-8: Dye study results in July 1997. a) Depth averaged concentrations within the first 1.5 hrs of an instantaneous release on July 30 (13:10-14:00). b) Maximum dye concentrations at the west (o), center (-) and east (x) side of the inlet after instantaneous dye release on July 30. c) Lateral temperature and dye transect 115 m from the neck. d) Longitudinal dye transect from the neck to the inlet on July 30 with flow measurements (11 am - 4 pm). e) Longitudinal temperature and dye transect from the neck to the inlet on July 31 with flow measurements (2 - 5 pm).

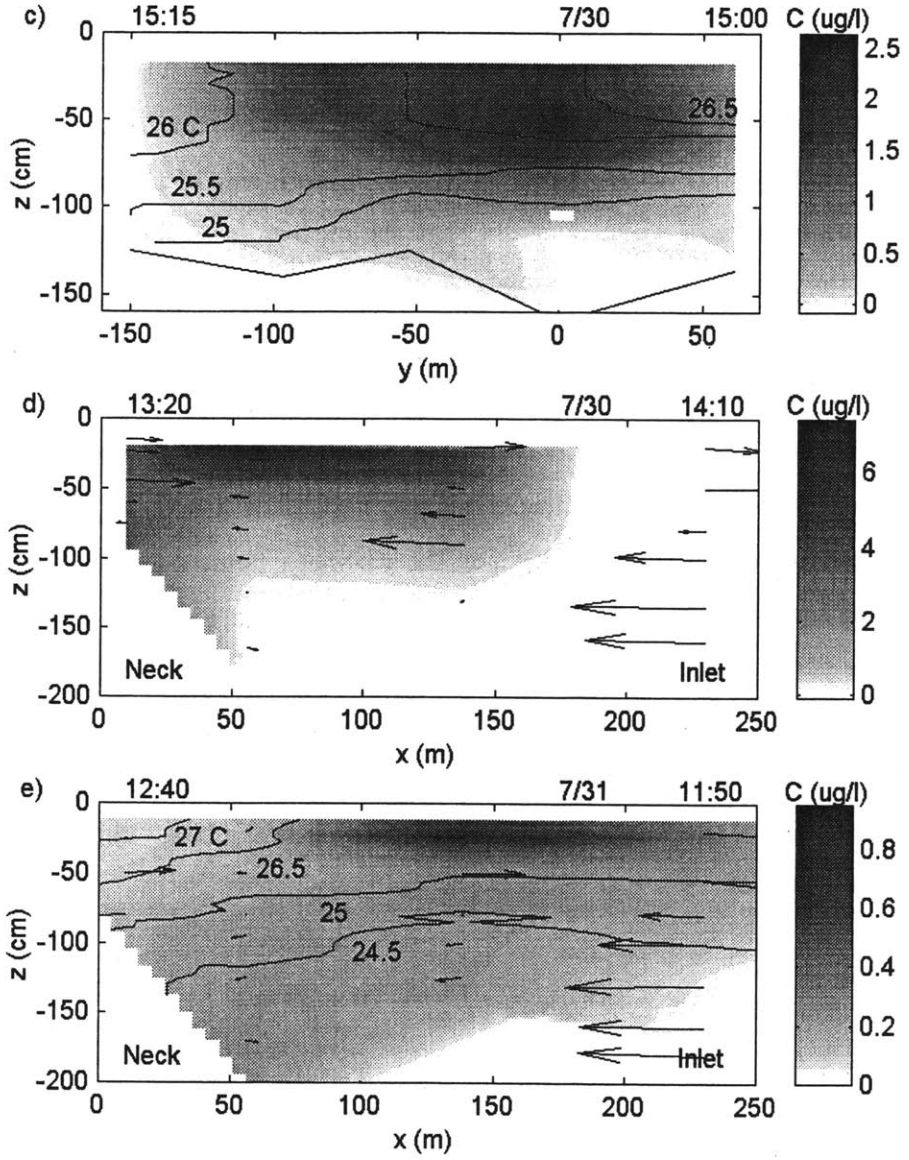

Figure 4-8 (cont).

The results from an instantaneous dye release on July 30 1997, summarized on figure 4-8, support this hypothesis. Figure 4-8a illustrates the lateral distribution of dye within the first 1.5 hrs of the release from the neck. As in the April study, the flow is short-circuiting through the wetland, seen by the fact that the pulse of dye advects faster than it disperses laterally. However, this short-circuiting is not associated with jet flow, but rather with the

wind and the wetland bathymetry, i.e. the fact that the lower forebay is very wide compared to its length ($W/L = 1.2$). *Thackston et al.* [1987] found that wide ponds have less hydraulic efficiency (i.e. more short-circuiting) than long ponds. The dye concentrations at the outlet of the wetland on figure 4-8b show that the pulse of dye leaves the wetland in 3.3 ± 0.2 hrs, which corresponds to a mean surface flow speed of $u_1 = L/t = 2.1$ cm/s. Again, the dye concentrations are not uniform across the lake inlet. However unlike the April study, the maximum concentrations occur at the center and eastern side of the lake inlet within the first few hours of release, which suggests that the outflow from the wetland is also being drawn from the western part of the wetland as schematically shown on figure 4-6b. Eight hours after the release, 70 ± 10 % of the injected dye remains in the wetland, some caught in the eastern dead-zone, and some in the western side zone of the wetland.

Since a shallow littoral wetland can in general be considered to have a uniform but different water density from the deeper pelagic regions of a lake, a symmetric wetland outflow is expected (point sink) as shown on the schematic figure 4-6. Wind stress, however, can alter this symmetry by promoting the flow parallel to the axis of the wind. In order to evaluate this effect in the Upper Mystic Lake system, we now use the mean flowspeed of $u_1 = 2.1$ cm/s along the transect from the neck to the inlet derived from the arrival of the dye peak on figure 4-8b, and the wetland outflow rates (Q_1 in table 4.3), to estimate the lateral areal extent of the water being drawn out towards the lake. This analysis yields an effective flow width of

$$W_{flow} = \frac{Q_1}{H_1 u_1} = 70 \pm 20 \ m \tag{4.11}$$

which corresponds to only 30% of the mean wetland width. This suggests that the relatively strong (2.9 m/s) northerly wind generates a preferential flow path along the eastern side of the wetland during this day.

Next consider in greater detail some of the lateral features of the flow. Figure 4-8c illustrates the lateral distribution of the water temperature and dye 115 m downstream of the neck 2.5 hrs after the release. The dye cloud has grown from its initial halfwidth of 5 m to 140 m on its unbounded western side. Assuming that the dye disperses according to Fickian diffusion, the lateral diffusivities in the wetland can be estimated from

$$D_y = \frac{{\sigma_2}^2 - {\sigma_1}^2}{2\Delta t}. \tag{4.12}$$

where 2σ corresponds to the halfwidth of the dye cloud, defined by the contour for which $C/C_{max} = 0.14$. This yields an estimate of $D_y = 0.3 \pm 0.2$ m^2/s, where the high uncertainty is a result of the low spatial resolution of the dye along the transect (figure 4-8a). The corresponding Peclet number is

$$Pe = \frac{UL}{D_y} = 20 >> 1$$

which confirms that the flow is short-circuiting through the wetland. Similar to the April study, the temperature contours exhibit a lateral structure. In particular, the surface water is warmer in the eastern side zone than the western side zone. This can be explained by differential heat absorption, which is consistent with the April observation that the Secchi depth is 20-30 cm shorter in the eastern side zone than in other parts of the wetland.

Next consider the vertical flow structure. Figures 4-8d and 4-8e summarize the dye concentrations and water speeds along the transect from the neck to the lake on the day of the release and the following day. Both figures illustrate a distinct two layer flow, with a 0.4-0.5 m thick upper layer flowing out of the wetland and a 1.2 m thick bottom layer flowing in from the lake. On July 31, the surface velocity measurement at $x = 140$ m deviates from the flow. Since the wind was less than average at this time (< 2 m/s), this feature is most likely due to the warming of the water in the eastern side zone, which may generate a weak, isolated lateral circulation. The bed intrusion from the lake extends along the whole wetland, and even into the upper forebay, as seen by the bed velocity measured near the neck. Some of this bed flow is recirculated in the deep channel, seen by the reversed flow direction at 1.7 m depth at $x = 60$ m.

In order to better understand the vertical flow structure in the wetland, consider three well documented exchange flow scenarios. Figure 4-9 summarizes each one of these scenarios, and the unique thermal signature that identifies them. The first flow scenario illustrated on figure 4-9a is that of a bottom wedge which travels along the bed without contact with the surface water. This flow structure occurs typically in deep and strongly stratified estuaries [*Fisher et al.*, 1979, p. 230], and is characterized by horizontal isotherms, except near the front of the bottom wedge. The second type of flow, previously observed in laboratory

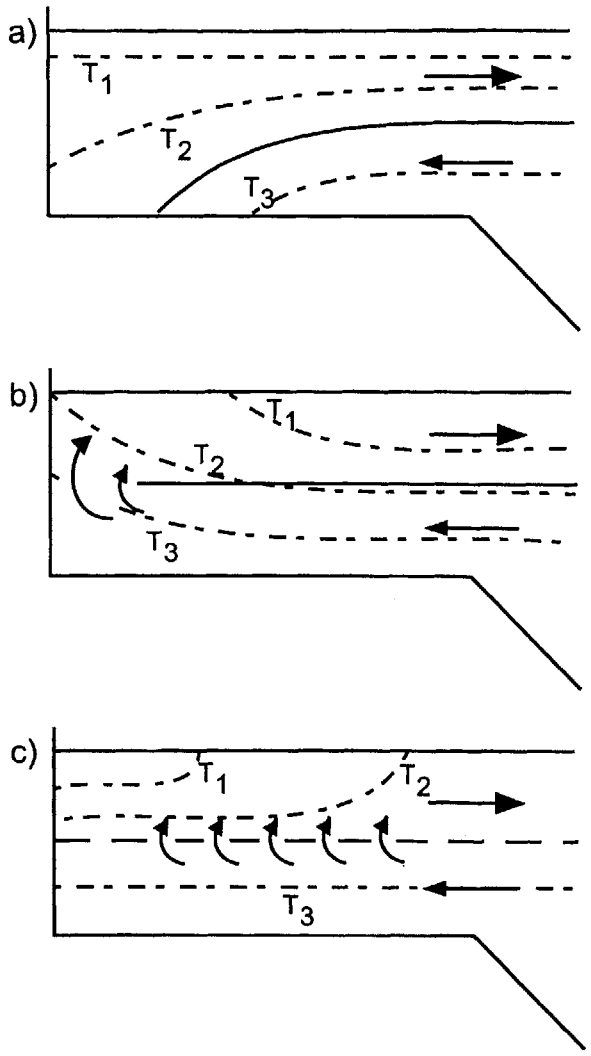

Figure 4-9: Typical vertical flow and thermal structures in lake sidearms and estuaries. a) Bottom wedge. b) Localized upwelling. c) Continuous upwelling.

experiments of laminar convective flows in shallow cavities [*Brocard and Harleman*, 1980], is that of a localized upwelling at the end of the sidearm (figure 4-9b). The thermal signature of this flow are isotherms that tilt upwards in the upwelling region, and increasing surface water temperatures towards the lake, as the colder upwelled water has had more time to equilibrate with the atmosphere. The last flow scenario is that of continuous upwelling along the length of the sidearm (figure 4-9c). This type of flow, both observed in sidearms of cooling lakes [*Adams and Wells*, 1984] and laboratory experiments of convective flow [*e.g. Jain*, 1980], results in a gradual cooling of the surface water towards the lake. This scenario is the most likely to occur in littoral wetlands, both because of the shallow water depth and water turbulence, which allows exchange between the two layers.

Figure 4-8e shows the wetland water temperatures along the transect from the neck towards the lake on July 31. The surface water is gradually cooling, from 27 °C at the neck to 25 °C at the lake inlet, similar to figure 4-9c, suggesting that the surface layer is continuously entraining water from the lower layer on its way towards the lake. The vertical entrainment velocity, w, and diffusivity of heat, K_{tz}, can be estimated by modeling the longitudinal temperature gradient in the region near the outlet of the wetland, where there is no heat exchange with the eastern dead-zone. For example, using

$$u_1 \frac{\partial T_1}{\partial x_1} = -(\frac{K_{tz}}{\Delta H} + w)\frac{T_1 - T_2}{H_1}$$

and the temperature measurements in the upper and lower layer, T_1 and T_2, gives an estimate for $(\frac{K_{tz}}{\Delta H} + w)$. Combining this with the heat budget in the lower layer, w and K_{tz} can be found individually. This analysis, summarized in more detail in Appendix 4.8.2, yields an estimate for the vertical diffusivity of heat as $K_{tz} = (1-4)10^{-5}$ m^2/s, which agrees well with the range of $10^{-5} - 10^{-4}$ m^2/s obtained from microstructure measurements in the wetland during summer days [*Nepf and Oldham*, 1997]. Similarly, the vertical entrainment velocity is estimated as $w = 10^{-5} - 10^{-4}$ m/s. For comparison, laboratory experiments suggest that interfacial mixing is related to the inertia and stratification of the flow by the following empirical formula [*Brocard et al.*, 1977, p. 112],

$$w_{emperical} \approx \frac{1.6 \cdot 10^{-3}}{g\Delta\rho/\rho}\left(\frac{u_1^3}{H_1} - \frac{u_2^3}{H_2}\right), \tag{4.13}$$

which yields $w_{emperical} \approx 1 \cdot 10^{-5}$m/s for the exchange flow in the Upper Mystic Lake system, in agreement with the heat analysis results.

Finally, consider in greater detail the longitudinal diffusion characteristics of the exchange flow. Figure 4-8d shows that 1 hr after the dye release, the center of the cloud has moved 60 m downstream which is in good agreement with the velocity measurements. In addition, the dye has dispersed longitudinally by 115 m. Using Fickian diffusion (4.12) and accounting for the advection of dye while the transect was taken, the longitudinal diffusivity was estimated as $D_x = 0.25 \pm 0.07$ m^2/s which is on the same order of magnitude as the lateral diffusivities, and matches the spreading of the dye observed at the outlet (figure 4-8b). Figure 4-8e illustrates the spatial dye distribution one day after the dye release. The low dye concentrations near the neck and at the inlet outline the river and lake flow into the wetland. Otherwise, the dye is relatively uniformly distributed across the wetland, except for the high concentrations at $x = 150$ m, which corresponds to the flushing out of the highly vegetated dead-zone on the western side of the neck (see figure 4-6b).

4.5 Analysis and Discussion

4.5.1 Exchange Flow Generation

In summer and fall, when river flows are low, exchange flows are generated by two interplaying factors, buoyancy and wind. In this section, we start by considering the various effects of wind on exchange flow generation, including the effects of barotropic, baroclinic seiching and surface wind drift. Then we consider the seasonal exchange flow generation, and evaluate the long-term effects of wind in promoting or destroying the density driven circulation.

Lake Barotropic Seiching

Wind along the main axis of a lake generates barotropic seiches, in which the entire water column in the lake oscillates up and down as if the lake were not stratified. The amplitude of the surface seiche can be assumed to scale on the steady surface setup in the lake, which is predicted as

$$\Delta\zeta = \frac{u_*^2 L}{2gH} \tag{4.14}$$

where $u_* = \sqrt{\bar{\tau}_w/\rho}$ is the wind friction velocity and is related to the wind speed by (4.5), and L/H is the length to depth ratio of the lake. For the Upper Mystic Lake, the average wind speed of 1.9 m/s yields

$$\Delta\bar{\zeta} = 1 \cdot 10^{-5}\ m.$$

Similarly, the maximum wind speed of 12.5 m/s, produces a vertical surface water displacement of

$$\Delta\zeta_{\max} = 6 \cdot 10^{-4}\ m.$$

The period of barotropic basin seiching is

$$P = \frac{2L}{\sqrt{gH}} = \frac{2 \cdot 960\ m}{\sqrt{9.81\ m/s^2 \cdot 15\ m}} = 2.6 \pm 0.1\ min. \tag{4.15}$$

Interestingly, this barotropic seiching period is on the same order of magnitude as the Helmholtz frequency, or the natural pumping mode or co-oscillations between the wetland and lake, given by *e.g. Hamblin* [1998]

$$\omega_h = \frac{2\pi}{P_h} = \sqrt{\frac{gH_iW_i}{A_wL_i}} = \sqrt{\frac{9.81 \cdot 1.4 \cdot 60}{51600 \cdot 60}} = (0.016 \pm 0.002)\ s^{-1} \Rightarrow P_h = 6 \pm 1\ min \tag{4.16}$$

where A_w is the wetland surface area, and, H_i, W_i, and L_i are the mean depth, width and length of the inlet separating the wetland from the lake (table 4.1). Assuming sinusoidal water level fluctuations in the lake and that the inlet is a rectangular channel, the maximum flow rate can be calculated based upon the non-dimensional surface seiche frequency, $\omega/\omega_h = P_h/P$, and the bed dissipation coefficient

$$\beta = \frac{\Delta\zeta A_w}{2L_iW_iH_i}(k_{en} + k_{ex} + \Lambda_i) \tag{4.17}$$

where $0.05 < k_{en} < 0.25$ and $k_{ex} = 1$ are the head loss coefficients associated with channel entrance and exit flows, and $\Lambda_i = \frac{C_f}{2}\frac{L_i}{H_i}$ is the bed drag along the inlet [*e.g. Mehta and Joshi*, 1988]. For the Upper Mystic Lake inlet with $C_f = 0.004$, $\Lambda_i = 0.1$ which yields $\beta << 1$. For such a no inertia configuration, *Mehta and Joshi* [1988] predict that the

amplitude of surface seiche induced flow at the inlet is

$$U_{\max} \approx \frac{2\pi\Delta\zeta A_w}{W_i H_i P} = \frac{2\pi \cdot 51600}{60 \cdot 1.4 \cdot 158\ s}(1 \cdot 10^{-5}, 6 \cdot 10^{-4})\ m = \begin{cases} 0.02\ cm/s & mean\ wind \\ 1\ cm/s & max\ wind. \end{cases} \tag{4.18}$$

Figures 4-4a and 4-5a show that the flow speeds at the inlet between the lower forebay and the lake range between 1-5 cm/s, and thus significantly exceed the surface seiche induced flow speeds. More importantly, the 3 min surface seiche generates horizontal excursions that are less than 1.8 m. Therefore, this analysis indicates that barotropic seiching in a small lake like the Upper Mystic Lake will have negligible effects on the exchange flow between the wetland and lake.

Lake Baroclinic Seiching

Wind blowing over a closed stratified basin also generates baroclinic seiches, which are much slower than the pre-discussed barotropic seiches. Thermistor chain data collected along the main wind axis of the Upper Mystic Lake reveal two dominant frequencies of basin scale (H1) internal seiches: First, an internal seiche of the first vertical mode (V1H1)[1] with a frequency of 0.5 cph ($P' = 2$ hrs), and second, an internal seiche of the second vertical mode (V2) with a frequency of 0.09 cph ($P' = 12$ hrs) [*Trowbridge*, 1995]. The frequency of the V1H1 oscillation is in good agreement with internal period predicted by a two layer model, i.e.

$$P' = \frac{2L}{\sqrt{\frac{g' H_{epi} \cdot H_{hypo}}{H_{epi} + H_{hypo}}}} = \frac{2 \cdot 960}{\sqrt{\frac{2.7 \cdot 10^{-2} \cdot 5 \cdot 10}{15}}} = 1.8 \pm 0.2\ hrs. \tag{4.19}$$

Here $g' = g(\rho_{hypo} - \rho_{epi})/\rho = (2.7 \pm 0.7)10^{-2}$ m/s^2 represents the reduced gravity in the lake based upon the observed temperature gradient between the lake epilimnion and hypolimnion (see section 4.2). The internal Helmholtz frequency for this system is

[1] A more detailed explanation of the vertical modes of internal seiches is found in e.g. *Münnich et al.* [1992].

$$\omega_h' = \frac{2\pi}{P_h'} = \sqrt{\frac{g' H_{2,i} W_{2,i}}{A_w L_i}} = \sqrt{\frac{3 \cdot 10^{-3} \cdot 1 \cdot 30}{51600 \cdot 60}} = (1.7 \pm 0.6) \cdot 10^{-4}\ s^{-1} \Rightarrow P_h' = 10 \pm 3\ hr \tag{4.20}$$

where $g' = g\,|\rho_2 - \rho_1|\,/\rho = (3 \pm 2) \cdot 10^{-3}$ m^2/s is the reduced gravity in the wetland, and not in the lake as in (4.19), $H_{2,i}$ is the mean water depth and $W_{2,i}$ the mean width of the lower layer at the inlet. The lake thermistor records indicate that the maximum vertical displacements in the thermocline region are ± 0.5 m [*Fricker*, 2000]. Assuming that these excursions decay linearly with depth, the maximum excursions of isopycnals at the level of the adjoining wetland are $\Delta\zeta' = \pm 0.1$ m. Adapting *Mehta and Joshi* [1988] theory for surface displacements to displacements of internal surfaces, the dissipation coefficient becomes

$$\beta' = \frac{\Delta\zeta' A_w}{2 L_i W_{2,i} H_{2,i}} (k_{en} + k_{ex} + \Lambda_i') \approx \frac{0.1 \cdot 51600}{2 \cdot 60 \cdot 30 \cdot 1}(1.5) = 2.$$

This in turns predicts the maximal seiche induced flows in the bottom layer at the inlet as

$$\begin{aligned} Q_{2,\max}' &= \frac{2\pi \Delta\zeta' A_w}{P'} \cdot const(P_h'/P') \\ &\approx \frac{2\pi \cdot 0.1 \cdot 51600\ m^3}{P'} \left\{ \begin{array}{l} 0.03 - 0.09 \\ 0.7 - 1.1 \end{array} \right\} = \begin{array}{ll} 0.1 - 0.3\ m^3/s & P' = 2\ hrs \\ 0.5 - 0.8\ m^3/s & P' = 12\ hrs \end{array} . \end{aligned} \tag{4.21}$$

These large seiche induced flowrates suggests that internal seiching in the lake may modify the baroclinic circulation driven by the density gradient between the wetland and lake. Note that this result is based upon the assumption that a diurnal surface layer is present in the lake. On windy days, when the wind blows from the far end of the lake, the lake water column may be fully mixed at the level adjoining the wetland, and will thus not exhibit internal displacements after the wind stops. Similarly, vertical mixing associated with convective cooling at night and during the fall is expected to impair these seiche induced flows.

In addition to the internal displacements, the baroclinic seiching mode also generates surface motion. The surface displacement scales on the internal displacements as [*Gill*, 1982, p. 122]

$$\Delta\zeta'_{surf} = \frac{g'H_{hypo}}{g(H_{epi}+H_{hypo})}\Delta\zeta' = \frac{2.7\cdot 10^{-2}\cdot 10}{9.81\cdot 15}0.5\ m = (9\pm 2)\cdot 10^{-4}\ m$$

and is thus much smaller than the internal displacements. Repeating the barotropic tidal inlet analysis (i.e. equations 4.17 and 4.18) but with P' and $\Delta\zeta'_{surf}$ replacing P and $\Delta\zeta$, the surface seiche induced flow is estimated as $0.03 - 0.05$ m^3/s, which is not significant compared to flow observed between the wetland and lake. Consequently, surface motion associated with the baroclinic seiching mode is not important in modifying the exchange flow.

Next consider the potential of lake hypolimnetic water to intrude into the wetland. Once fully established, the seasonal thermocline in the lake is at 5 m depth, or 2 m below the maximum depth of the inlet. Consequently, the ± 0.5 m vertical displacements of the thermocline are not large enough for hypolimnetic water to intrude into the wetland during summer and fall. This is in agreement with the Wedderburn number criteria, *i.e.*

$$We\# = \frac{g'H_{epil}^2}{Lu_*^2} < 0.5\ \frac{H_{epil}}{H_i}, \tag{4.22}$$

which suggests that for the thermocline to upwell into the wetland requires a wind speed of

$$W_{10} > \sqrt{2\frac{g'H_{epil}}{LH_i}}10^3 = \sqrt{2\frac{2.7\cdot 10^{-2}\cdot 5}{960\cdot 1.4}}10^3 = 14\ m/s$$

which has never been observed during the 5 year monitoring period in this system.

To summarize, the analysis presented in this section suggests that basin scale internal seiches in a small lake like the Upper Mystic Lake may modify the density driven lateral circulation between the lake and its adjoining littoral wetland or sidearm on summer days. However, as long as the lake thermocline is located at a significant greater depth than the wetland, lake hypolimnetic water is not expected to upwell into the wetland.

Wetland Seiching

Besides lake seiching, the wind also generates barotropic and internal seiching inside the wetland. The period of the wetland seiches can be estimated from (4.15) and (4.19), by replacing the numerator of $2L$ by $4L$, since the wetland has an open flow boundary (or

node) at the inlet. The results of this analysis are that the barotropic adjustment period in the wetland of around 3 min is too fast to significantly modify the exchange flow. The period of wetland internal seiches, however, is much slower, or

$$P'_W = \frac{4L}{\sqrt{\frac{g' H_1 \cdot H_2}{H_1 + H_2}}} = \frac{4 \cdot 200}{\sqrt{\frac{3 \cdot 10^{-3} \cdot 0.5 \cdot 1}{1.5}}} \approx 7.0 \pm 2.3 \; hrs, \tag{4.23}$$

and may modify the baroclinic exchange flow.

Lets now revisit the flow reversal observed in the bottom layer at the inlet on July 30 at 6 pm (figure 4-5a). In the afternoon, the wind is blowing steadily from the north at 3 m/s which leads to an upwards tilt of the thermocline in the northern end of the lake and in the wetland. At 4:50 pm, the wind stops and sets off an internal seiche both in the wetland and lake. While the lake thermistor data is not available for the time of this study, figure 4-5b shows that the lake surface mixed layer has deepened from 0.8 m at 3 pm to 1.15 m at 6 pm, which is consistent with a downwards moving internal seiche in the lake. This is also supported by the fact that the water in the lower layer in the wetland is colder than the water at the same depth in the lake at 6 pm. However, our previous analysis (4.21) suggests that lake internal seiching by itself is not likely to reverse the flow in the lower layer. Therefore another mechanism is likely contributing to the flow reversal. For example, the wetland internal seiching will generate flows in the bottom layer that are retreating towards the lake 1 hour after the wind stops, because it corresponds to approximately $P'_W/4$ for the highly stratified late summer afternoon (4.23). To summarize, the observed flow reversal in the bottom layer at the inlet on July 30 coincides with the onset of internal seiching in the wetland and lake, but the data available from that time is not conclusive about whether that is the main mechanism behind the reversal.

Wind Drift and Stirring

The 1D, steady and linear model derived by *Hansen and Rattay* [1965] and *Officer* [1976] for estuarine circulation is a simple tool widely used to characterize the effects of wind drift and vertical mixing on baroclinic circulation. In order to account for bathymetry in shallow littoral wetlands, I modified this model for non-rectangular cross sections, whose width varies with depth according to

$$W(\xi) = (1+\gamma)\bar{W}\,(1+\xi)^{\gamma}\,. \tag{4.24}$$

Here $\xi = z/H_{\max}$ represents the non-dimensional vertical coordinate, $H_{\max}$ is the maximum water depth, $\bar{W}$ the mean width, and γ the shape factor of the cross-section shown on figure 4-10a. By neglecting lateral cross-sectional variations and nonlinear feedback terms, and assuming that the density gradient, $\partial\rho/\partial x$, as well as the vertical eddy viscosity, K_{mz}, are uniform over the depth, the along channel velocities become

$$\begin{aligned} u(\xi) &= \frac{g\frac{\partial\rho}{\partial x}H_{\max}^3}{12\left(2+\frac{\gamma}{2}\right)^2\rho K_{mz}}\left[1-\left(2\left(2+\frac{\gamma}{2}\right)^2+1\right)\xi^2-2\left(2+\frac{\gamma}{2}\right)^2\xi^3\right] \\ &\quad +\frac{\bar{\tau}_w H_{\max}}{(4+\gamma)\rho K_{mz}}\left[1+(4+\gamma)\xi+(3+\gamma)\xi^2\right] \end{aligned} \tag{4.25}$$

where x is the positive axis from the wetland to lake. For a parabolic cross-section, (4.25) reduces to

$$\begin{aligned} u(\xi)|_{\gamma=0.5} &= \frac{4g\frac{\partial\rho}{\partial x}H_{\max}^3}{243\rho K_{mz}}\left[1-\frac{89}{8}\xi^2-\frac{81}{8}\xi^3\right] \\ &\quad +\frac{2\bar{\tau}_w H_{\max}}{9\rho K_{mz}}\left[1+\frac{9}{2}\xi+\frac{7}{2}\xi^2\right]. \end{aligned} \tag{4.26}$$

This analysis portrays the net along channel flow as a linear superposition of a density and wind driven circulation. The exchange flow contributed by the density gradient can be estimated by integrating the velocity profile given by (4.26) over the upper layer, i.e. from the zero crossing to the surface, yielding

$$\begin{aligned} \Delta Q_{buoy} &= \frac{2\bar{W}g\frac{\partial\rho}{\partial x}H_{\max}^4}{81\rho K_{mz}}\int_{-\frac{4+2\sqrt{166}}{81}}^{0}(1+\xi)^{0.5}\cdot\left(1-\frac{89}{8}\xi^2-\frac{81}{8}\xi^3\right)d\xi \\ &\approx 5.27\times10^{-3}\frac{\bar{W}g\frac{\partial\rho}{\partial x}H_{\max}^4}{\rho K_{mz}}. \end{aligned} \tag{4.27}$$

Similarly, the contribution by the wind can be quantified as

$$\Delta Q_{wind} = \frac{\bar{W}\bar{\tau}_w H_{\max}^2}{3\rho K_{mz}}\int_{-2/7}^{0}(1+\xi)^{0.5}\cdot\left(1+\frac{9}{2}\xi+\frac{7}{2}\xi^2\right)d\xi \tag{4.28}$$

$$= 4.11 \times 10^{-2} \frac{\bar{W}\bar{\tau}_w H_{\max}^2}{\rho K_{mz}}.$$

For the wind to dominate buoyancy, then $|\Delta Q_{wind}/\Delta Q_{buoy}| > 1$, which is satisfied by the following criteria for a parabolic cross section

$$|We\#| = \frac{buoyancy}{wind} = \left| \frac{g\frac{\partial \rho}{\partial x} H_{\max}^2}{\bar{\tau}_w} \right| < 8. \tag{4.29}$$

Notice, here we write the ratio between the buoyancy forcing and wind as a modified Wedderburn number, which differs from that used to predict upwelling (see eq. 4.22) by that the buoyancy term is here associated with a lateral density gradient and not with vertical stratification. Also notice that the sign of the Wedderburn number is relevant: If $We\# > 1$ then the wind promotes the density driven circulation, whereas if $We\# < 1$ then the wind surpresses it. Lastly, the critical value of the Wedderburn number varies slightly with cross section, as derived in Appendix 4.8.3.

Another interesting result of this model is that the buoyancy and wind driven circulations have different shapes as portrayed on figure 4-10b. Consequently, a moderate wind will not fully arrest the exchange flow when it is blowing from the opposite direction. Specifically, with an opposing wind the minimum exchange flow is approximately 40% of the baroclinic circulation existing without wind. In the limit of very strong winds, the flushing of the wetland will be solely determined by the barotropic wind driven circulation shown on figure 4-10b. Lastly, the model accounts for the effect of wind stirring through the vertical diffusivity of momentum, K_{mz}. As expected, along channel flow is inversely related to K_{mz}, such that a high K_{mz} reduces the exchange flow.

This 1D, linear and steady model has been extensively used to predict the water circulation in long, partially mixed estuaries. However, to the authors knowledge, it has not been used in shallow freshwater system and it is unclear how well this model performs there. One concern is that the model does not take into account the feedback between circulation and heating, but relies on the density gradient as an input. Unlike partially well mixed estuaries, the density gradient in shallow freshwater systems can vary significantly over time. For example, $|\Delta\rho/\Delta x|$ is observed to vary from -0.002 kg/m^2 to 0.003 kg/m^2 during the July study in the Upper Mystic Lake system. In addition, the model assumes that the density gradient is constant in space, whereas the July observations show

a)

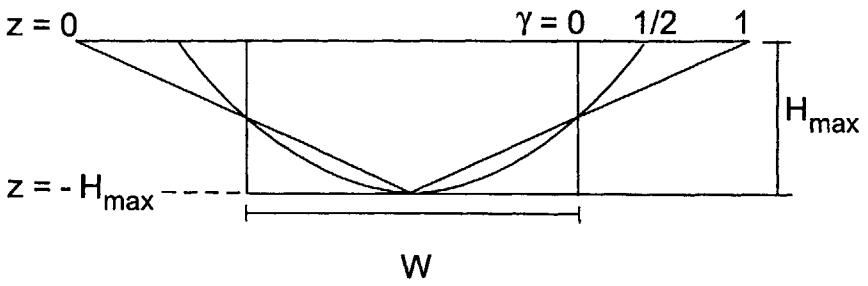

b)

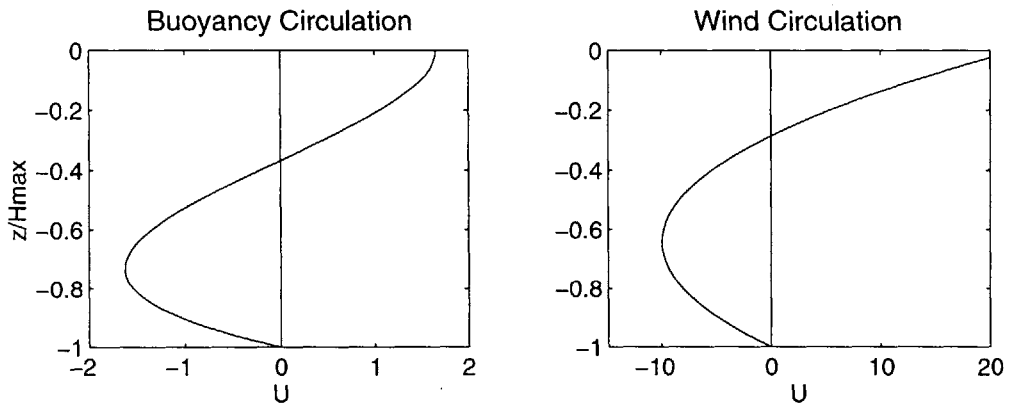

Figure 4-10: Schematic of Hansen-Rattay model adapted for non-rectangular cross sections. a) Cross-section shapes. b) Non-dimensional buoyancy- and wind-driven velocity profiles for a parabolic cross section ($\gamma = 0.5$).

that it ranges spatially from 0.0001-0.003 kg/m^2, with the highest gradient of 0.001-0.003 kg/m^2 being localized within 100±30 m around the inlet between the wetland and lake. This observation is in agreement with heat budget computations that show that horizontal temperature gradients are only appreciable up to 100 m from a lake shore [*Stefan et al.*, 1989]. The practical application of the Hansen-Rattay model in shallow freshwater systems is limited by the availability of spatial and temporal water temperature records. Another complication is that wind effects are more difficult to quantify in small freshwater system than large estuaries, both because of wind sheltering and wind directionality. Thus if the wind speed is not measured locally, then the wind shear stress must be adjusted by

$$\bar{\tau}_w = \left(\rho_a C_{10} W_{10}^2\right) \lambda \cos\theta \tag{4.30}$$

where θ is the angle between the wind direction and the main flow axis, and $\lambda(\theta)$ is the wind sheltering coefficient, which varies with fetch and is thus very site specific. Given the uncertainty in wind sheltering coefficient, wind speed and direction, the uncertainty in wind shear stress can easily be as large as 50%. Yet another concern is that the model assumes quasi-steady state, while both the wind and temperature gradients that generate the flow vary over time. Following *Monismith et al.* [1990], the sidearm spinup time can be estimated from the balance between the unsteady inertia and the pressure terms as

$$t_{spinup} \sim \left(\sqrt{g\frac{1}{\rho_0}\frac{\partial\rho}{\partial x}\frac{H}{L}}\right)^{-1}. \tag{4.31}$$

For a short (L = 200 m), shallow (H = 1.5 m) sidearm with a mild density gradient ($\Delta\rho/\Delta x = 0.002 \pm 0.001$ kg/m^2), such as the lower forebay, (4.31) yields a spinup time of 0.7±0.2 hrs which is short compared to period of the flow forcing (1-20 days). This suggests that exchange flows in small, shallow littoral regions such as wetlands have a small inertia and can be reasonably modeled assuming quasi-steady state. Lastly, the model assumes a constant vertical eddy diffusion coefficient K_{mz}. Since there is no tide that dominates the vertical mixing in shallow freshwater systems, K_{mz} may vary during the day as the exchange flow progresses and with variable wind conditions, making it hard to select a value of K_{mz} a priori. Consequently, it is important to make site specific measurements of vertical diffusivites, for example using a microstructure profiler.

Taking these factors into consideration, the model is now tested by predicting the flow

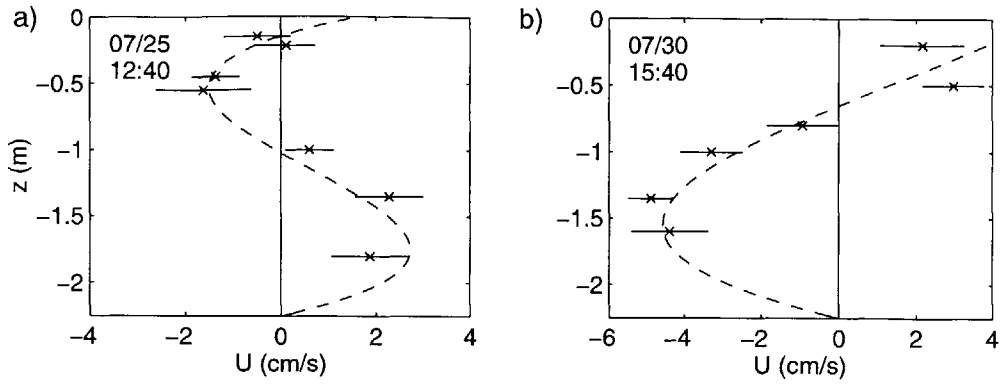

Figure 4-11: Comparison between Hansen-Rattay analytical solutions (dashed) and observations (-x-). a) July 25, $\Delta\rho/\Delta x = -0.002$ kg/m^2 and $W_{10} = 3.9$ m/s. b) July 30, $\Delta\rho/\Delta x = 0.001$ kg/m^2 and $W_{10} = 2.2$ m/s. Best fit was obtained using a triangular cross section ($\gamma = 1$).

in the channel between the lower forebay and Upper Mystic Lake on two windy summer days. Figure 4-11 compares the model analytical solutions to field observations. The wind speed and density gradient used in the predictions correspond to the value that best fits the data within the uncertainty of the observations. The turbulent eddy viscosity is taken from observations in the same system, and is not a fitting parameter. The chosen value of $K_{mz} = 7 \cdot 10^{-5}$ m^2/s corresponds to the upper bound of vertical heat diffusivities, K_{tz}, observed on windy days [*Nepf and Oldham*, 1997] and accounts for that $\mathrm{Pr} = K_{mz}/K_{tz} = 0.7$ in wall turbulent shear flow [*Hinze*, 1975, p. 747]. Figure 4-11a shows the circulation on a day when the wetland is cooling and the wind blowing from north-east, opposing the density driven circulation. For this condition, the model predicts a three layer flow profile at the lake inlet, with a wind-driven surface outflow to the lake, superimposed on a baroclinic circulation. The net flow at this time is 0.3 m^3/s, which corresponds to 40% of the estimated baroclinic exchange flowrate if there were no wind. Figure 4-11b, however, shows the circulation when the wetland is warming and a northerly wind is promoting the baroclinic circulation. The resulting flow is a two layer velocity profile, in which the wind doubles the exchange flow above that contributed by the density gradient. The close match between the simulations and field data suggests that within the uncertainty of the input variables, the simple linear 1D quasi-steady model may be used to predict exchange flows in shallow freshwater systems. In addition, this analysis highlights the importance of winds

in promoting and surpressing the density driven circulation. In the following section, we consider the long-term wind effects during the open water season (when the wetland is not frozen).

Seasonal Exchange Flow Evolution

The buoyancy forcing in shallow freshwater systems is generated by differential heating and cooling between the wetland and lake. Figure 4-12 summarizes the long-term water temperatures made during summer and fall of 1997. The solid line corresponds to the weighted average of the near-surface and near-bed temperatures measured in the lower forebay, whereas the dashed line corresponds to the water temperature within the top 2 m in the lake. First consider the fall season, for which both wetland and lake water temperatures are available. Figure 4-12b shows that the buoyancy forcing is characterized by synoptic cooling, i.e. there are extended time periods (e.g. Julian Days 265-279 and 290-307) when the wetland is $1 - 2^o$ C colder than the lake water. Since the temperature difference between the wetland and lake has been observed to occur within 100 m around the inlet, the corresponding density gradient is $0.001 - 0.002$ kg/m^4. The wind at this time of the year is predominantly blowing from the north (figure 4-3c). Consequently, the wind will mostly oppose the density driven circulation generated by differential cooling, similar to the July 25 scenario discussed on figure 4-11a. In order to better quantify the effect of wind during this time period, the long-term temperature difference between the wetland and lake water on figure 4-12b are combined with the wind measurement from the southern end of the lake, accounting for wind directionality using (4.30), to yield the timeseries of Wedderburn numbers shown on figure 4-12c. Incorporating the uncertainty associated with the density gradient and wind stress estimates, the Wedderburn number criteria (4.29) developed from the Hansen-Rattay model suggests that the wind surpresses the density driven circulation 10-25% of the time, and promotes it 7-12% of the time during this two month fall period.

Next consider the summer season. The temperature measurements in the wetland on figure 4-12a suggest that the buoyancy forcing is characterized by strong diurnal variations, as well as synoptic variations. This is consistent with detailed temperature measurements during the two shaded time periods on figure 4-12a, when a $\pm 1^o$ C temperature difference was observed between the wetland and lake. The density gradient associated with this differential heating and cooling was ± 0.003 kg/m^4, or on the same order of magnitude as

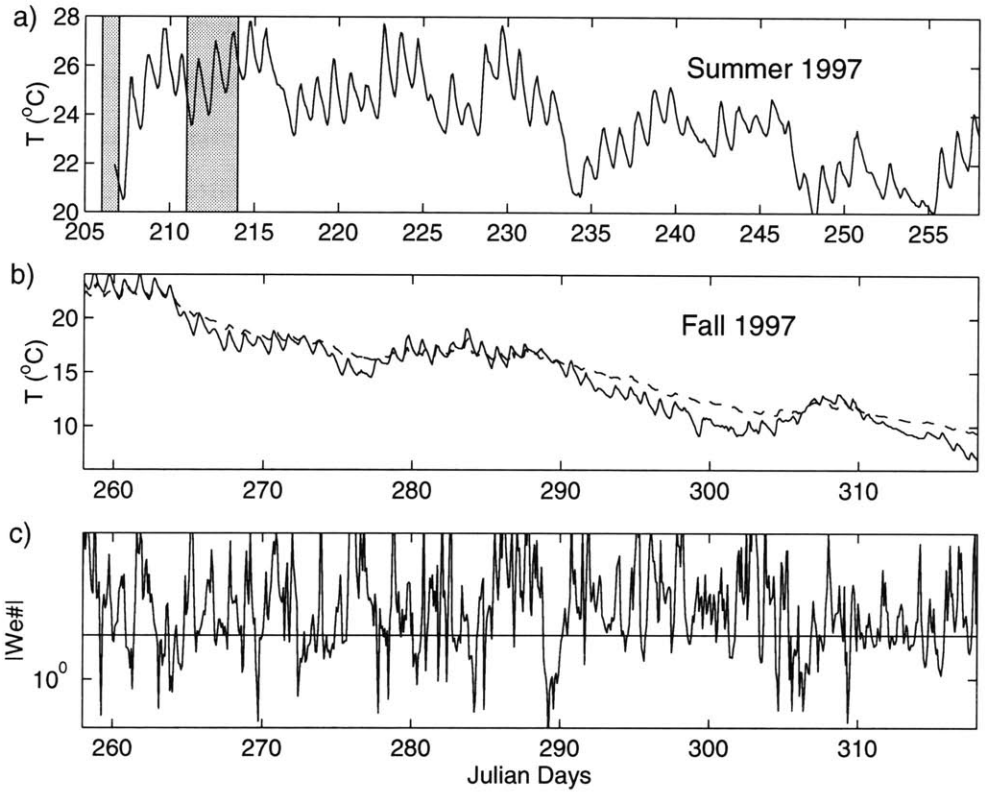

Figure 4-12: Relative importance of wind and buoyancy in summer and fall of 1997. a) - b) Weight-average water temperatures wetland (solid) and surface water lake temperatures (dashed). c) Wedderburn numbers.

that observed during the fall. Because of the diurnal variability in the density gradient, the summer southerly winds (figure 4-3c) are expected to equally promote and destroy the baroclinic circulation. While the wind speeds are slightly smaller during summer than fall (figure 4-3d), they are compensated for by less wind sheltering from the south. Consequently, the summer southerly winds are expected to be as important in modifying the baroclinic exchange flow between the wetland as the fall northerly winds.

Lastly, given the symmetry of the annual heating cycle, the buoyancy forcing during spring is expected to follow an opposite trend to that in fall, and be characterized by extended periods of synoptic heating. This is consistent with the observations during the April study, where the wetland water was persistently $1-2^{o}$ C warmer than the lake water (figure 4-4b). At this time period of the year, the winds are typically strong and from the north, and can promote the density driven circulation. However, as discussed in section 4.4.1, the high spring river flows significantly constrain the wind- and buoyancy-driven exchange flows between the wetland and lake.

To summarize, long-term meteorological observations in the Upper Mystic Lake system suggest that the buoyancy forcing is relatively constant over the course of the year, but the timescale of variation differs. The buoyancy forcing is characterized by synoptic variations in spring and fall, and diurnal variations in summer. Winds modify these shallow, density-driven exchange flows 20-40% of the time during summer and fall, when river flows do not constrain the flow.

4.5.2 Effect of Exchange on Flushing and Lake Transport

Unlike estuarine exchange flows, freshwater exchange flows can vary significantly over the course of the day, often reversing direction at night. When considering the transport of material from a littoral wetland to a lake, the net exchange over the day is of much higher significance than the temporal variations of the flow. This net exchange cannot be characterized from flow measurements alone, because they do no distinguish where the water comes from and do not account for the effect of mixing [*Hamblin*, 1998]. For example, velocity profiles cannot give insight whether upon flow reversal, the same water that left the wetland during the day reenters at night. Instead, characterizing the net exchange requires a conservative tracer, such as the dye released in the July study into the lower forebay in the Upper Mystic Lake system. Figure 4-13 summarizes the mass of dye remaining in

wetland, $M_{left}(t)$, on three different days after the release. The dye in the wetland decays as a result of the exchange flow occurring between the wetland and lake. The net diurnal flushing timescale can be estimated based upon these measurements as

$$\bar{t}_{net} = \frac{\int_0^\infty M_{left}(t)dt}{M_{in}} \approx \frac{\sum M_{left}\Delta t}{M_{in}} = 0.9 \pm 0.1 \ days. \tag{4.32}$$

Since the measurements in figure 4-13 do not resolve for the tail of the distribution, (4.32) is overestimating the net wetland flushing. Another estimate can be derived by fitting these measurements to an exponential curve as shown on figure 4-13, which yields $\bar{t}_{net} = 1.2 \pm 0.1$ days. This flushing timescale incorporates both the river flushing and net diurnal exchange flushing, i.e.

$$\bar{t}_{net} = \frac{AH}{Q_R + \Delta\bar{Q}_{net}} \tag{4.33}$$

from which the effective net exchange flowrate can be estimated as

$$\Delta\bar{Q}_{net} = \frac{AH}{\bar{t}_{net}} - Q_R = \frac{51,600 \cdot 1.3 \ m^3}{1.1 \ days} - 0.06 \ m^3/s \approx 0.6 \ m^3/s, \tag{4.34}$$

which corresponds closely to the maximum exchange flow observed at the neck during this study (table 4.3). While this is just one observation, this high net exchange rate suggests that the exchange flow is an efficient lateral transport mechanism between the wetland and lake. There are many factors that can contribute to a high exchange efficiency in the Upper Mystic Lake system. For example, the wakes and shear flow dispersion associated with the flow through the contraction between the wetland and lake enhances mixing and can contribute significantly to transport. The latter has been well documented in estuaries, where the interaction between irregular bathymetry and tides generates a residual circulation called "tidal pumping" [*Fisher et al.*, 1987, p. 237]. In addition, the synoptic variability between the wetland and lake water temperature, specifically in fall (and spring) as shown on figure 4-12b, indicates that there are extended periods when there is no flow reversal at night and therefore more effective exchange. To the authors' knowledge, this synoptic variability has not been reported in previous sidearm studies. Besides these site specific processes, there are two other processes that are generally expected to enhance net exchange between a shallow wetland and lake. The first one is that, when diurnal flow

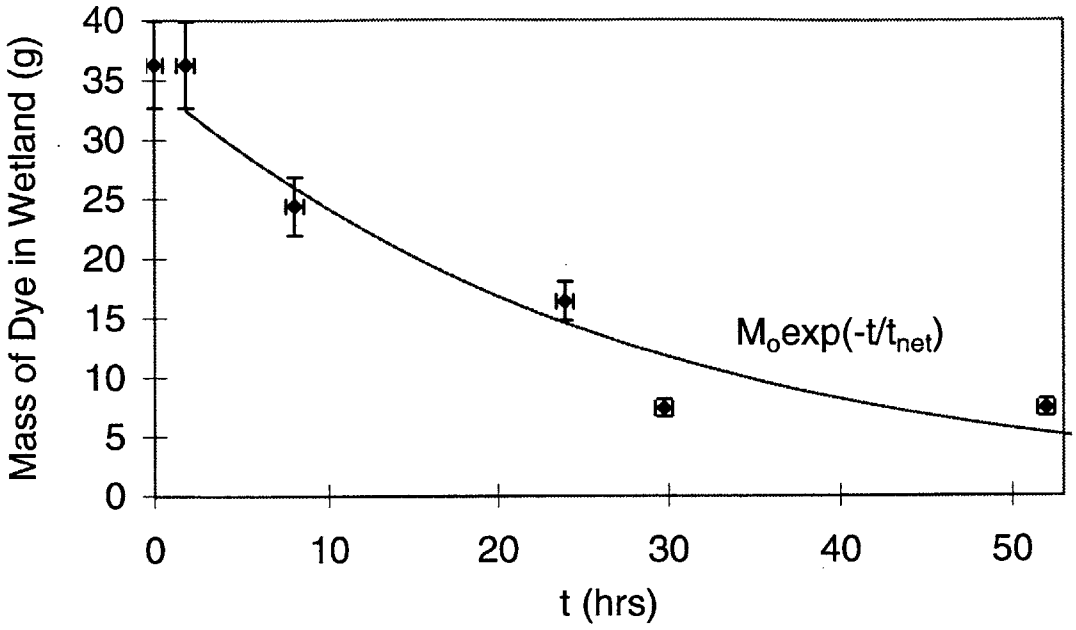

Figure 4-13: Mass retained in wetland after dye release on July 30, 1997.

reversal occurs, the different vertical mixing structure during the day (stabilizing period) and night (destabilizing period) can generate a net exchange flow, referred to by *Imberger* [1987] as a thermal siphon. Second, wetland water entering the surface layer of the lake can be transported and/or mixed within the lake, so even when flow reversal occurs, not the same water is pulled back into the wetland.

Finally, consider in greater detail how exchange flows impact wetland flushing. In the Upper Mystic Lake system, the net flushing timescale with exchange flow present is approx 1.2 days. However, if no exchange flows were present, the wetland flushing time would be

$$\bar{t}_R = \frac{AH}{Q_R} = \frac{51,600 \cdot 1.3\ m^3}{0.06\ m^3/s} = 13 \pm 1\ days,$$

or ten times slower. This comparison therefore demonstrates that unconstrained density and wind driven exchange flows can dramatically enhance wetland flushing. With this enhanced

flushing, the capacity of the wetland to remove contaminants, and thermally mediate the temperature of the lake inflow is impaired. Consequently, littoral wetlands that exchange with lakes play a very different role in lake water quality than wetlands that do not exchange with the lake. Specifically, instead of being considered as transformers, they need to be considered as "communicators" in the sense that they communicate properties from the shoreline (e.g. watershed runoffs) to the lake interior. This communication capacity will be reduced if these littoral regions are very densely vegetated, because of the drag imposed on the flow by the plants.

4.5.3 Feedback between Exchange Flow and Heating

Sidearm studies have identified density currents as an important heat dissipation mechanism in cooling lakes [*e.g. Jain*, 1980]. By analogy, littoral wetlands potentially play an important role in the thermal dynamics of natural lakes. Using the exchange flow observations at the inlet between the wetland and lake, i.e. $\Delta Q = (\Delta Q_1 + \Delta Q_2)/2$ in table 4.3, and the meteorological measurements at the site, the relative contributions of atmospheric heating and advective heat fluxes can be evaluated for both the wetland and lake in the Upper Mystic Lake system. The results from this analysis, summarized in table 4.4, show that heat fluxes associated with exchange flows are 5-50% of the surface atmospheric flux that acts on the wetland. Consequently, exchange flows contribute significantly to the wetland heat budget. However, these localized exchange flows are less important in the lake heat budget, because lakes are generally much larger than littoral wetlands (here $A_L \approx 10A_W$). The same does not apply for river flows. In spring, when river flows are high, table 4.4 shows that the Upper Mystic Lake receives an additional 25% on top of the atmospheric heating because of the river inflow. This suggests that river flows may significantly contribute to the formation of the seasonal thermocline in lakes, whereas exchange flows do not. *Carmack* [1979] came to a similar result based upon water temperature and river flow measurements in the much larger Kamloops Lake in British Columbia. Finally, since river flows are not as strong during fall (see for example figure 4-3a), they are not expected to play as important a role in the lake destratification process as they do in lake stratification process.

Date	Diurnal Average Surface Heat Flux $\bar{\phi}/\rho C_p$ (^{o}C m/day)	Advective Heat Fluxes in		
		Wetland	Lake	
		$\frac{\Delta Q}{A_W}(T_L - T_W)$ (^{o}C m/day)	$\frac{\Delta Q}{A_L}(T_W - T_L)$ (^{o}C m/day)	$\frac{Q_R}{A_L}(T_W - T_L)$ (^{o}C m/day)
4/14	2.3	-0.9	0.1	0.6
4/15	3.3	-0.6	0.1	0.3
4/17	0.7	-0.0	0	0.1
7/25	-6.5	0.3	-0.0	0.0
7/30 am	2.4	-0.2	0.1	0.0
7/30 pm	"	-1.2	0.0	0.0
7/31	3.6	-1.3	0.1	0.0

Table 4.4: Diurnal (P = 1 day) heat balance analysis for the lower forebay and Upper Mystic lake during the 1997 April and July studies.

4.6 Conclusions

Field observations show that wetland circulation and flushing dynamics can vary significantly with season. During spring, when river flowrates are typically high, the wetland flow regime is jet dominated. This results in short-circuiting, where a large portion of the river exits the wetland in a much shorter time than the nominal residence time, while another portion recirculates inside the wetland on both sides of the jet. The flushing of the wetland is predominantly determined by the river flow at this time. During summer, however, when river flows are typically low, the wetland flow regime is exchange flow dominated. These exchange flows vary over the diurnal cycle as a result of differential heating and cooling between the shallow wetland and deeper pelagic region in the lake. Surface wind drift can either surpress the density driven circulation, or promote it by a factor of two to three, depending on direction. Wind driven internal seiches in both the wetland and lake may also modify the exchange episodically. Despite this temporal variability, these exchange flows can enhance the net diurnal wetland flushing by a factor of 10 from the river flushing timescale. With this enhanced flushing, the capacity of the wetland to remove contaminants and thermally mediate lake inflow is impaired. Instead, these littoral wetlands effectively transport material originating from the watershed to the lake interior.

4.7 Acknowledgments

This work was funded by the National Institute of Environmental Health Sciences, Superfund Basic Research Program, Grant No. P42-ES04675. The authors would like to thank Rocky Geyer for his interest and development of this work, Harry Hemond, David Senn and Terry Donohue for their help in designing the field studies. Special thanks to our colleagues who participated in the April field program: David Senn, Wendy Pabich, Katja Knauer, Jenny Jay, Dan Brabander, Carolyn Oldham, Kathryn Linge, Chrissy Reilly; in the June field program: Marnie Bell, Shu-Fen Yun and Daniel Feller. The Winchester boat-club receives special thanks for their interest in our research and for allowing us to launch our boats from their docks during the busy summer months, and to the Medford boat-club for providing a pole for our anemometer.

4.8 Appendix

4.8.1 Wind over the Upper Mystic Lake

Wind speed and direction were measured at 10 m above the surface of the Upper Mystic Lake with a cup anemometer set up on the flag pole at the Medford boat club on the South shore of the lake. Measurements were taken every minute, averaged into 10 min bins and stored in a CR10 datalogger. The monthly averaged mean wind and prevalent direction are listed in table 4.5, and the monthly maximum winds in table 4.6.

(m/s)	April	May	June	July	August	Sept.	Oct.	Nov.	Dec.
1994	-	-	2.4	1.7	1.8	1.9	2.0	2.6	2.8
1995	-	1.9	1.5	1.7	2.0	-	-	-	-
1996	2.7	2.0	1.9	1.9	1.4	1.9	2.0	2.3	2.3
1997	2.9	-	-	2.1	1.6	1.8	1.9	2.5	2.5
1998	2.6	1.8	1.6	1.6	1.4	1.9	2.4	2.2	-
$\bar{W}_{10}$	2.7	1.9	1.9	1.8	1.6	1.9	2.1	2.4	2.5
1994	-	-	S	S	S	N	N	NW	N
1995	-	SE	S	S	N	-	-	-	-
1996	S	NW	S	S	S	N	N	N	N
1997	NW	-	-	NW	S	S	N	NW	NW
1998	NW	N/S	S	S	S	S	N	NW	-
Direct.	NW	N/S	S	S	S	S/N	N	NW	N

Table 4.5: Monthly mean wind speed (m/s) and prevalent wind direction over the Upper Mystic Lake in 1994-1998.

(m/s)	April	May	June	July	August	Sept.	Oct.	Nov.	Dec.
1994	-	-	7.1	5.9	6.6	9.1	8.0	10.5	9.6
1995	-	6.5	8.1	9.1	8.1	-	-	-	-
1996	8.9	7.7	8.3	10.0	5.2	8.4	10.5	10.7	8.8
1997	10.1	-	-	8.1	6.8	8.8	8.1	**12.5**	11.3
1998	(9.9)	(7.8)	8.8	6.8	6.4	8.2	10.6	9.7	-

Table 4.6: Monthly maximum wind speed (m/s) over the Upper Mystic Lake in 1994-1998.

4.8.2 Vertical Diffusivity and Entrainment

In July, when the river flowrates are low compared to the exchange flowrates, a distinct two layer flow pattern is observed in the wetland. Figure 4-9c shows the typical flow during daytime, where the upper layer of thickness H_1 flows out of the wetland at speed u_1, and the lower layer of thickness H_2 flows in from the lake at speed u_2. As the water flows through the upper layer towards the lake, it is cooling both because it entrains some water from the colder lower layer and also because of vertical diffusion of heat between the two layers. Following Jain's [1980] sidearm analysis, the entrainment velocity at the interface between the two layers, w, can be assumed to be constant. Consequently, the flow in both layers vary linearly at the rate

$$\frac{\partial H_1}{\partial t} + \frac{\partial (H_1 u_1)}{\partial x} = w; \quad \frac{\partial H_2}{\partial t} + \frac{\partial (H_2 u_2)}{\partial x} = -w$$

Neglecting longitudinal diffusivities, the corresponding governing equations for the depth-averaged water temperatures in the upper, T_1, and lower, T_2, layers are

$$\frac{\partial T_1}{\partial t} + u_1 \frac{\partial T_1}{\partial x_1} = -(\frac{K_{tz}}{\Delta H} + w)\frac{T_1 - T_2}{H_1} + \frac{\phi_1}{\rho C_p H_1} \tag{4.35}$$

$$\frac{\partial T_2}{\partial t} + u_2 \frac{\partial T_2}{\partial x_2} = \frac{K_{tz}}{\Delta H}\frac{T_1 - T_2}{H_2} + \frac{\phi_2}{\rho C_p H_2}. \tag{4.36}$$

Here $\Delta H = (H_1 + H_2)/2$ represents the distance for the water temperature gradient between the two layers, ϕ_i the net surface heat flux per surface area in each of the layers, $\rho = 1000$ kg/m^3 is the density and $C_p = 4180$ J/kg^{o}C the specific heat of water. The heat flux entering the upper layer, ϕ_1, incorporates the fraction of short wave (solar) radiation absorbed in that layer, long-wave radiation and diffusive fluxes due to conduction and evaporation. The

Date	Time	x (m)	H_1 (m)	H_2 (m)	T_1 (°C)	T_2 (°C)	K_{tz} (m^2/s)	w (m/s)
7/30	13:45	184	0.4	1.1	25.64	24.82	-	-
	14:09	250	0.7	1.3	25.13	24.70	$(3\pm1)\cdot10^{-5}$	$(1\pm0.2)\cdot10^{-4}$
7/31	12:16	138	0.4	1.1	25.52	24.49	-	-
	11:51	250	0.7	1.1	25.33	24.35	$(1\pm0.7)\cdot10^{-5}$	$(4\pm7)\cdot10^{-6}$
7/31	18:15	138	0.3	1.1	27.68	25.83	-	-
	18:24	250	0.7	1.3	26.76	25.40	$(3\pm1)\cdot10^{-5}$	$(2\pm1)\cdot10^{-5}$

Table 4.7: Estimation of vertical diffusivities and entrainment based upon two layer heat model. The observed water temperatures in the upper and lower layers, T1 and T2, have been temporally corrected. The uncertainity in the water temperatures are 0.05 and 0.6 C respectively.

lower layer, however, receives the remaining fraction of the short-wave radiation, S, which is given by

$$\phi_1 = S\exp(-\eta H_1)$$

where the light extinction coefficient, η, is inversely related to the Secchi depth, z_{sd}, i.e. $\eta = 1.7/z_{sd}$ [*Wetzel*, 1983, p. 68]. During the July study, $z_{sd} = 1.05$ m in the lower forebay which suggests that the lower wetland layer receives 30-50% of the incoming solar radiation.

Table 4.7 summarizes the water temperatures measured near the outlet of the wetland at $x = 250$ m. Notice that some of the measurements are taken within half an hour apart from one another during the peak surface heating time, when the water temperatures are increasing at a rate 0.6 °C/hour. By neglecting this transient behavior (*i.e.* set $\partial T_i/\partial t = 0$), (4.35) will overestimate the rate of entrainment and (4.36) will yield the unrealistic result of negative diffusion rate. Therefore, estimating the diffusion and entrainment rate requires that we decouple the transient behavior from the spatial behavior. This can be done by recognizing that the water entering the lower forebay has had enough heating time within the upper forebay to reach thermal equilibrium with the atmosphere (see section 4.4.2). Similarly, the water which enters the wetland at the bed (figure 4-9c) originates from the lake where it has had enough time to reach equilibrium. Consequently, in the absence of vertical entrainment or diffusion, there would be no spatial temperature gradient in the wetland and the water temperature would simply vary with time as stationary water, *i.e.*

$$\frac{\partial T_{1,2}^s}{\partial t} = \frac{\phi_{1,2}(t)}{\rho C_p H_{1,2}}. \tag{4.37}$$

With entrainment and diffusion present, then the water temperature will continue to vary in time according to (4.37). The spatial temperature gradient present at any given time in the wetland can thus be characterized by

$$u_1 \frac{\partial T_1}{\partial x_1} = -(\frac{K_{tz}}{\Delta H} + w)\frac{T_1 - T_2}{H_1} + \frac{\frac{\partial \phi_1}{\partial x_1}\Delta x}{\rho C_p H_1} \tag{4.38}$$

$$u_2 \frac{\partial T_2}{\partial x_2} = \frac{K_{tz}}{\Delta H}\frac{T_1 - T_2}{H_2}, \tag{4.39}$$

which is obtained by substracting (4.37) from (4.35) and (4.36). The last term in (4.38) represents the component of the atmospheric heat flux at the surface which counteracts the diffusion and entrainment from the colder lower layer. This term originates from the fact that conductive and evaporative heat fluxes as well as back-radiation at the surface are all a function of water temperature. Using empirical relationships for these heat flux terms [*e.g. Fisher et al.*, 1979, p. 163], this terms can be estimated as

$$\frac{\partial \phi_1}{\partial x_1}\Delta x = -\left(1.5 \cdot 10^{-3}\rho_a C_{pa} W_{10} + 1.5 \cdot 10^{-3}\rho_a L_w W_{10}\frac{\partial q}{\partial T_1} + 2.2 \cdot 10^{-7}(273 + T_1)^3\right)\frac{\partial T_1}{\partial x_1}\Delta x$$

$$\frac{\partial q}{\partial T_1} = 0.0038\frac{L_w}{R_v}\frac{1}{(273 + T_1)^2}\exp(\frac{L_w}{R_v}\left[\frac{1}{273} - \frac{1}{273 + T_1}\right])[1/^oC]$$

where $\rho_a = 1.2$ kg/m^3 is the density of air, $C_{pa} = 1012$ J/kg ^{o}C the specific heat of air, $L_w = 2.5 \cdot 10^6$ J/kg the latent heat of evaporation, $R_v = 461$ J/kg ^{o}C the vapor gas constant, W_{10} the wind speed at 10 m height and q the specific humidity of water. For the conditions during the July study ($T_1 = 26$ ^{o}C and $W_{10} = 2$ m/s),

$$\frac{\partial \phi_1}{\partial x_1}\Delta x \approx -21\Delta_x T_1 \ [W/m^2] \tag{4.40}$$

which is small compared to the advective heat flux that it can be neglected. Similarly, the lower layer does not get any significant heat flux since ϕ_2 is only a function of solar radiation which is spatially uniform ($\Rightarrow \partial\phi_2/\partial x_2 = 0$).

Using (4.37) to temporally adjust the water temperatures, then (4.39) yields the vertical diffusion rate

$$\frac{K_{tz}}{\Delta H} = \frac{u_2(H_2^j + H_2^{j+1})}{2\Delta x} \frac{T_2^{j+1} - T_2^j}{(T_1 - T_2)^j + (T_1 - T_2)^{j+1}},$$

and (4.38) the entrainment velocity

$$w = -\frac{u_1(H_1^i + H_1^{i+1})}{2\Delta x} \frac{T_1^{i+1} - T_1^i}{(T_1 - T_2)^i + (T_1 - T_2)^{i+1}} - \frac{K_{tz}}{\Delta H}. \tag{4.41}$$

The results from this analysis are summarized in table 4.7.

4.8.3 Hansen-Rattay Model for Rectangular and Triangular Cross-Sections

For a rectangular cross-section, (4.25) reduces to

$$\begin{aligned} u(\xi)|_{\gamma=0} &= \frac{g\frac{\partial \rho}{\partial x} H_{\max}^3}{48\rho K_{mz}} \left[1 - 9\xi^2 - 8\xi^3\right] \\ &\quad + \frac{\bar{\tau}_w H_{\max}}{4\rho K_{mz}} \left[1 + 4\xi + 3\xi^2\right]. \end{aligned} \tag{4.42}$$

The exchange flow contributed by the density gradient can now be estimated as

$$\begin{aligned} \Delta Q_{buoy} &= \frac{\bar{W} g \frac{\partial \rho}{\partial x} H_{\max}^4}{48\rho K_{mz}} \int_{-\frac{1+\sqrt{33}}{16}}^{0} \left(1 - 9\xi^2 - 8\xi^3\right) d\xi \\ &\approx 5.42 \times 10^{-3} \frac{\bar{W} g \frac{\partial \rho}{\partial x} H_{\max}^4}{\rho K_{mz}}. \end{aligned} \tag{4.43}$$

Similarly, the contribution by the wind can be quantified as

$$\begin{aligned} \Delta Q_{wind} &= \frac{\bar{W}\bar{\tau}_w H_{\max}^2}{4\rho K_{mz}} \int_{-1/3}^{0} \left(1 + 4\xi + 3\xi^2\right) d\xi \\ &= \frac{\bar{W}\bar{\tau}_w H_{\max}^2}{27\rho K_{mz}}. \end{aligned} \tag{4.44}$$

For the wind to dominate buoyancy, then $|\Delta Q_{wind}/\Delta Q_{buoy}| > 1$, which is satisfied by the following Wedderburn number criteria

$$|We\#| = \frac{buoyancy}{wind} = \left| \frac{g\frac{\partial \rho}{\partial x} H_{\max}^2}{\bar{\tau}_w} \right| < 7. \tag{4.45}$$

For a triangular cross-section, (4.25) reduces to

$$\begin{aligned} u(\xi)|_{\gamma=1} &= \frac{g\frac{\partial \rho}{\partial x} H_{\max}^3}{75\rho K_{mz}} \left[1 - \frac{27}{2}\xi^2 - \frac{25}{2}\xi^3 \right] \\ &\quad + \frac{\bar{\tau}_w H_{\max}}{5\rho K_{mz}} \left[1 + 5\xi + 4\xi^2 \right]. \end{aligned} \tag{4.46}$$

The exchange flow contributed by the density gradient can now be estimated as

$$\begin{aligned} \Delta Q_{buoy} &= \frac{2\bar{W} g\frac{\partial \rho}{\partial x} H_{\max}^4}{75\rho K_{mz}} \int_{-\frac{1+\sqrt{51}}{25}}^{0} (1+\xi) \cdot \left(1 - \frac{27}{2}\xi^2 - \frac{25}{2}\xi^3 \right) d\xi \\ &\approx 4.85 \times 10^{-3} \frac{\bar{W} g\frac{\partial \rho}{\partial x} H_{\max}^4}{\rho K_{mz}}. \end{aligned} \tag{4.47}$$

Similarly, the contribution by the wind can be quantified as

$$\begin{aligned} \Delta Q_{wind} &= \frac{2\bar{W}\bar{\tau}_w H_{\max}^2}{5\rho K_{mz}} \int_{-1/4}^{0} (1+\xi) \cdot \left(1 + 5\xi + 4\xi^2 \right) d\xi \\ &= 4.22 \times 10^{-2} \frac{\bar{W}\bar{\tau}_w H_{\max}^2}{\rho K_{mz}}. \end{aligned} \tag{4.48}$$

For the wind to dominate buoyancy, then $|\Delta Q_{wind}/\Delta Q_{buoy}| > 1$, which is satisfied by the following Wedderburn number criteria

$$|We\#| = \frac{buoyancy}{wind} = \left| \frac{g\frac{\partial \rho}{\partial x} H_{\max}^2}{\bar{\tau}_w} \right| < 9. \tag{4.49}$$

Bibliography

[1] Adams, E. E., S. A. Wells, Field measurements on side arms of Lake Anna, VA, *J. of Hydr. Engineer., 110*(6), 773-793, 1984.

[2] Armi, L., and D. M. Farmer, Maximal two-layer exchange through a contraction with barotropic net flow, *J. Fluid Mech., 164*, 27-53, 1986.

[3] Aurilio, A. C., R. P. Mason, and H. F. Hemond, Speciation and fate of arsenic in three lakes of the Aberjona Watershed, *Environ. Sci. Technol., 28*, 577-585, 1994.

[4] Brocard, D. N., G. H. Jirka, and D. R. F. Harleman, A model for the convective circulation in side arms of cooling lakes, *Tech. Rep. 223*, R. M. Parsons Lab for Water Res. and Hydrod., Mass. Inst. of Technology, 1977.

[5] Brocard, D. N., and D. R. F. Harleman, Two-layer model for shallow horizontal convective circulation, *J. Fluid Mech., 100*, 120-146, 1980.

[6] Carmack, E. C., Combined influence of inflow and lake temperatures on spring circulation in a riverine lake, *J. of Physical Oceanogr., 9*, 422-434, 1979.

[7] Chu, V. H., and W. D. Baines, Entrainment by buoyant jet between confined walls, *J. Hydraul. Eng., 115*(4), 1989.

[8] Dalziel, S. B., Maximal exchange in channels with nonrectangular cross section, *J. of Physical Oceanogr., 22*, 1188-1206, 1992.

[9] Farmer, D. M., and L. Armi, Maximal two-layer exchange over a sill and through the combination of a sill and contraction with barotropic flow, *J. Fluid Mech., 164*, 53-76, 1986.

[10] Farrow, D. E., and J. C. Patterson, On the response of a reservoir sidearm to diurnal heating and cooling, *J. Fluid Mech., 246*, 143-161, 1993.

[11] Fisher, H. B., E. J. List, R. C. Y. Koh, J. Imberger, and N. H. Brooks, *Mixing in inland and coastal waters*, Academic Press, Inc., London, 1979.

[12] Fricker, P. D., and H. M. Nepf, Bathymetry, stratification, and internal seiche structure, *J. Geophysical Res.*, 2000 (in press).

[13] Fricker, P. D., The effect of stratification and bathymetry on internal seiche dynamics, PhD thesis, Mass. Inst. of Technology, 2000.

[14] Geyer, R. W., Influence of wind on dynamics and flushing of shallow estuaries, *Estuarine, Coastal and Shelf Science*, 44, 713-722, 1987.

[15] Gill, A. E., *Atmosphere-Ocean Dynamics*, Academic Press, Inc, San Diego, 1982.

[16] Hamblin, P. F., Exchange flows in lakes, in Physical processes in lakes and oceans, *Coastal and Estuarine Studies*, 54, 187-198, 1998.

[17] Hansen, D. V., and Rattay, Jr. M., Gravitational circulation in straits and estuaries, *J. of Marine Res., 23*, 104-122, 1965.

[18] Hicks, B. B., R. L. Drinklow, and G. Grauze, Drag and bulk transfer coefficients associated with a shallow water surface, *Boundary-Layer Meteorology, 6*, 287-297 ,1974.

[19] Hinze, J. O., *Turbulence*, Mc Graw Hill, New York, 1975.

[20] Horsch, G. M., and H. G. Stefan, Convective circulation in littoral water due to surface cooling, *Limnol. Oceanogr.*, 33(5), 1068-1083, 1988.

[21] Imberger, J., Hydrodynamics of lakes, *Australian Water and Waster Association*, 12th Federal Convention, Adelaide, Australia, 401-423, 1987.

[22] James, W. F., and J. W. Barko, Estimation of phosphorus exchange between littoral and pelagic zones during nighttime convective circulation, *Limnol. Oceanogr.*, 36(1), 179-187, 1991.

[23] Jain, S. C., Density currents in sidearms of cooling ponds, *J. of the Energy Div. ASCE, 106*(EY1), 1980.

[24] Linden, P. F., and J. E. Simpson, Gravity-driven flows in a turbulent fluid, *J. Fluid Mech., 172*, 481-497, 1986.

[25] Mehta, A. J., and P. B. Joshi, Tidal inlet hydraulics, *J. of Hydr. Engineer., 114*(11), 1321-1338, 1986.

[26] Monismith, S. G., J. Imberger, and M. L. Morison, Convective motions in the sidearm of a small reservoir, *Limnol. Oceanogr., 35*(8), 1676-1702, 1990.

[27] Nepf, H. M., and C.E. Oldham, Exchange dynamics of a shallow contaminated wetland, *Aquat. Sci., 59*, 193-213, 1997.

[28] Nunes Vaz, R. A., G. W. Lennon, and J. R. de Silva Samarasinghe, The negative role of turbulence in estuarine mass transpor, *Estuarine, Coastal and Shelf Sci., 28*, 361-377, 1989.

[29] Officer, C. B., Physical oceanography of estuaries (and associated coastal waters, John Wiley & Sons, Ney York, 1976.

[30] Solo-Gabriele, H., Metal transport in the aberjona river system: monitoring, modelling, and mechanisms. PhD thesis, Mass. Inst. of Technology, 1995.

[31] Stefan, H. G., M. Horsch, and J. W. Barko, A model for the estimation of convective water exchange in the littoral region of a shallow lake during cooling, *Hydrobiologia, 174*, 225-234, 1989.

[32] Sturman, J. J., G. N. Ivey, and J. R. Taylor, Convection in a long box driven by heating and cooling on the horizontal boundaries, *J. Fluid Mech., 310*, p. 61-87, 1996.

[33] Sturman, J. J., and G. N. Ivey, Unsteady convective exchange flows in cavities, *J. Fluid Mech., 368*, p. 127-153, 1998.

[34] Sturman, J. J., C. E. Oldham, and G. N. Ivey, Steady convective exchange flows down slopes, *Aquat. Sci., 61*, 260-278, 1999.

[35] Thackston, E. L., F. D. Jr. Shields, and P. R. Schroeder, Residence time distributions of shallow basins, *J. Environ. Eng., 113*(6), 1319-1332, 1987.

[36] Trowbridge, P. R., Rapid redox transformations of arsenic and characterization of the internal seiches in the Upper Mystic Lake, Medford, Massachusetts, Masters thesis, Mass. Inst. of Technology, 1995.

[37] Wetzel, R. G., *Limnology*, Saunders College Publishing, Forth Worth, 1983.